Development of a Laser-Based Automated Mechanical Mobility Measurement System for One-Dimensional Experimental Modal Analysis

By

Barry L. Agee

Thesis submitted to the Faculty of the

Virginia Polytechnic Institute and Sate University

in partial fulfillment of the requirements for the degree of

Master of Science

in

Mechanical Engineering

APPROVED:

Larry D. Mitchell

Larry D. Mitchell, Chairman

Alfred L. Wicks

Alfred L. Wicks

Robert L. West Jr

Robert L. West

February, 1992
Blacksburg, Virginia

c.2

Development of a Laser-Based Automated Mechanical Mobility Measurement System for One-Dimensional Experimental Modal Analysis

By

Barry L. Agee

Committee Chairman: Larry D. Mitchell

Abstract

A laser-based automated mechanical mobility measurement system has been developed that can obtain a very high spatial resolution of frequency response functions (FRFs) for experimental modal analysis where one-dimensional structural motion predominates. With this system FRFs are measured and recorded in a format that is readily imported into a popular modal analysis software. A scanning laser Doppler velocimeter is coupled to a multi-channel FFT analyzer system for efficient data collection and management of spatially distributed FRFs. The objectives in designing this measurement system is to take advantage of the laser's non-contacting nature, its high spatial resolution, and its fast point-to-point movement. By using the scanning capabilities of the laser, experimental mobility FRF data can be collected in those structures that have dominant response in one direction at up to 16,000,000 positions. Moreover, the laser does not mass load the structure thus making the structure time invariant unlike "roving" accelerometers. The design and implementation of this automated mechanical mobility measurement system is presented. Instrumentation interfacing and control issues as well as software development issues are addressed in this thesis. Procedures required to implement the laser-based measurement system are presented. The performance of the laser-based system is presented along with an illustrative example of its use on a free-free rectangular plate where the vibration response is primarily in one direction.

To Marvin H. Agee

Acknowledgements

First, I would like to thank my advisor Dr. Larry Mitchell for his advice and friendship through my undergraduate and graduate studies at Virginia Tech. I thank him for providing me the opportunity to pursue an advanced degree with him and for being there to help answer those difficult questions whenever called upon. I would also like to thank committee members Dr. Al Wicks and Dr. Bob West for their frequent advice and suggestions on this research project. Also thanks go to the VPI Laser Team especially, Mr. Teck Awa, Mr. Xiandi Zeng, and Dr. Roberto Arruda for their hard work toward the timely completion of this project. I would also like to thank the Virginia Center for Innovative Technology, Zonic Corporation, and the Department of Mechanical Engineering for financial support of this research. I wish to thank my family and friends for their support. Most of all, thanks to my parents Gladys and Lester Agee for their encouragement and guidance throughout the years. Finally, I have a special thanks for Robin Heath for her friendship and support during this endeavor. This task would have been very difficult to complete without her often needed words of encouragement and endless support.

Contents

List of Figures

List of Tables

Nomenclature

Roman Characters*

$V(t)$	instantaneous velocity signal
$H(f)$	true frequency response function
$\mathcal{F}$	Fourier Transform
$x(t)$	time-domain representation of signal x
$y(t)$	time-domain representation of signal y
$S_x(f)$	frequency-domain representation of signal x
$S_y(f)$	frequency-domain representation of signal y
$G_{xx}(f)$	autospectrum of signal x
$G_{yx}(f)$	cross spectrum of two signals y and x
$H_1(f)$	estimate of the true frequency response function
Y_{ij}	mechanical mobility
V_i	velocity response at point i
F_j	force at point j
^cH	estimate of the true frequency response function
H_2	estimate of the true frequency response function
$F(t)$	instantaneous force signal
f_D	Doppler shift frequency
V'_{LOS}	line-of-sight velocity with respect to a fixed laser source
f_C	laser carrier frequency
f_{CO}	low-pass filter cut-off frequency
R_1	circuit resistance
R_L	load resistance
E_{in}	input voltage to filter circuit
E_{out}	output voltage to filter circuit
C_1	circuit capacitor
X	horizontal scan direction
Y	vertical scan direction
x,y,z	global Cartesian coordinate system
$\bar{x},\bar{y},\bar{z}$	laser local Cartesian coordinate system
dl	mirror separation distance
O	origin of global coordinate system
$\bar{O}$	origin of laser local coordinate system

$\bar{R}_P$	range between laser local origin and arbitrary point, P
P	arbitrary point in space
R_o	range between coordinate system origins
a,b,c	laser local origin coordinates in global coordinate system
[RT]	rotation matrix
l,m,n	direction cosines
A,B,C,D	arbitrary registration points on the structure
$\mathscr{E}_{RMS}$	RMS error
V_{cmd}	ZETA voltage amplitude command
V_t	true output voltage
$f_i(V_t)$	command voltage to true voltage transform function
$g_i(\theta)$	true voltage to scan angle transform function
$X(V_t)$	horizontal distance traveled due to V_t
$Y(V_t)$	vertical distance traveled due to V_t
V_z	true outward normal velocity
V_{out}	analog laser velocity output
V_{Hx}	correlated laser-head motion, x-direction
V_{Hy}	correlated laser-head motion, y-direction
V_{Hz}	correlated laser-head motion, z-direction
$H_i(f)$	head motion model transfer function
$n_i(f)$	measurement noise
$R_{L,max}$	upper-bound laser range
$R_{L,min}$	lower-bound laser range
d	optimum laser working distance

Greek Characters*

$\gamma^2(f)$	coherence function
λ	laser light wavelength
Ω	resistance in Ohms
μF	capacitance in microfarad
$\theta_{\bar{x}}$	mirror rotation angle about the $\bar{x}$-axis
$\theta_{\bar{y}}$	mirror rotation angle about the $\bar{y}$-axis
ϕ	arbitrary angle
$\Delta\theta_{\bar{x}\,i}$	difference between measured and computed rotation angle about $\bar{x}$
$\Delta\theta_{\bar{y}\,i}$	difference between measured and computed rotation angle about $\bar{y}$
ΔX_{max}	maximum global Cartesian horizontal distance between registration nodes
ΔY_{max}	maximum global Cartesian vertical distance between registration nodes

*Nomenclature is listed in order of appearence.

Chapter 1

Introduction

1.1 Rationale for Research

There is an ever increasing demand to shorten the product design and development cycle while at the same time improving product quality. This demand to decrease the time to take a product from conceptional design to finished product has prompted the need for better designs in less time. Pursuit of this goal is being aided by the integration of computer modelling into the design cycle. Computer modelling technology provides an analytical technique that allows a design to be simulated and tested before expensive hardware prototypes are built. This powerful design approach provides a real potential for decreasing the design cycle time and costs as well as improving the quality of the designs.

The formulation of a computer model in terms of a structure's dynamic properties is now integral to the design process. The modern design process is heavily dependent on the accuracy of the computer dynamic models. The quantitative reliability of these models is a fundamental requirement, thus, placing a premium on techniques for validating existing models and methods for generating new experimental or theoretical models.

The finite element method (FEM), lumped-mass models, and transfer matrix continuum techniques represent the common analytical techniques employed in developing dynamic models. For many, the experimental method of choice is experimental modal analysis (EMA) [1]. Increased computer technology has allowed the analytical methods to generate refined dynamic models with thousands of degrees of freedom. Although in theory the experimental models may incorporate thousands of degrees of freedom, technology and time constraints have deterred this development. Typically, experimental models contain four hundred or less degrees of freedom, all of which are translational degrees of freedom.

Test setup usually is the most time consuming task of the entire experimental modal measurement. Calibration, cabling, checking, and preliminary modal survey work typically require 50% or more of the total test time on a large modal test. With a new instrument like a laser Doppler velocimeter (LDV) and with a new automated mobility measurement system (AMMS), experimental time to move transducers around can be decreased significantly. The net test duration may be reduced to 1/8 of its conventional testing value. With test setup and transducer movement requiring less of the total test time, more time is available for collecting dynamic information and performing data analysis.

This research develops a high-technology product that addresses the short-falls of the experimental modeling technique. A laser-based engineering tool is developed that is capable of measuring structural dynamic properties at a resolution and quality comparable to the currently available analytical techniques.

1.2 Project Summary

This project proposed to develop the first of a series of four high-technology products. The product developed and described in this thesis is a coupled scanning laser velocimeter/fast Fourier transform (FFT) system. This system will allow the non-contacting determination of the dynamic properties of a measured structure with data collection times that will be 1/8 to 1/300 of conventional methods. Such dynamic properties can be used for qualitative non-destructive testing, on-line product inspection, maintenance inspection, quality control, defect localization, multipoint on-line monitoring, experimental modal analysis, mathematical model development, and experimentally based structural modification.

The structural dynamics measurement system developed from this research is centered around a laser velocity measurement instrument capable of providing structural surface vibration data to a high-speed computerized data acquisition system. Figure 1.1 provides a laser Doppler instrument system schematic identifying the major laser head components. The optical scanner unit sequentially positions the laser beam to the response measurement locations. The optical detector senses the back-scattered radiation and adds

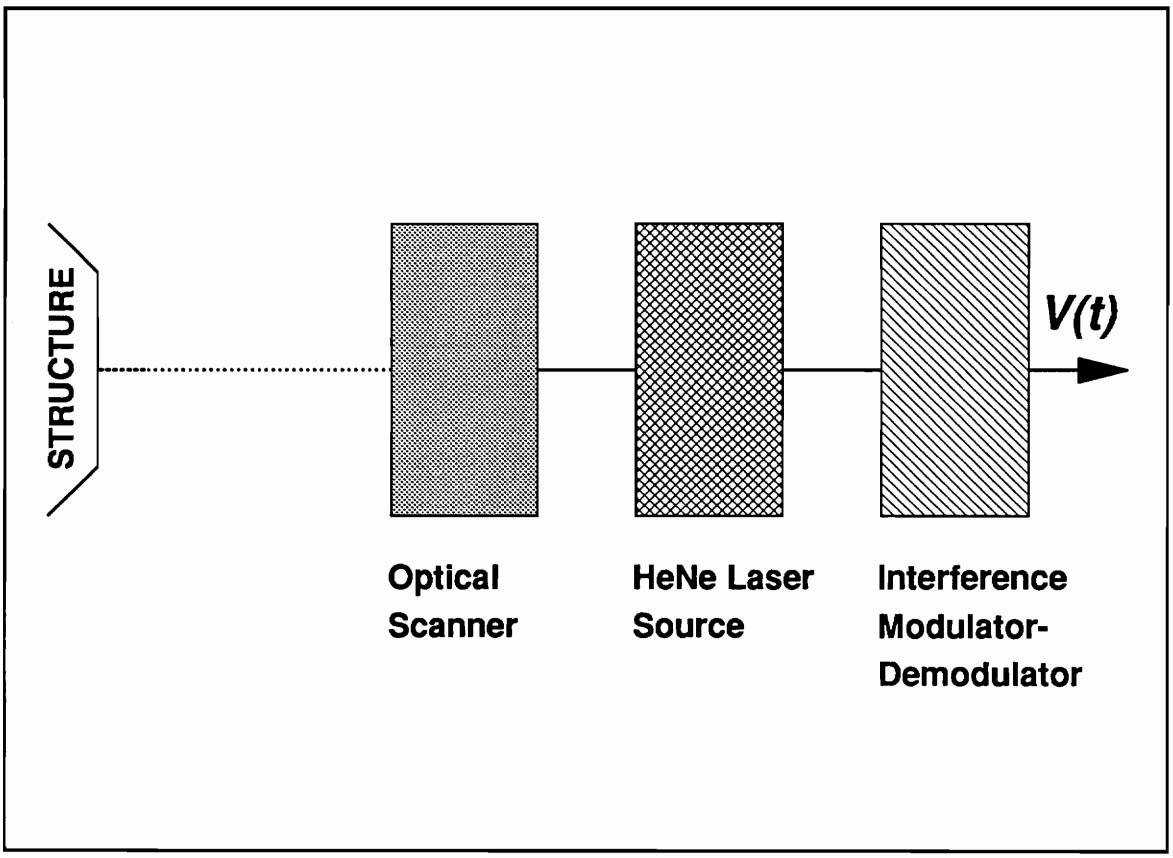

Figure 1.1 Laser Measurement System Schematic, (adapted from Mitchell, [1]).

it to an internal reference laser beam. The constructive and destructive interference patterns are modulated-demodulated in quadrature to produced a phase-preserved signal proportional to the velocity of the measurement point. Thus, the output of the laser system is an instantaneous analog velocity signal, $V(t)$. It is this velocity signal that all of the remaining AMMS system is design to capture and process.

The equipment required to assemble a laser-based mobility measurement system is shown in Fig. 1.2. As shown in this figure, the scanning laser is used to measure surface vibration. The programmed laser beam movement is controlled by an external digital-to-analog converter (DAC) source. The vibration data is acquired by the signal conditioner and analog-to-digital conversion (ADC) equipment. The entire process is controlled by a powerful multi-tasking control computer workstation that integrates the instruments into a measurement system. The computer workstation also provides real-time acquisition displays for interactive monitoring and provides a means for electronic FRF data storage. Post-processing software for modal analysis as well as a popular finite element method (FEM) software can also be installed on the workstation.

1.3 Thesis Overview

Chapter 1 of this thesis provides rationale and supporting information for the research detailed in the remainder of the thesis. The section entitled research product overview provides an executive summary of the research project including project objectives, research goals, and the scope of the research. Additionally, Chapter 1 contains the

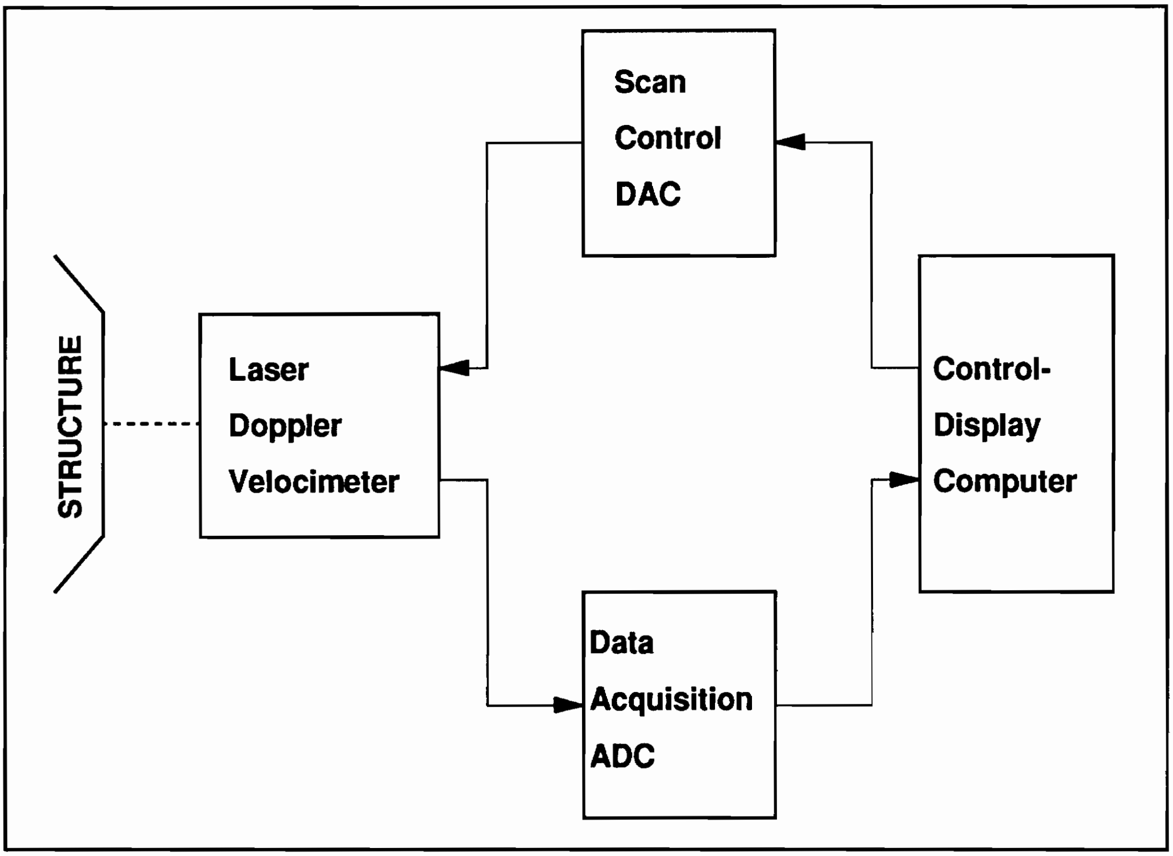

Figure 1.2 Instrumentation Schematic Diagram.

literature review on laser applications and conventional instrumentation for automated structural dynamic measurements. A brief review of conventional vibration analysis and signal processing is presented so that an appreciation for the automated test system developed by this research can be had. A brief discussion of resonance, mode shapes, experimental modal testing, and spatial aliasing is presented in Chapter 1.

Chapter 2 fully details the laser-based automated mobility measurement system (AMMS). System schematics and wiring diagrams are presented for the system in Chapter 2. A section highlighting the features of the system is included. The major equipment used in this research is described and hardware interfaces are detailed. The laser Doppler technique is presented and the principles of the Vibration Pattern Imager (VPI Sensor) instrument is discussed. Other major equipment including the System 7000 FFT analyzer and the HP 9000/series 300 computer are discussed in Chapter 2.

Chapter 3 details the software technology required to the develop the AMMS system. This chapter outlines the software development and instrument control. Specifically, the software architecture is introduced with a overview of the automation process. This consists of a flow chart of the modal test automation process. Next, the automated modal test scenario is discussed in detail. Chapter 3 presents the AMMS product development tools and software architecture. The Laser Systems Integrator (LSI) software modular presented. A complete description of the LSI user interface is presented as well as examples of all the major menu panels. A "walk-through" of the LSI menu system is also given in Chapter 3.

The task of determining the laser position with respect to the structure is detailed in Chapter 4. First, the concept of starting the experimental dynamics measurement with a wireframe or solid I-DEAS model is discussed. Second, the laser positioning algorithm development is presented. Third, sensitivities and performance measurements of the algorithm are presented. Finally, the process required to take the algorithm from computer simulations to the vibration laboratory is discussed. Chapter 4 also contains the instrument calibration procedures and typical calibration results for the laser galvanometer scanner system and digital-to-analog (DAC) voltage devices.

Chapter 5 discusses an application of the automated mobility measurement system to a free-free flat rectangular plate. Procedures for correcting line-of-sight (LOS) velocity measurements for laser view angle are presented. A procedure for correction of correlated laser head motions is also presented. In Chapter 5, typical laser-based mobility FRFs are presented and discussed. Additionally, a comparison of laser-based mobility data versus conventional accelerometer data is presented.

Chapter 6 presents conclusions about the research project and the automated mobility measurement system. Recommendations for using the AMMS system as a practical structural dynamics measurement tool engineering are provided. Finally, recommendations are offered to improve future versions of the AMMS system.

1.4 Research Project Overview

1.4.1 Introduction

The newly developing technology of applying laser velocimetry measurements to structural dynamics provides the analyst with a powerful tool for acquisition of experimental vibration data. By utilizing retro-reflected laser light to measure structural vibrations the measurement now can be accomplished without dynamically altering the structure. The mass and local stiffness effects typically added by a conventional acceleration transducer is avoided. This becomes a significant consideration when testing small lightweight components or when using multiple degree-of-freedom (MDOF) curve-fitting algorithms that require very consistent FRFs.

Furthermore, a laser velocimeter offers two additional advantages over conventional equipment and techniques. One of them is the fact that the laser beam can be focused to a spot diameter approaching 0.5 mm. This allows for vibration data acquisition in locations physically impossible with conventional transducers. The laser's capability to measure dynamics of small parts makes modal analysis techniques practical for quality inspection or diagnostics. For example, one laser application of this capability was to measure the deflection shapes of the small intake and exhaust valves in a reciprocating compressor crankcase [2]. In this application, the confines of the compressor cylinder bore (and mounting difficulties) would have allowed only one or two measurement points with a conventional accelerometer. This would have been a sparse dynamic measurement to say the least! Moreover, the accelerometer mass loading would have grossly changed the valve's dynamics. However, by using the laser velocimeter, approximately twelve (12) FRF locations were measured inside a 60 mm diameter cavity. This represented an order of magnitude increase in the FRFs collected in the tight confines of the cylinder bore. Furthermore, the laser provided the capability to expand the number of response point to several hundred in this relatively small cavity, if required. In this particular problem sufficient experimental dynamic information was obtained from the twelve or so response points to determine that the critical mode shape was such that it chopped the exhausting freon gas stream. This chopping frequency was, in turn correlated with high frequency noise emissions.

Non-contacting measurement of small parts is prompting a growing interest in applying the laser velocimeter to a quality inspection program. These attributes of the laser are being researched as an application for non-destructive testing (NDT) of circuit boards. The individual components on the circuit boards (ICs, resistors, etc.) can be targeted with the laser beam and monitored in a non-contacting fashion. This inspection process, currently in the development stages, may provide a reliable means to pre-test the "structural" integrity of the solder joints or pin connections prior to the electrical circuit inspection. This pre-electrical inspection could provide improved production rates as the "structurally" defective parts could be culled out of the production process before entering the electrical testing phase of inspection. Ideally, the defective region could be localized by monitoring the response spectrums on components of the circuit board assembly.

Traditionally, the task of measuring structural dynamic information has been an expensive and time-consuming task. However, the laser's ability to acquire mechanical vibration data at a high spatial resolution without contacting the structure during measurement is in itself an extremely desirable attribute. Additionally, the laser velocimeter can simplify the experimental test setup. By using the scanning capabilities of the laser, complete high-speed coverage of a large structure from a small number of view positions is possible. Thus, eliminating many separate transducers, cables, and power supplies. By simplifying the modal test setup, test reliability is improved and more time is available for data collection and analysis. Further discussions of applying the automated laser-based mobility measurement system to large modal tests is the topic of Chapter 5 of this thesis.

1.4.2 Objective of the research

The objectives of this research were primarily to advance the practicality of using laser-based vibration measurements for one-dimensional experimental modal analysis (EMA) and non-destructive testing (NDT) applications. Furthermore, this research was to expand and improve the function of the Ometron VPI Sensor to include spatially related, wide frequency band velocity vector measurement. Ultimately, the effort of this research was to develop and implement an engineering tool that would provide quality structural dynamics information with high-speed data acquisition capabilities. The development of this high-technology vibration measurement system was the logical first step in a series of laser-based products.

1.4.3 Goals of the Research Project

- Integrate a high speed multi-channel FFT analyzer (Zonic System 7000) with the scanning laser velocimeter (Ometron VPI Sensor) with a reduction in existing hardware components and with a minimum development of new hardware.
- Develop a computer-controlled automated technique to spatially acquire broadband mobility FRFs for dynamic analysis of structures in one-dimensional vibration.

1.4.4 Scope of the Research

- Develop the instrumentation interfaces required to fully integrate the laser velocimeter with a multi-channel FFT analyzer.
- Develop an automated measurement system that utilizes I-DEAS, a commercially available engineering software package by:
  - a.) Using the I-DEAS Test family modelling and wireframe meshing capabilities as a pre-processor to the automated measurement task.
  - b.) Using the modal analysis capabilities of the Test family software as the post-processor for estimation of modal parameters and mode shape animation.

- Develop a technique to locate the relative position of the laser with respect to the test structure.
- Develop the software required to implement the automation of laser-based mobility measurements.
- Test the laser instrument to determine its usefulness as a wideband velocity transducer for experimental modal analysis.

1.5 Literature Review

There is an increasing demand to perform experimental modal analysis of large structures. A large modal analysis experiment traditionally is a labor intensive task. A desirable goal is to shorten the test setup time and expedite the collection of vibration data. Partial automation of this modal test task is one way to make sure it is performed with a sufficient quantity of vibration response locations.

NASA investigators, Hunt and West [3,4], have developed and implemented a successful space shuttle inspection program based on EMA and machinery predictive maintenance (PM) technology [5]. In this experimental modal work large amounts of vibration data are necessary for meaningful post-flight quality inspection. Comparison of orbiter pre-flight FRFs to post-flight FRFs has been shown to effectively reveal cracks, flaws, or other structural damage to the air control surfaces. However, there is a major shortfall of this modal inspection program; the test setup time plus the post-test tile cleaning is a significant amount of the total test time. Setup usually requires more than 90% of the shuttle modal inspection time. Additionally, the spatial resolution of the measured FRF is limited by the number of accelerometer response points. Approximately 350 accelerometers currently are being used in the shuttle modal inspection system.

Other investigators, Oliver and Barker [6,7], have used a LDV for non-destructive testing (NDT) purposes. In this work, a laser Doppler velocimeter was used in an application to detect composite material delaminations and broken solder joints. By using wideband frequency excitation and an RMS level measurement technique, delamination flaws were detectable in a composite honeycomb panel. Additionally, these investigators were able to detect broken solder joints on a circuit board. By measuring the RMS vibration level of both a "good" circuit board and a "defective" board, the solder joint flaws were easily detectable when the difference of the two measurements were taken.

A basic vibration measurement system requires both an excitation transducer and a response transducer, two (2) data acquisition channels, and a digital signal processing capability. To be a viable product for experimental modal measurement a laser Doppler velocimeter must effectively compete with other instruments and other transducers. With conventional instruments as the number of response measurements increases so does the requirements for transducers, data acquisition channels, and analyzer channels. But with a scanning laser system, the necessary equipment list remains the same for one data point or 16,000,000 points. As a structural measurement technique, the laser-based measurement is fundamentally different than conventional measurement systems. A laser system takes vibration data serially. In other words, a sequential point-to-point measurement is performed. Other FFT systems [8,9] developed by various analyzer manufacturers acquire many channels of data in a parallel arrangement; up to 1000 simultaneous channels. Still other vibration data acquisition systems use fewer analyzer channels and a data scanner [10,11] to process data in a semi-parallel fashion. The operation of the data scanners is based on a multiplexer switching device in which many channels can be monitored with a relatively few number of analyzer channels.

Consequentially, large modal tests require many response transducers, cables, and conditioning amplifiers. Researchers Mitchell, et al [1] have shown that even a product reliability of 99% for this dynamic test equipment does not guarantee a high overall test system reliability. In fact, with a large modal test consisting of 400 response locations the overall system reliability can be a low as 20% for conventional accelerometer-based modal testing.

Other requirements of a large accelerometer-based modal test such as the space shuttle modal inspection program is the number of simultaneous (parallel) response channels to record. Advancements in microprocessor design and digital signal processing techniques have led to development of high speed multi-channel FFT analyzers. The Zonic System 7000 [8] is such a high performance FFT analyzer that can be configured to operate from 4 to 1000 parallel channels and maintain real time rates up to 5 kHz in large configurations. This is accomplished mainly because the System 7000 can be configured to have separate parallel FFT processors for each group of 8 input channels. The NASA shuttle inspection team of Hunt, West, et al [3,4] has developed its modal test system around a large multi-channel configuration of a Zonic System 7000.

There is a significant commitment of resources in multiple-channel signal analyzers. Other data acquisitions alternatives are available at the expense of the parallel signal processing capability. To cut instrumentation expenses for a large modal test a 2- or 4-channel FFT analyzer coupled to a data scanner may be used. The PCB 537B Data Harvester [10,11] is a computer-controlled multiplexer device that can automatically switch acquisition channels. The Data Harvester provides continuous power to ICP sensors, ranges automatically or manually, monitors overloads, and indicates faulty sensor operation. The Data Harvester is usually controlled over the IEEE-488 bus, but it has RS-232 and RS-422 communication capability. This model is configured on a 8-to-1 multiplexer module. The 8-channel plug-in modules are mounted in a chassis and will support either 4 or 16 eight-channel modules for a maximum of 128 channels per rack. Additional channels can be included by chaining racks together. A smaller, less-featured model 533 [10,11] is also available from PCB.

For large modal tests, the Tektronix SI5010 Programmable Scanner [12] is another popular multiplexed data scanner that is controllable over the IEEE-488 bus. It provides 16 channels which can be switched to 1, 2, or 4 common ports using a matrix switching scheme. Up to three 16-channel modules can be plugged into a single rack and multiple racks can be combined for systems requiring more that 48 channels. This scanner is useful for voltage mode inputs only; it does not provide power for ICP transducers.

Other tools exist to assist in the collection and management of large amounts of modal data. Fastscan 2600FS [13] data acquisition and scanner control software from Tektronix provides a convenient tool for automating large modal tests. This PC-based software integrates Tektronix FFT analyzers with a PC and data scanner. This software supports the Tektronix SI5010 over GPIB, PCB 537B Data Harvester over GPIB, and PCB 533A over RS-232C. Fastscan switches the scanner, acquires and stores data at each vibration measurement point, and applies the correct transducer calibration factor. For automating modal tests, it creates and maintains a transducer calibration database for each transducer serial number.

A structural laser Doppler velocimeter must compete with parallel-signal FFT analyzers and with data scanner instruments. However, it also directly competes with piezoelectric transducers. Inexpensive and lightweight accelerometers are being used more frequently in large automated modal testing. The Structcel and Flexcel accelerometers by PCB represent the latest progress to make a good, lightweight, inexpensive transducer [11,14]. These low-cost accelerometers are frequently integrated with a data scanner and control software to produce an economical automated modal analysis system.

There are two tradeoffs with an accelerometer/scanner data acquisition system. First, regardless of how light the accelerometers are, the test structure is mass loaded. Second, there still exists the problem of potential spatial aliasing; acquiring too few response points per spatial waveform. To address these short-falls of traditional modal testing equipment, Ometron Inc. has developed a intermediate laser product. Ometron attempted to bridge the gap between single frequency and wideband structural vibration measurement by adding extensions to the basic VPI Sensor product. One of these product extensions includes integration of the VPI Sensor and Ometron 9000 series console to a dual-channel FFT analyzer. With the add-on software option, Random/Service Data Acquisition Software (R/S-DAS) [15] allows multi-mode vibration analysis on a chosen component or structure. This software scans the laser beam in a user-defined manner, interfaces with several dual-channel FFT analyzers, and displays the FRF results. The R/S-DAS software supports the dual-channel spectrum analyzers from: Hewlett Packard, Bruel and Kjaer, Solartron, and Ono Sokki.

The next development towards a automated measurement system, by Ometron, was implementation of a auto-positioning feature in the VPI Sensor [16]. This optional handset feature give the user the ability to manually store up to 510 different laser beam positions. The positions are stored by directing the beam to the measurement points and electronically storing the beam locations. This feature is a partial step toward full automation of a structural dynamics measurement system. However, the obvious disadvantage of this feature is the tedious requirement to aim the beam at each response location.

1.6 Experimental Structural Dynamics

1.6.1 Noise and Mechanical Vibration

Noise and vibration in the environment or in industry are caused by particular processes where dynamic forces excite structures. The effects of noise and vibration range from annoyance, fatigue and reduced comfort, to safety and even health hazards. On machines, vehicles and buildings the effect may be wear, reduced performance, faulty operation or any degree of irreversible damage [17].

Vibration and noise are closely related. Most noise and vibration problems are related to resonance phenomena. Resonance occurs when the dynamic forces in a process excite the natural frequencies or modes of vibration, in the surrounding structures. Therefore, this is one reason for studying vibration modes. A second reason for studying modes is that they form the basis for a complete dynamic description of a structure. Still other reasons to study modes include dynamic motion control for precision machining, for vehicle ride comfort, for a feel of quality, for fatigue prevention, etc.

This thesis will not attempt to discuss the vast field of experimental structural dynamics. It is beyond the scope of this thesis. However, it is necessary to present the basic linear input-output relationship used to dynamically characterize a structure and later, how this process can be automated with current state-of-the-art scanning laser equipment.

1.6.2 Single Input-Single Output Model

Figure 1.3 illustrates a single input-single output (SISO) model with output noise used for two-channel frequency-domain measurement. Simply stated, the response of a structural system (in displacement, velocity, or acceleration) is directly related to the dynamic force applied. This relationship is called the frequency response function (FRF) for a linear system in the frequency domain. In Fig 1.3 the mechanical or structural system FRF is represented by $H(f)$.

Determination of the FRF of most systems is not intuitive; one can not simply determine the FRF by inspection. Luckily, this simple SISO model can be described mathematically and measured experimentally. In the section that follows, the two-channel FRF and Coherence function will be mathematically defined.

First, it assumed that the reader is familiar with the Discrete Fourier Transform (DFT) and the Fast Fourier Transform (FFT). References [18, 19, 20] provide a thorough presentation of the Fourier Transform material. Therefore, this work will not be presented in this thesis. However, the mathematical formulation of the FRF and Coherence function will be presented here. It begins with the assumption that all time-domain signals have been Fourier Transformed into the frequency domain given symbolically by the forward

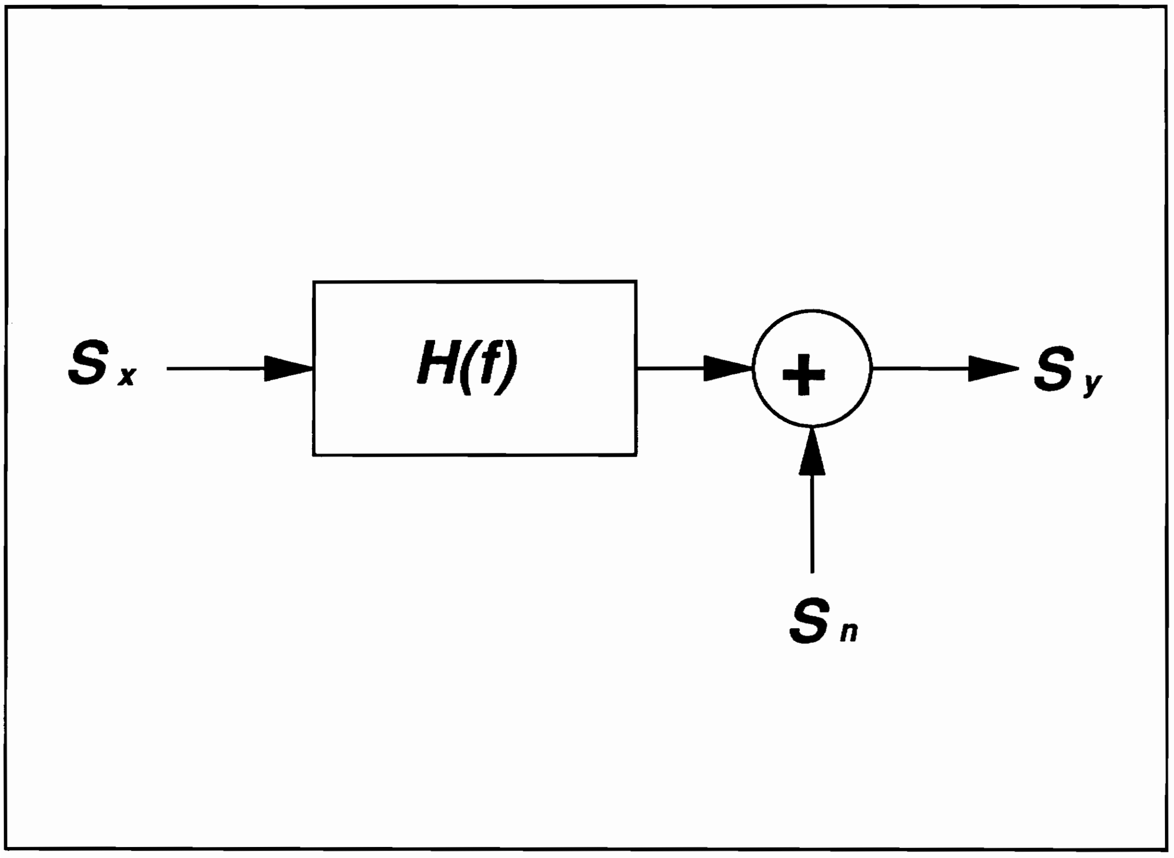

Figure 1.3 Block Diagram for $H_1(f)$ Model with Output Noise.

Transform relation:

$$x(t) \;\Rightarrow\; \mathscr{F} \;\Rightarrow\; S_x(f) \tag{1.1}$$

where,

$x(t)$	=	time-domain representation of the signal x
$S_x(f)$	=	frequency domain representation of the signal x
$\mathscr{F}$	=	Fourier Transform

Note that the transformation from the frequency domain back to the time-domain is accomplished by the Inverse Fourier Transform given symbolically by:

$$S_x(f) \;\Rightarrow\; \mathscr{F}^{-1} \;\Rightarrow\; x(t) \tag{1.2}$$

where $\mathscr{F}^{-1}$ denotes the Inverse Fourier Transform

Hence, Eqs. (1.1) and (1.2) are referred to as the Fourier Transform pair. The definition of the frequency response function requires that two other functions be introduced. The **Autospectrum,** G_{xx} , function is defined as taking the Fourier Transform of a signal, x and multiplying it by its complex conjugate, x^* as follows:

$$G_{xx}(f) \;=\; S_x^*(f)\; S_x(f) \tag{1.3}$$

where * indicates the complex conjugate of the function.

The **Averaged Autospectrum** is then defined as:

$$\bar{G}_{xx}(f) \;=\; \frac{1}{N}\sum_{n=1}^{N} G_{xx,n}(f) \tag{1.4}$$

where N is the number of measurement ensembles.

The second function needed to compute the FRF and Coherence function is the **Cross Power Spectrum**, or simply **Cross Spectrum**, G_{xy}. The **Cross Spectrum**, G_{xy}, is defined as taking the Fourier Transform of two signals separately, conjugating one of them, and then multiplying the result together as follows:

$$G_{xy}(f) = S_x^*(f)\, S_y(f) \tag{1.5}$$

It follows that the **Averaged Cross Spectrum** can then be defined as:

$$\bar{G}_{xy}(f) = \frac{1}{N}\sum_{n=1}^{N} G_{xy,n}(f) \tag{1.6}$$

With these two averaged functions defined in Eqs. (1.4) and (1.6) the **Frequency Response Function**, *H(f)*, can be defined using the two-channel measurement as:

$$H(f) = \frac{\bar{G}_{xy}(f)}{\bar{G}_{xx}(f)} \tag{1.7}$$

When *H(f)* is defined by Eq. (1.7) and Fig. 1.3, it is standard convention to call this FRF estimator, $H_1(f)$. Furthermore, a recent ANSI (American National Standard Institute) standard defines mechanical mobility as:

$$Y_{ij} = \frac{V_i}{F_j} \quad ; \quad F_k = 0 \; ; \; k \neq j \tag{1.8}$$

where V_i is the velocity response at point i to the force, F_j, applied at point j. The condition on Eq. (1.8) requires the external forces applied at all other points, F_k, and directions are zero. This means that we excite at only one point and direction on the structure at one time [21]. Since a LDV instrument measures a vibrating structure's surface velocity, the usual laser-based frequency response function, $H_1(f)$, is in mobility *(V/F)* form.

The other function computed with and monitored with the AMMS system is the **Coherence Function,** γ^2. It is also derived from the two-channel mobility measurement. The averaged cross spectrum and averaged autospectrum define the **Averaged Coherence Function** as:

$$\gamma^2(f) = \frac{\bar{G}_{xy}(f)\ \bar{G}^*_{xy}(f)}{\bar{G}_{xx}(f)\ \bar{G}_{yy}(f)} \tag{1.9}$$

The coherence function is a measure of the power in the output signal caused by the input. If the coherence is 1.0, then all the output power is caused by the input. If the coherence is 0.0, then very little of the output is caused by the input or there can be nonlinearity in the structure or leakage in the measurement system. If there is noise, then the coherence will be less than 1.0. Note that the coherence is also a function of frequency, The coherence can be unity at frequencies where there is no interference and low at frequencies where the noise is high. It is very common for the antiresonance region of the FRF to have low coherence. This is due to the poor signal-to-noise levels at these frequencies.

It is primary goal of the AMMS system to measure the signals required to compute the mechanical system's mobility frequency response function, $H(f)$ and the coherence function, γ^2. The experimental FRF measurement technique is summarized by the following general approach:

1. Apply a measurable input force, $x(t)$.
2. Measure the corresponding output response, $y(t)$.
3. Transform the force and response time-domain signals into the frequency domain by use of a Fast Fourier Transform (FFT) giving $S_x(f)$ and $S_y(f)$. (see Fig. 1.3)
4. Form the Averaged Cross Spectrum, $\bar{G}_{yx}(f)$ and the Averaged Autospectrum, $\bar{G}_{xx}(f)$ of the input.
5. For measurements with noise on the output, (which is a good assumption with an LDV), use Eq. (1.7) for estimation of the mobility frequency response function, $H_1(f)$, or other unbiased estimator [22,23,24].
6. Monitor the coherence function, γ^2, for an indication of experimental measurement quality.

1.6.3 Resonance Phenomena and Mode Shapes

The FRF of a structure can be determined experimentally. Generally, what is obtained in the experiment is a measurement of the complex FRF containing both real and imaginary or magnitude and phase information as a function of frequency. This experimental FRF can be curve-fit to provide an estimation of the modal parameters; mode shapes, natural frequencies, and modal damping.

Corresponding to each natural frequency of a structure is a mode shape. A mode shape is a vibration shape formed when a structure is excited at its natural frequency. Figure 1.4 demonstrates what is meant by the term mode shape. In this figure, the first three modes of a pinned-pinned (simple) beam are illustrated. Note: (1.) the vertical scaling is exaggerated to emphasize the motion, and (2.) only one freeze-frame of the oscillatory motion is shown. Mode 1 is a simple bulging shape similar to the static deflection curve. This mode is the called the first mode as it occurs at the first natural frequency of the beam. The two curves labeled Mode 2 and Mode 3 are the next two beam mode shapes. Logically, they occur at the beam's second and third natural frequency.

Generally, as the natural frequency increases, the mode shapes of structures become more complex in shape with an increased number of nodes. Also as structural geometry becomes more complicated so do the mode shapes. Notice in Fig. 1.4, as the mode number increases the "wavelength" of the mode shape decreases. Thus, as higher natural frequencies are examined, more closely spaced response points need to be measured to avoid the phenomenon of spatial aliasing (discussed later). The vibration testing of a simple structures like beams obviously does not require a high-tech instrument like a scanning laser velocimeter. However, the ability of the laser to obtain very high spatial resolution without mass loading the structure is a valuable asset. When tasked with

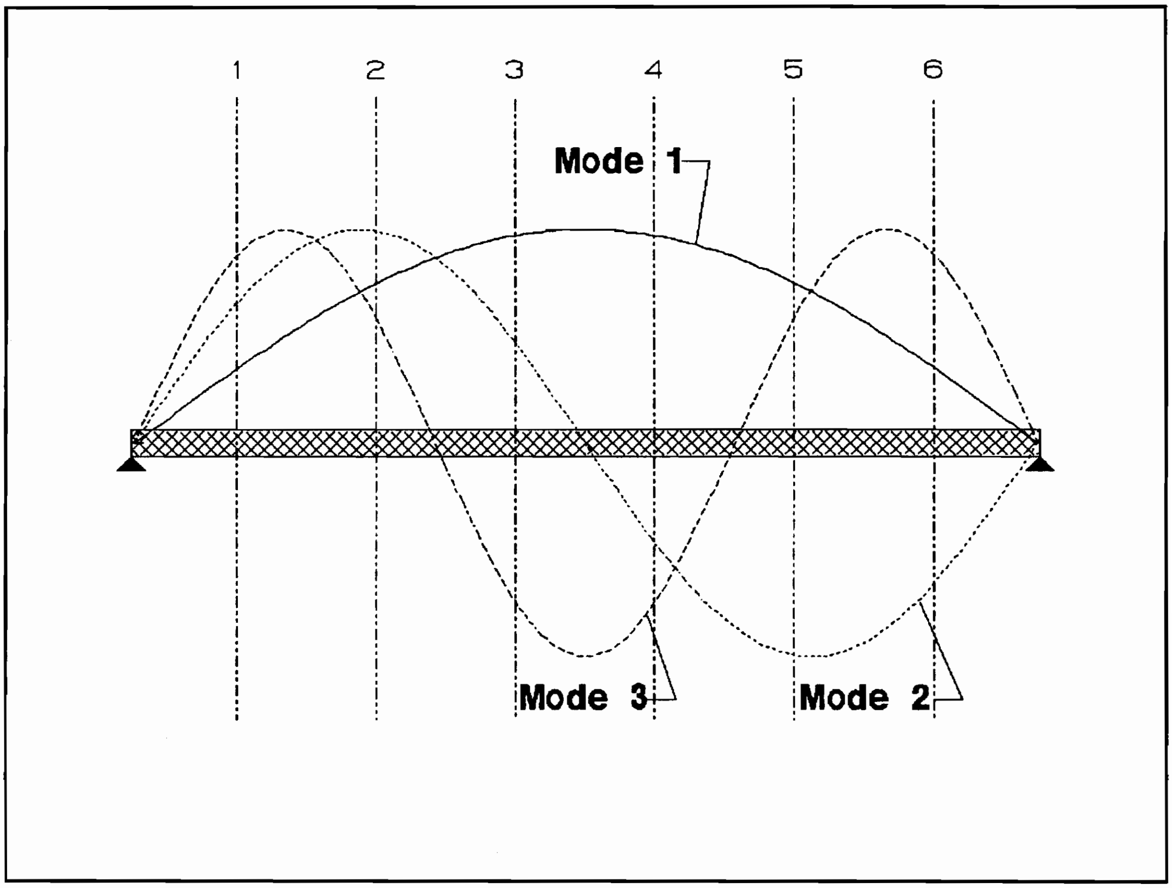

Figure 1.4 First Three Flexible Mode Shapes for a Pinned-Pinned Beam.

characterizing dynamic responses of structures with complex geometry the laser has proved its effectiveness [2,25]. Furthermore, the scanning laser may soon replace accelerometers in large scale modal testing requiring hundreds of transducers. The post-flight modal inspection of NASA's space shuttle [3,4] may benefit significantly from a automated laser-based dynamic measurement system like the one described in this thesis. Thus, it is the purpose of this thesis is to describe the procedure for automation of an experimental technique to obtain quality data for FRF measurement.

1.6.4 Experimental Structural Vibration Testing

Figure 1.5 shows a view of how a simple beam structure would be experimentally tested with conventional test equipment. In Fig 1.5 an electro-mechanical shaker is attached to the structure. The shaker transforms a power-amplified signal from a signal generator (sine, random, etc.) to an excitation force. The shaker is not usually connected directly to the structure. Normally what is attached to the structure is a force gage transducer or load-cell transducer. A force gage is a piezoelectric device that produces a voltage proportional to the force that produces a strain in the piezoelectric crystal. By mounting the force gage on the structure, the force-time history input to the structure can be accurately monitored throughout the test. The force gage can be attached either by stud mounting or by a thin film of high-strength adhesive. The force is usually transmitted from the shaker through a stinger that is designed to transmit axial loads effectively but not bending moments.

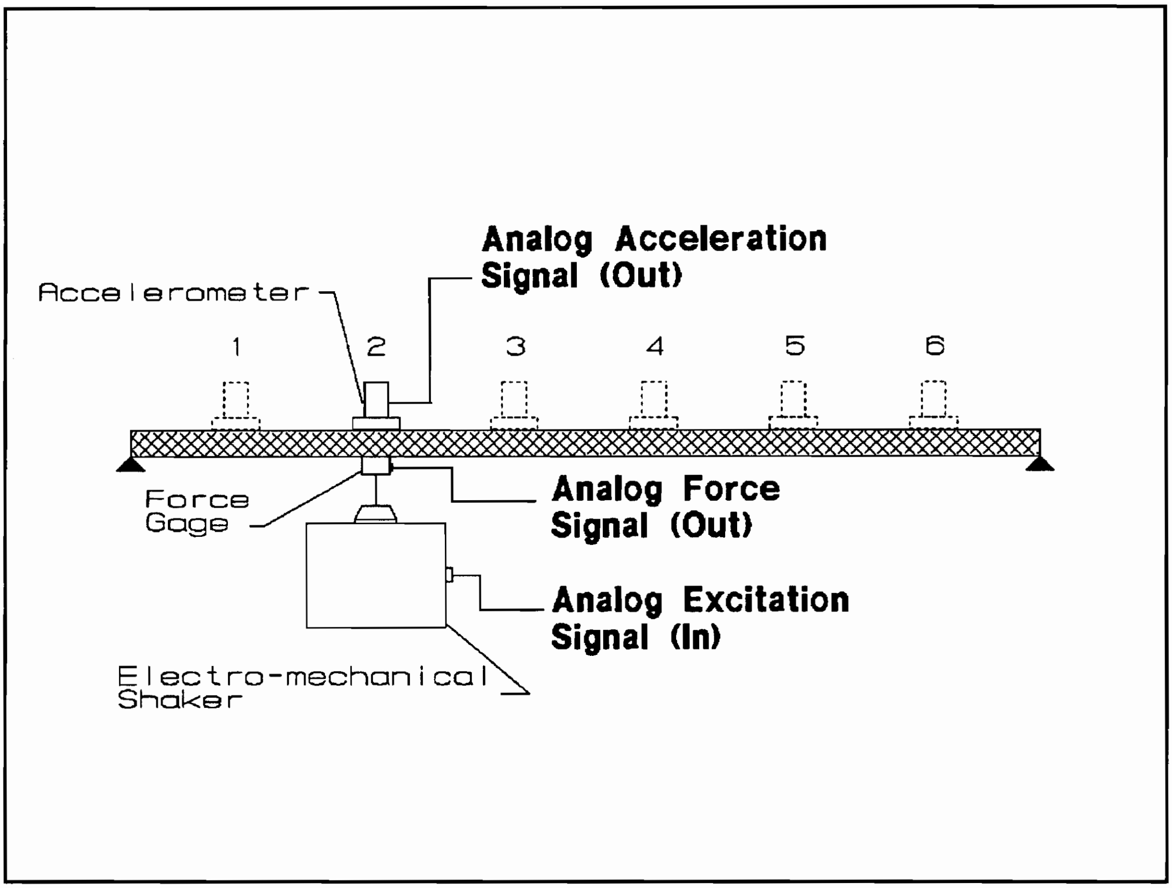

Figure 1.5 Experimental Modal Test Setup of a Simple Beam Showing Force and 6 Response Locations.

Also illustrated in the experimental setup shown in Fig. 1.5 are typical miniature accelerometers. Accelerometers are also piezoelectric transducers that generate a charge or voltage proportional to the acceleration of their base. The following list of features account for why accelerometers are one of the most popular transducers for EMA. They are:

- Relatively low-cost and rugged transducers
- Easily attachment by stud, wax, or high strength adhesive
- Highly sensitivity (up to 1 Volt per g)
- Low noise transducers with high dynamic range (>90 dB)
- Usable over a wide frequency range (<1 Hz to >10 kHz)
- Highly linear response (+/- 0.1 dB over usable range)
- Reasonably lightweight

The above list is only a partial list of accelerometer features. However, the accelerometer is being replaced with the newer technology of laser Doppler velocimetry in some structural dynamic applications for the following reasons:

- Mass loading of the test structure is unavoidable with accelerometers. At higher frequencies (i.e. complicated mode shapes) the mass of the accelerometer can introduce measurement errors in the FRF [26].

- The accelerometer has a spatial resolution limitation. Its finite size limits its ability to be placed spatial.
- It must be manually placed on the structure. This often requires surface preparation and introduces the possibility for human error in locating the transducer or not securely attaching it. Furthermore, the desired location may not be physically accessible.
- The effects of the environment can alter the output of an accelerometer. The temperature of the mounting surface must be below certain limits.
- A scanning laser may be <u>automated</u> to acquire FRFs without influencing the measurement.

1.6.5 Spatial Aliasing

In Fig. 1.5, an accelerometer was shown in one of many possible locations on the beam. For simplicity, the figure shows only six test positions. In reality, the beam in this figure is oversampled. The minimum sample points needed for reliable measurement of the first three modes is three (i.e., *2* x *number of waves* = 2(1.5) = 3). The waveform in the spatial domain also must obey the Shannon sampling theorem [19], which states the sample frequency must be equal to or greater than twice the highest frequency to prevent aliasing. Based on this reasoning, the more cycles in a waveform per unit length the greater the number of measurement points required. The laser velocimeter is the ideal instrument for obtaining this increased spatial resolution. In a test involving the laser instead of accelerometers, the experimental set-up would be identical to Fig 1.5 except the accelerometers would not be present. The laser-based system required for this measurement is presented in the following chapter.

Chapter 2

The Laser-Based Automated Mobility Measurement System

2.1 System Overview

There are two major modes of operation of EMA measurement systems. First and foremost, they are used to acquire modal data for comparison with and/or to be used to update finite element method (FEM) models. The second EMA application is the use of EMA's system identification capabilities to develop a modal space model of the test structure. This experimentally based model can be used with analytical models of the other machine components to assemble the overall model of the machine assembly. Moreover, the EMA model can be used as an analytical model that can be modified to correspond to an engineer's "what-if" redesign alternatives. This latter use of the experimental model as a basis for structural modification has some acknowledged limitations. The model limitation being the lack of rotational degrees of freedom. However, this lack of rotational degrees of freedom are quickly being removed by recent developments in rotational transducers [25] and in spatial data manipulation [26].

The main application that will be addressed by this thesis is the development of a laser-based automated mobility measurement system that will be compatible with FEM models where 1-D modes are expected. Compatibility with and measurements at the FEM nodal points is possible with the system. Moreover, the system measures, records, and labels all of the FRF files thus eliminating this extremely tedious and time-consuming task in high spatial measurement density test scenarios.

2.2 Description of the Laser-Based Measurement System

It is the goal of this research to develop an automated laser-based system to scan a predefined structure and obtain frequency response functions (FRFs). It is to manage the response node location/direction and then store the FRF data in a retrievable format for use in an engineering test data analysis program. The automated system being presented in this paper consists of two instruments that require interfacing and control by a Hewlett-Packard (HP) 9000/series 300 workstation. Figure 2.1 shows the major equipment required to implement this automated mobility measurement system (AMMS). One of the major instruments of this system is a laser Doppler velocimeter, (VPI Sensor) manufactured by Ometron Limited of London, England [16]. The other major component is the FFT analyzer (System 7000 or Workstation 7000) manufactured by Zonic Corporation of Milford, Ohio [8].

Figure 2.2 diagrams the physical arrangement of the laser-based Automated Mobility Measurement System (AMMS). The AMMS system works in the following manner. The

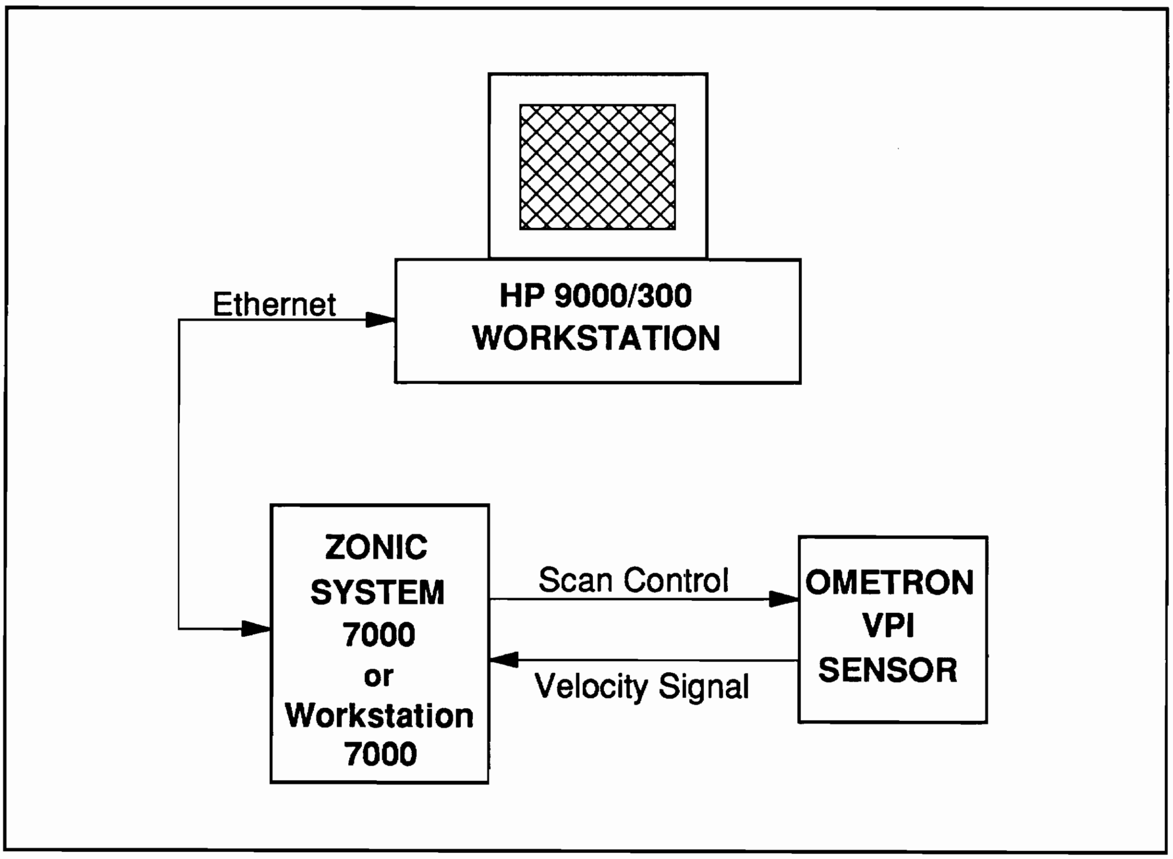

Figure 2.1 Major Instruments of the AMMS System.

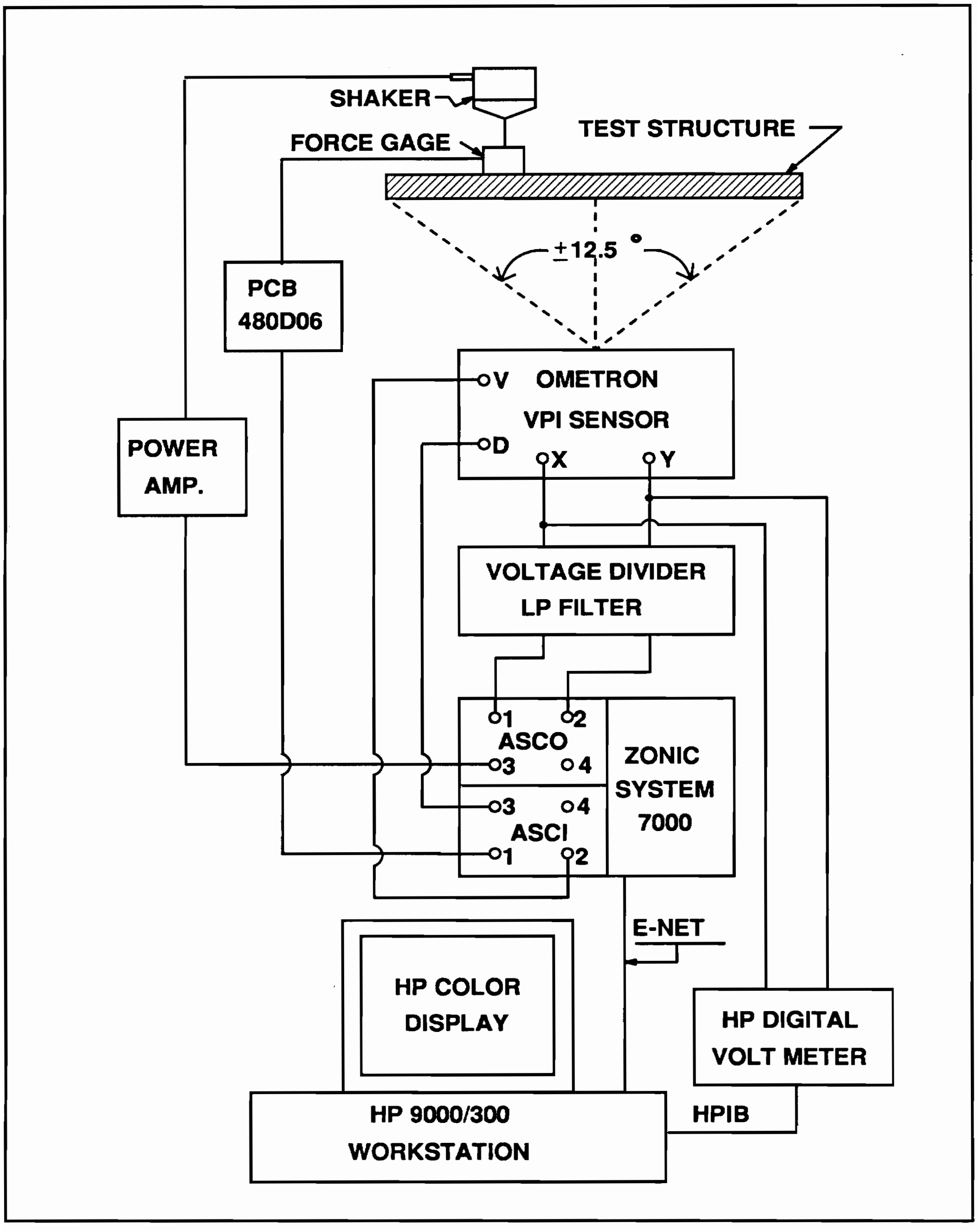

Figure 2.2 Automated Mobility Measurement System Schematic, (after Agee, [29]).

laser's scan is controlled by ASCO channel 1 and 2 of the System 7000 analyzer. DC voltages are applied, respectively, to the X and Y galvanometer drives for the scanning mirrors. The ASCOs are automatically calibrated before the scan is started to maintain scan accuracy. A voltage divider/low-pass filter is used in the scan circuit to match the FFT DACs output level to the laser scan control input. This maintains the full range of X and Y positions available from the 12-bit ASCOs. However, in the prototype system the output was limited to ± 2000 DAC steps to prevent overdriving the mirror system. At full-scale the ASCO output is ± 5.1 V DC (after division by 2). The VPI Sensor external scan input is rated for ± 5 V DC so in the prototype unit the scanners were limited by software to 4000 DAC steps instead of 4096. In this system, ASCO channel 3 is used to supply the drive signal for the structural excitation system.

From Fig. 2.2 the velocity from the laser demodulator circuitry is fed to ASCI channel 2 while the force signal is supplied to ASCI channel 1. The ASCI channel 3 carries the laser Doppler envelop signal which can be monitored to determine when the retro-reflective light energy is approaching the limit of detectability. In such cases the laser will have to be re-focused or the surface specially prepared. The System 7000 FFT analyzer forms the FRF of channel 2 (response) over channel 1 (force) using the conventional $H_1(f)$ estimator as defined in Chapter 1. It is possible to tee-off the excitation signal (ASCO channel 3) and route it into the remaining available ASCI channel 4. Because the laser has a slightly lower signal-to-noise ratio than a corresponding accelerometer, it is recommended that a FRF estimator that is unbiased in the presence of noise in the output be used. Thus the use of H_1 or ${}^cH$ is recommended when using the current LDV system. With the present trend of product improvements, it is expected that future refinements in LDV technology will result in a vibration measurement instrument that will approach the signal-to-noise performance of today's typical piezoelectric accelerometers. Consequently, the use of the H_2 estimator is not recommended as it is a biased estimator in the presence of output noise [22, 23, 25].

To aid in understanding the system diagram (Fig 2.2) the following is a summary of the various cabling in the diagram and what signal they are carrying:

ASCI channel-1 carries the analog force, $F(t)$ signal. It originates from the piezoelectric force transducer attached to the structure by measuring the applied force. Typical values range from 10 mV to 5 V depending on the sensitivity of the gage and the signal conditioning gain settings. The force signal frequency content ranges between 0.1 Hz to 20 kHz depending on test conditions and the force transducer capabilities. This time-domain signal is Fourier Transformed to the frequency domain, averaged, and then used to compute the FRF at each laser position.

ASCI channel-2 carries the analog velocity, $V(t)$ signal output of the laser head. The voltage is proportional to the relative line-of-sight velocity of the test structure at the measurement point. Typical amplitude values for this signal range from 20 mV to 10 V with a frequency content 0.1 Hz to 20 kHz, again, depending on the vibration test conditions. The time-domain velocity signal is transformed in to the frequency domain by the FFT process. The velocity signal is averaged, and then through the use of H_1 or ^cH its used to compute the estimate of the mechanical system's FRF.

ASCI channel-3 monitors the Doppler envelope signal. This frequency-modulated signal also originates from the laser head. This signal can be sampled to indicate laser beam focus, electronic saturation, and overall quality of the velocity signal. The Doppler signal is generally a very high frequency FM signal that is difficult to capture when the FFT analyzer is setup to measure lower vibration frequencies. However, by passing the signal through a full wave rectifier [30] and a low-pass filter, the resulting signal has a much lower frequency with a fluctuating DC offset. This rectified and filtered signal can now be captured at the analysis frequency of the analyzer setup.

ASCO channel-1 and-2 control the X and Y laser scanners. The scan control signals are analog DC signals that provide control voltages to the laser positioning galvanometer circuits. These DC signals can range from +10 V to -10 V. The galvanometer input is limited to ±5 V. Therefore, the ASCO outputs are voltage divided by a factor of 2 to provide the ±12.5° laser scan angle. The 12-bit DAC provides DC output in approximately 5 mV steps. The internal signal generator located in the Zonic System 7000 synthesizes the DC voltages as a zero-frequency sine wave.

In single shaker tests, ASCO channel-3 synthesizes the excitation signal. The structure must be excited by an dynamic force to measure the FRF. The signal generator supplies the random (or other) excitation signal to an audio power amplifier which drives the electro-mechanical shaker for forced input to the structure. Amplitude and frequency vary according to the particular test, but is linearly related to the force transducer signal.

The System 7000 is controlled over a dedicated ethernet network. The HP 9000/series 300 computer contains the software necessary to control the analyzer. The analyzer is initialized over the network and then microcode is downloaded to it. All data taking and signal processing commands are delivered to the System 70000 over the network. The System 7000 is completely controlled by software instructions; there are no controls on the instrument itself. By being on the network, the System 7000 may be accessed by any remote workstation with appropriate software (one user at a time).

The HPIB (IEEE-488) shown in Fig 2.2 is for calibration purposes only. The HPIB is used to control an HP 3478 digital voltmeter. For each pair of scanner drive channels a calibration correction between the ZETA [31] DC amplitude command and the actual output voltage must be made to correct for the ASCO zero offset and slope error. The output voltages to the scanners can be off as much as 10 DAC steps if these effects are not corrected for. Instead of manually stepping the ASCOs through 4096 voltages for both X and Y channels, a small looping program is used to record the difference between the commanded voltage and the actual voltage. In reality, an adequate calibration curve can be determined from only three (3) data points instead of the 4096. In this way a linear calibration equation can represent the correction factors instead of a look-up table. An added benefit of the equation method is it saves program I/O time and valuable disk space. The ASCO calibration procedure will only be performed on instrument cold start-up as the ASCO offset and slope errors have been found to stable over time, but do not repeat themselves from a cold start-up.

The computer workstation shown in Fig. 2.2 is used to run the I-DEAS software, to control the FFT analyzer, and to monitor the progress of the data acquisition. The time histories, the FRFs, and the associated coherence functions are displayed in a real-time manner during data acquisition. Data taking can be interrupted at any time to make test adjustments and the programmed scanning can be restarted at the point in which it left off.

2.3 Summary of the AMMS System Features

The key features of the instrumentation complex (Fig. 2.2) that make up the automated mobility measurement system are:

- Safe, low power (<1 mW) scanning laser velocimeter which does not require precision alignment and optical bench setups typical of holographic systems.
- Included scan view angle of 25° in both the horizontal and vertical directions.

- Full-scan view of the structure can be made for 8.8 x 8.8 mm up to 17.7 x 17.7 m without the use of special surface coatings. Special coatings increase the usable range and allow measurements on structures up to 97 x 97 m.
- Full scan view allows up to 4000 x 4000 or $16(10)^6$ vibration response data points.
- Uncorrelated motion of the laser head itself is averaged out of the FRF, if conventional H_1 or ^cH estimation methods are used.
- The system depends upon an EMA geometry description in an I-DEAS Universal file format.
- Universal file geometry and four (4) reference points are used to determine the laser head's own position in space. The accurate determination of this position is key in the automated data acquisition scenario.
- Velocity response measurements made by the laser are controlled by a node group Universal file. The control computer uses the geometry Universal file and the laser head position to develop the list of points to scan.
- Effective response transducer movement rates are less than 60 ms per point.

- The system provides complete modal data management by labeling each FRF with the node number and response direction; relieving the user of the massive record-keeping task.
- The system automatically calibrates and corrects the FRFs for scan view angle.
- Calibrated and labeled FRF data is automatically stored in the I-DEAS associated data file (ADF) format with an option for storage as a ZETA binary or ZETA ASCII function file.

2.4 Laser Doppler Velocimeter

2.4.1 VPI Sensor - Principles of Operation

The VPI Sensor instrument is an industrially engineered interferometer developed for mechanical vibration measurement. The VPI Sensor functions as a non-contacting velocity transducer capable of remote measurements of the velocity of a solid surface. The VPI Sensor is based on the Michelson[1] interferometer in which a 1 mW Helium-Neon (HeNe) laser light beam is divided into two beams, the measuring and reference beams. Figure 2.3 shows the optical paths of the laser beams within the VPI Sensor. As shown in Fig. 2.3, the path of the reference beam is contained entirely within the VPI Sensor optical unit while the measuring beam is focused on the vibrating test structure. The retro-reflected part of the measurement beam is mixed with the reference beam. The

[1] Albert A. Michelson, (1852-1931) an American physicist, who in 1907 received the Nobel prize in physics for using his interferometer for his careful measurement of the standard meter [32].

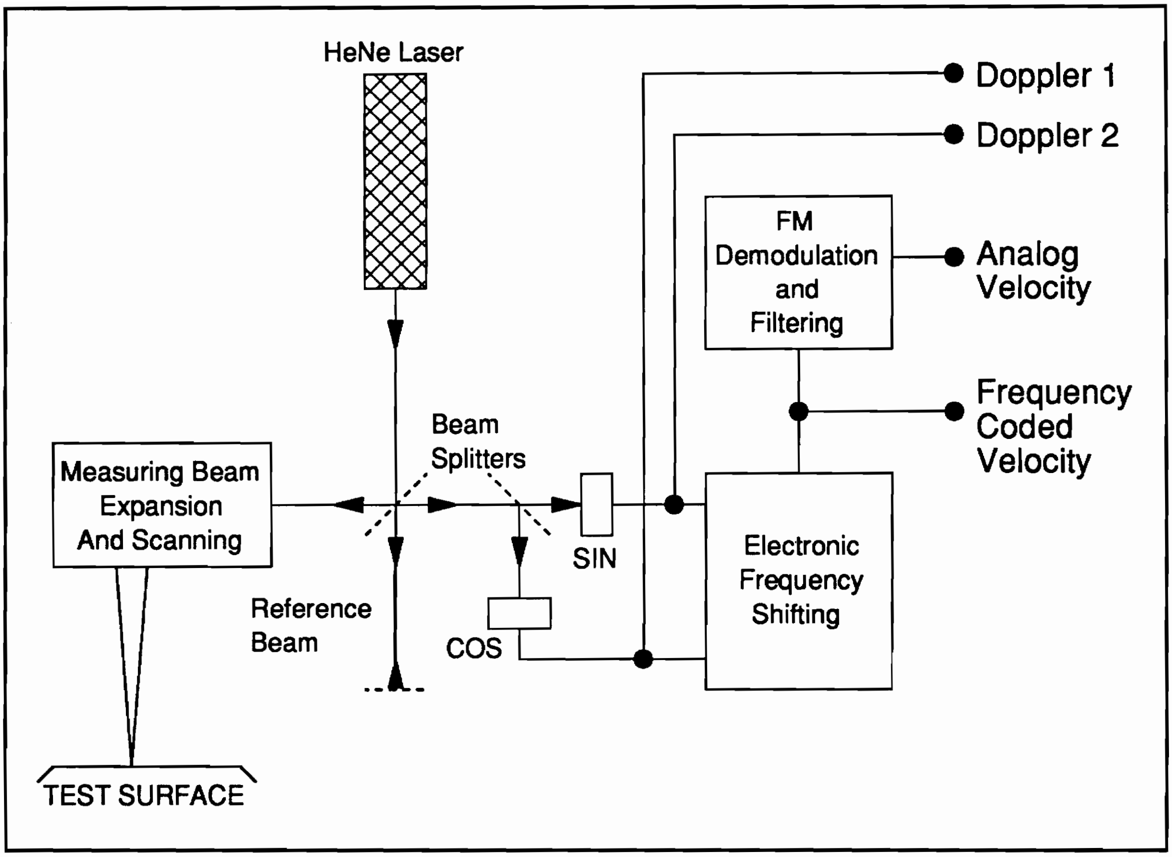

Figure 2.3 VPI Sensor Optical Path, (adapted from Ometron, [16])

two beams interfere with one another at the detectors depending on the Doppler shifting of the measurement beam. This results in intensity modulations of the re-combined beam due to interference between the reference and measurement beams.

In the same way that sound waves reflected from, or emitted by a moving object are subject to a frequency change (the well known Doppler[1] [32] effect heard on ambulance sirens, etc.), a beam of light reflected from a moving surface is also changed in frequency, Doppler shifted. When light is scattered back from a vibrating target it will undergo a frequency shift proportional to the velocity of the target. As the target moves towards the light source the back-scattered light frequency increases, as the target moves away the back-scattered light frequency lowers. If the target is vibrating, the back scattered beam will be frequency modulated at the surface vibration frequency, f_{vib}, with a deviation from the laser carrier frequency, f_c, by the amount equal to the Doppler shift frequency, f_D. The Doppler shift frequency, f_D is directly proportional to the velocity of the target surface. Therefore, to track this shifted frequency is to have a direct measure of the target's velocity relative to the motion of the laser source.

If the surface of the vibrating structure is moving at a constant velocity the intensity of light at the detector oscillates at a constant frequency, f_D. The relationship between the

[1] Christian Johann Doppler, (1803-1853), a Austrian, who in 1842 called attention to the fact that the color of a luminous body must be changed by relative motion of the body and the observer. In his works Doppler mentions the more familiar application of his principles to sound waves [32].

wavelength of the laser light beam used (λ), the line-of-sight surface velocity (V'_{LOS}) and the frequency of this oscillation (f_D), presented here without proof is:

$$V'_{LOS} = \frac{f_D \lambda}{2} \tag{2.1}$$

where,

f_D	=	the Doppler shift frequency (Hz)
λ	=	the laser light wavelength (m)
V'_{LOS}	=	the speed (m/s) of the retro-reflective surface with respect to a <u>stationary</u> laser source

For realistic surface vibrations, the Doppler shift frequency is a very small fractional change in the frequency of the light wave (typically 1 part in $1(10)^8$ or less) [16]. However, the change can be measured very accurately using optical interferometry in conjunction with electronic frequency measurement.

Referring back to Fig. 2.3, the recombined laser beam is shared between two independent detection channels in such a way that the path difference presented to one channel is effectively one quarter of a wavelength longer than that presented to the other. The configuration results in a 90° phase shift between the signals from the two channels (denoted "sin" and "cos" signals in Fig. 2.3). The direction of motion to the surface determines which signal leads the other in phase angle. The sine and cosine signals at the Doppler shift frequency, f_D, are fed to a dual-channel balanced modulator where they are modulated by internally generated "sin" and "cos" signals at a carrier frequency f_C. Summation of the two modulated outputs yields a single, frequency shifted output at f_C

$+ f_D$ or $f_C - f_D$, depending on the direction of the motion of the surface. In this way, electronic mixing results in essentially the same frequency-shifted Doppler signals as those obtained using optical frequency shifting techniques. Thus, established frequency tracking methods (FM demodulation) can be used to derive an analog voltage representing the instantaneous velocity of the moving surface [16]. To remain brief here, reference [33] is suggested for further reading on the laser Doppler technique.

2.4.2 VPI Sensor Description and Specifications

The VPI Sensor's HeNe laser light source is ideally suited for velocity measurements. The laser light is highly coherent; meaning the beam remains in-phase over time. Its monochromatic in that it contains a very narrow band of light frequencies. Additionally, its highly directional properties coupled with the ability to focus the spot to diameters on the order of 0.5 mm make the laser the ideal candidate for this non-contacting method of measuring surface vibrations. The following information summarizes the VPI Sensors attributes and specifications:

- Laser-based non-contacting transduction of vibrating surface velocities.
- Useable in high temperature, polluted, radioactive, and hazardous areas where conventional transducers are not appropriate.
- The laser is a Class 2 HeNe laser which does not require specialized glasses. Output beam power is <1 mW. However, precautions are necessary to avoid continuous direct viewing of the beam.

- The laser system does not require specialized optical alignment fixtures; simple tripod or bench mounting installation is all that is required.
- The laser beam is movable by a set of scanning mirrors. This set of *X* and *Y* mirrors are moved by galvanometers and allow the measurement beam to be placed anywhere in a 25° x 25° scan area. This scanning capability is a key element in the success of the automated vibration measurement system being developed and described here.
- Structures with flat black finishes through fully retro-reflective surfaces provide acceptable velocity signals.

The distance at which the VPI Sensor can detect vibration increases with the increase in diffuse reflectivity. Table 2.1 summarizes the typical working distances in meters (m). The following are approximate working distances.

Table 2.1: VPI Sensor Typical Maximum Working Distance

Velocity Range	Matte Black Surface	Matte White Surface	Retro-reflective Surface
Low	4m	40m	220m
Medium	2m	20m	110m
High	0.7m	7m	70m

The above working distances for matte black surfaces are conservative since successful tests have been run at 45m on the low range. In Table 2.1 above, the distance values greater than 5m require the "long" lens. Additionally, it should be recognized that a laser Doppler system will not function properly on a mirrored or high gloss surfaces. Other laser attributes are:

- The laser scanning mirrors permit movement of the measuring position across a ±12.5° horizontal and vertical field of view. This converts to a view plane of 8.8 x 8.8mm to 97 x 97m. The number of data points that can be taken in this area is $16(10)^6$ (4000 x 4000).
- Primary instrument output is an analog voltage proportional to surface velocity. Other outputs are provided for Doppler signals and Doppler envelope.

The frequency response of the VPI Sensor is dependent upon the vibration level as follows in Table 2.2.

Table 2.2: VPI Sensor Usable Vibration Levels

Vibration Range	Vibration Level	Frequency Range -3dB
Low	0-0.01m/s	0.5-1,000 Hz
Medium	0-0.1m/s	0.5-9,500 Hz
High	0-1.0m/s	0.5-20,000* Hz

*The laser has only been tested to 20 kHz on the high range, however the manufacturer claims response to 100,000 Hz.

- The working depth of field is controlled by the loss of focus. The depth of field depends upon the lens used, the surface finish, and velocity range.

Table 2.3: VPI Sensor Typical Depth of Field

Velocity Range	Focus Distance	Surface Finish	Short-Range Lens	Long-Range Lens
Low	2m	Matte White	-2/+5.5m	---
Low	7m	Matte White	---	-3.5/+3.5m
Medium	2m	Matte White	-0.8/+2m	---
Medium	7m	Matte White	---	-2/+2m
High	2m	Matte White	-0.3/+0.3m	---
High	7m	Matte White	---	-0.5/+0.5m

2.5 The System 7000 Parallel Signal Processor

2.5.1 System 7000 FFT Analyzer - Description and Specifications

The Zonic System 7000 or Workstation 7000 Parallel Signal Processor is a multichannel, real-time, FFT computational analyzer and data acquisition system. The System 7000 used in this AMMS system development has 16-input channels and could be expanded to 1000 fully parallel and independent channels. However, the AMMS utilizes only three of the input channels (force, velocity, and Doppler envelop) for conventional H_1 FRF estimates. A fourth input channel can easily be activated for ${}^{c}H$ FRF measurements. As explained earlier, one of the cost saving attributes of the laser-based AMMS system is that only three (3) FFT analyzer input channels are required, meaning there is no need for large multi-channel FFT processors when using a scanning laser for large modal tests.

Features of the System 7000 include a baseband frequency analysis ranges up to 150 kHz. Real-time analysis rates can be maintained at up to 5 kHz even in large system configurations of 1000 channels [8]. The particular System 7000 used in this development work was outfitted with 4 channels of signal generation output. The AMMS system utilizes three (3) of those outputs. Output channels 1 and 2 are used for DC voltage to the X and Y laser scanner control respectively. Output channel 3 supplies the forcing function to the excitation system for the modal test. Several output waveforms are available including those that are most frequently used in experimental modal analysis situations: sine dwell, continuous random, and burst random.

The System 7000 schematic configuration is shown in Fig. 2.4 below. In Fig. 2.4 the main modules of the analyzer are illustrated. In this figure, the block labeled "Analog Signal Conditioning Input Module", (ASCI) are the input channels used to capture the velocity, force and Doppler envelope signals for FRF processing and monitoring. The block labeled "Analog Signal Conditioning Output Module", (ASCO) are the signal generator output channels driving the X and Y laser scanners and providing the excitation force to the structure. A dedicated ethernet link is used to network the System 7000 to a HP 9000/series 300 computer. It is over this network connection that the instrument is controlled and data acquisition instructions are passed to the System 7000.

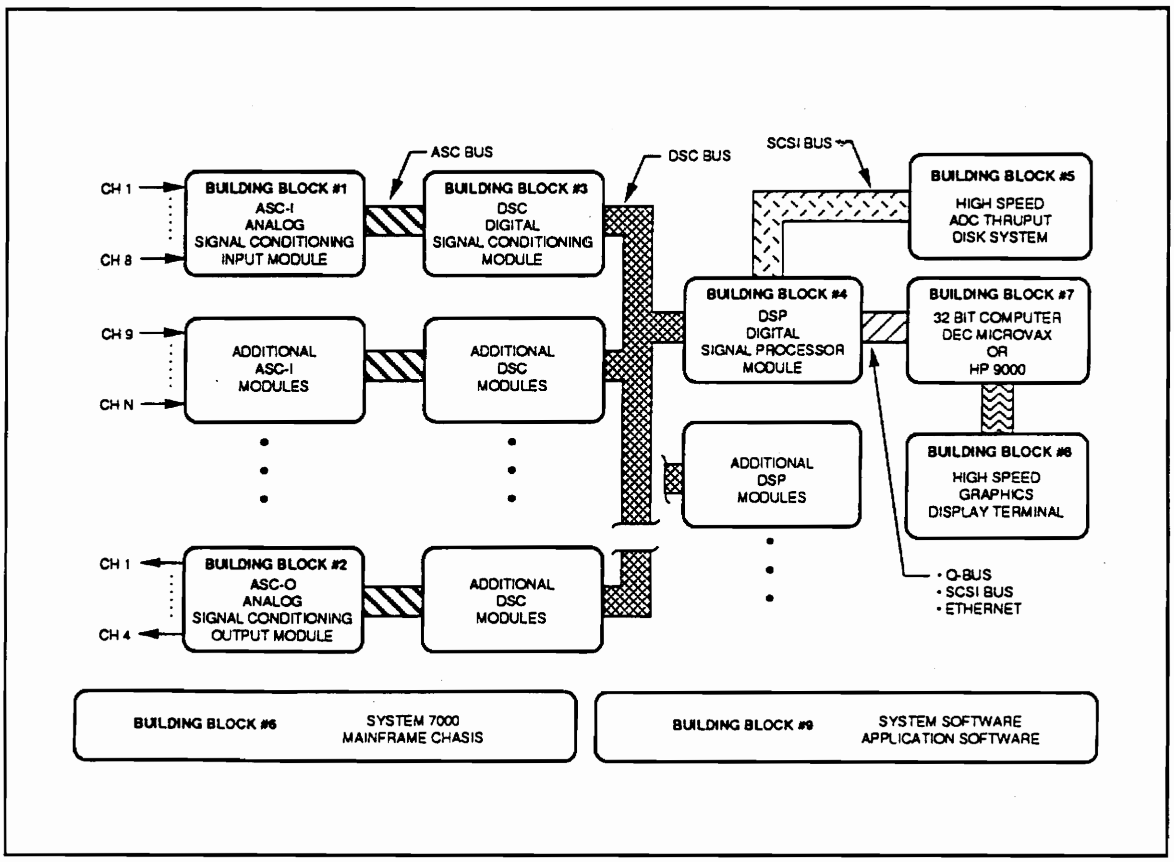

Figure 2.4 Zonic System 7000 Parallel Signal Processor, (after Zonic, [8]).

2.5.2 Interfacing the System 7000 with the VPI Sensor

Figure 2.5 shows the VPI Sensor's laser head connections that require interfacing to the System 7000 or VPI electronics box. In Fig 2.1, the connectors on the left-hand side of the laser head box are inputs to the laser head. The inputs include both *X* and *Y* scan control signals. The scan control signals are carried over the blue Lemo connector cable. Another required input to the VPI Sensor is the laser head electronics power supply. The power to the electronics is furnished by the orange Lemo connector cable. The only other required inputs to the VPI Sensor head is the HeNe laser power supply. It is supplied by a separate external laser power supply with a two-pronged connector. This commercial power supply has a switch with a key that can be removed to prevent any accidental turn-on of the laser. An optional input to the laser head is the local handset that allows the user to manually position the beam. When the handset is combined with the optional programmed scanning card, the user can register up to 510 beam locations for programmed scanning [16].

As shown in Fig. 2.5, the VPI Sensor laser head has five analog outputs, summarized as follows:

- <u>Coaxial Velocity</u>, is the output of BNC velocity connector. Typically the filtered BNC output is a ±10 V full-scale analog signal. If the VPI Sensor has been modified to provide an improved frequency response, then this is an unfiltered velocity signal and the full-scale output is approximately ±3.3 V.

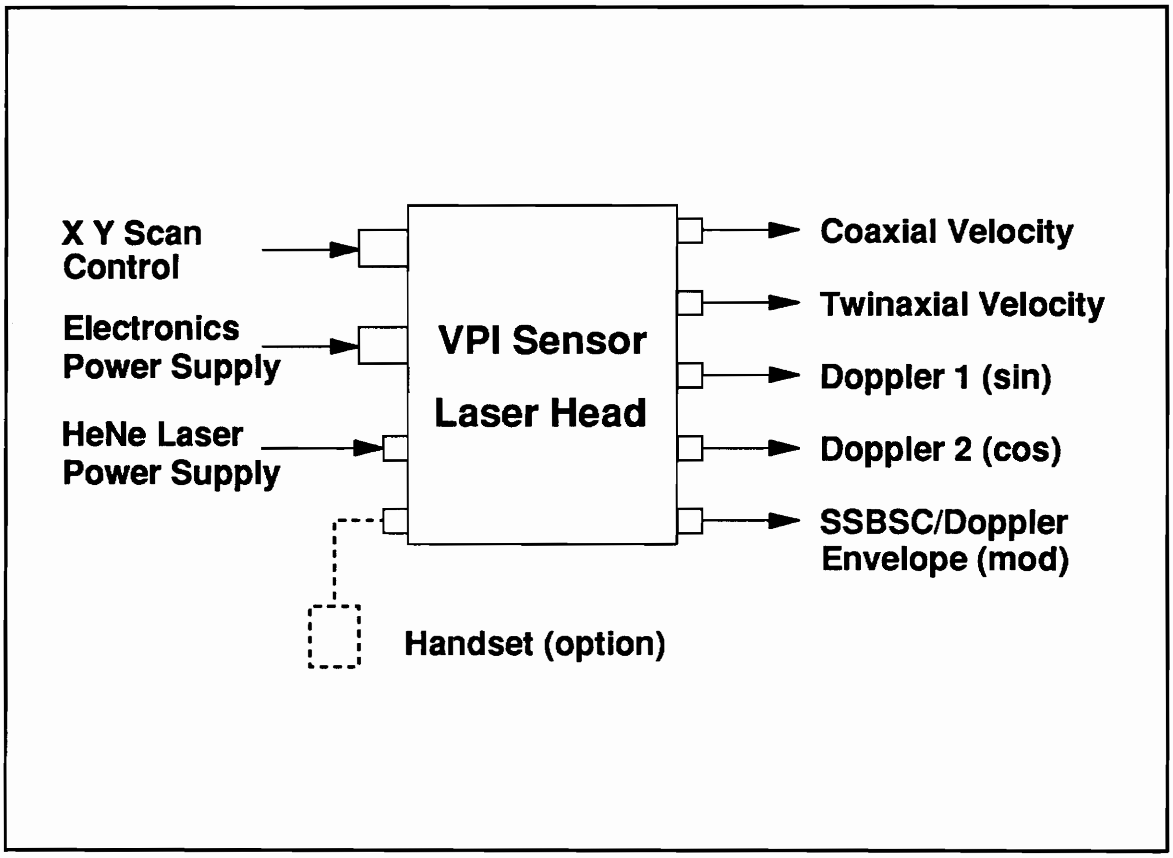

Figure 2.5 VPI Sensor Instrument Interface.

The coaxial BNC velocity signal is the one used in the AMMS system. It is normally, connected to ASCI channel 2 for computation of the FRF.

- Twinaxial Velocity, is the differential output of the BNO twinaxial connector. The full-scale velocity signal output is ±1 V on the twinaxial connector. The differential BNO signal is more noise immune that the BNC coaxial, thus, its recommended for longer signal cable runs. The BNO is designed to match the differential input of the EG&G Princeton Applied Research lock-in amplifier. It is not used in the AMMS system.

- Doppler 1 and Doppler 2, are the BNC connectors that provide the basic analog interferometer signals in quadrature (sine and cosine). Both signals show modulation at a frequency which is directly proportional to the instantaneous velocity of the test surface.

- SSBSC or Doppler Envelope, The BNC connector labeled SSBSC typically is a 0.1 V FM square wave carrying velocity information with high accuracy. However, the VPI Sensor used in the development work of the AMMS system had a different signal on this BNC socket. The Sensor was modified to provide a full-wave rectified Doppler envelope signal. The fluctuating mean level of this signal is normally monitored by ASCI channel 3 in the AMMS system.

The instrumentation used in the development of the AMMS system requires little modification to fully implement into reality. However, two hardware problems existed. First, the output of the System 7000 ASCO channels is rated for ±10 V DC and the input to the VPI Sensor external scan control circuit is rated for ±5 V DC. You can see the potential problems here. If left in this configuration three undesirable things could happen: (1.) The scan control boards in the laser head could be over driven by as much as a factor of two causing avoidable circuit damage, (2.) The galvanometers may deflect too much and cause damage to the optical mirrors, and (3.) If the ASCOs were limited to ±5 V DC the scanning system would have only ±1024 DAC steps over the ±12.5° scan angle. In other words, only half of the dynamic range of the ASCO would be utilized. Solution: Design a voltage divider circuit for each scan channel to match the ASCO output voltage range to the laser's input range. This impedance mis-match can be easily solved by an inexpensive resistor circuit.

The second hardware problem is that the ASCOs contain some high frequency noise (hash) riding on the DC output that could cause the mirrors to jitter. Solution: add a low-pass filter in the voltage divider circuit. Set the cut-off point, f_{CO}, at approximately 800 Hz to cut the higher frequency noise without adversely affecting the transient response of the mirrors. With a half-power point set at 800 Hz and a slope of about 6 dB per octave the noise problem is virtually eliminated. The LP-filter was combined with the voltage-divider to make a convenient "blackbox" to be inserted into the scan control wiring between the ASCO output BNC and the laser's external scan control BNC.

Figure 2.6 shows the schematic diagram of the required voltage divider/LP-filter circuit designed and built for interfacing the VPI Sensor to the System 7000. The values of the circuit resistor, R_1, and the laser electronics resistance, R_L, must be equal ($\approx$ 20 kΩ) to have an exact factor of 2 voltage reduction across output terminals, E_{out}. Therefore; when $R_1 = R_L$ and E_{in} is DC, C_1 (0.01 μF) looks like an <u>open</u> and $E_{out} = \frac{1}{2}E_{in}$. When E_{in} is AC at frequencies approaching f_{CO}, C_1 begins to look like a <u>short</u> to ground and $E_{out} \rightarrow 0$. Hence, we have a simple and economical low-pass filter circuit.

For the prototype AMMS system, the input impedance of the laser electronics was slightly different for each channel. The X channel input had a measured impedance of 19.17 kΩ while the Y channel measured 20.30 kΩ. This slight impedance difference of the channels is well within the ±5% tolerance for a typical 20 kΩ resistor. So the resistors for the voltage divider-LP filter circuit were hand picked for their resistance values which most closely matched the impedance of the electronics. If the AMMS calibration procedure presented in Chapter 5 is used, hand picked resistors are not necessary.

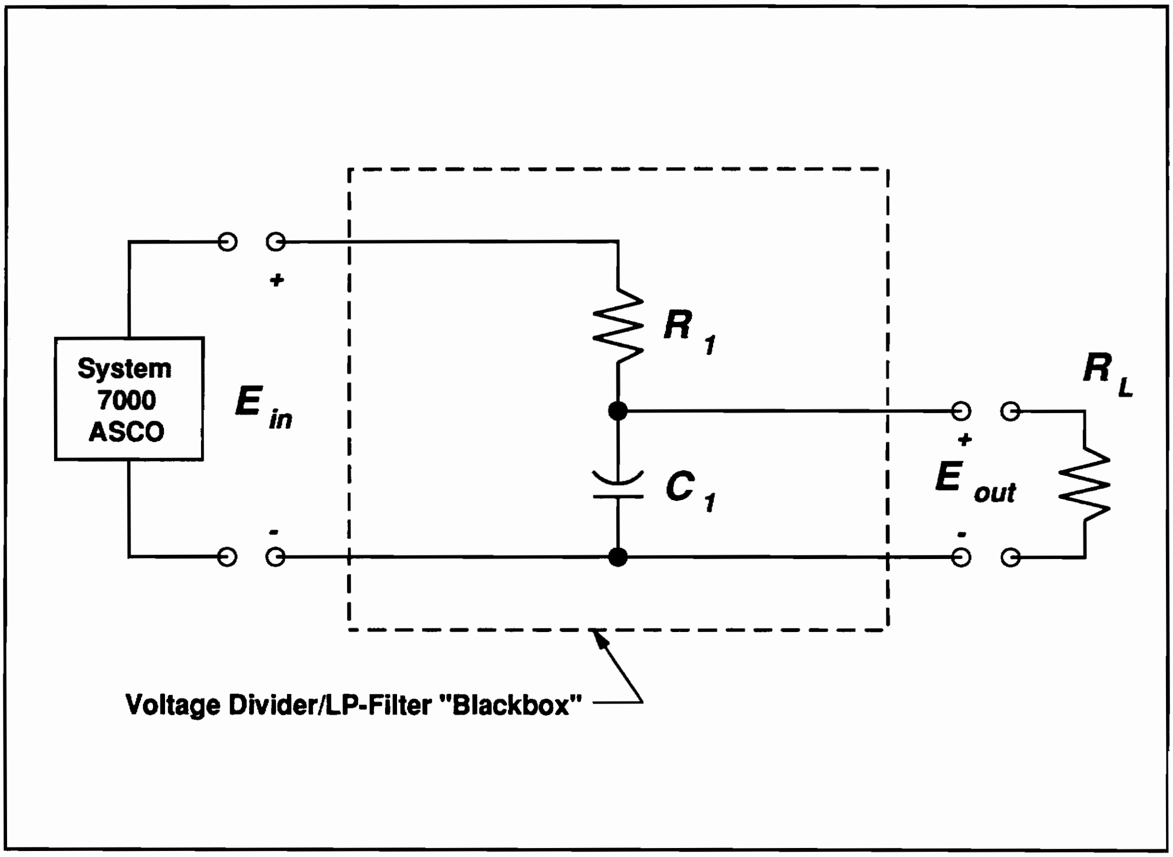

Figure 2.6 Voltage Divider - Low-Pass Filter Circuit for Interfacing the System 7000 ASCOs to the VPI Sensor External Scan Inputs.

Chapter 3

Development of the Automated Mobility Measurement System Software

3.1 Overview of the Automation Process

To develop the concept of a laser-based automated mobility measurement system into an engineering product required a significant amount of effort in the area of software development. To begin the software development process, the fundamental design goal was to develop software that was logically organized and user friendly. If the end-user had the knowledge of how to conduct a conventional modal test, then there would only be a minimum amount of training to use this automated product. Developing software for this high technology product required a concentrated effort in three technical areas: user interfacing, instrument control, and laser-to-structure position determination. The first two technical areas (user interfacing and instrument control) are discussed in the following sections of this chapter. The process to determine the laser's position in space with respect to a structure is the topic of Chapter 4.

To better understand the automation software development task it is first beneficial to have a perspective overview of the automation process. Figure 3.1 shows the flow chart of the modal test automation process. This figure can also be viewed as a division of the software development tasks. The left side of Fig 3.1 labeled "I-DEAS Test" can be considered as existing software (i.e. no computer programming required). The right side of Fig 3.1 labeled "AMMS" is the remaining software necessary to complete the product being developed in this research. Communication between the two sides (I-DEAS Test and AMMS) only requires a data exchange process. Universal files and associated data files (ADF) are the normal data exchange protocols for this system. It should be clear that the AMMS system is not operated under the I-DEAS Director-Observer family which allows user programs to interface with I-DEAS models directly. The AMMS system is a "stand-alone" system that only requires I-DEAS Universal files.

The following is a brief walk-through of the flow chart of the automation process shown in Fig. 3.1. First, the automation process starts with an I-DEAS wireframe geometry model of the test structure. Second, the structure is registered with respect to the laser position. Third, from the registration process and the geometry model the relative position of the laser to the structure is determined. Fourth, the process returns to the I-DEAS Test model and the nodes to scan are defined. Fifth, using the relative position information and the selected nodes, a scan list of X and Y coordinates is generated. Sixth, automated FRF data acquisition begins. Seventh, the FRF is labeled with its node number and stored in an I-DEAS ADF format. Eighth, the laser is moved to the next node for

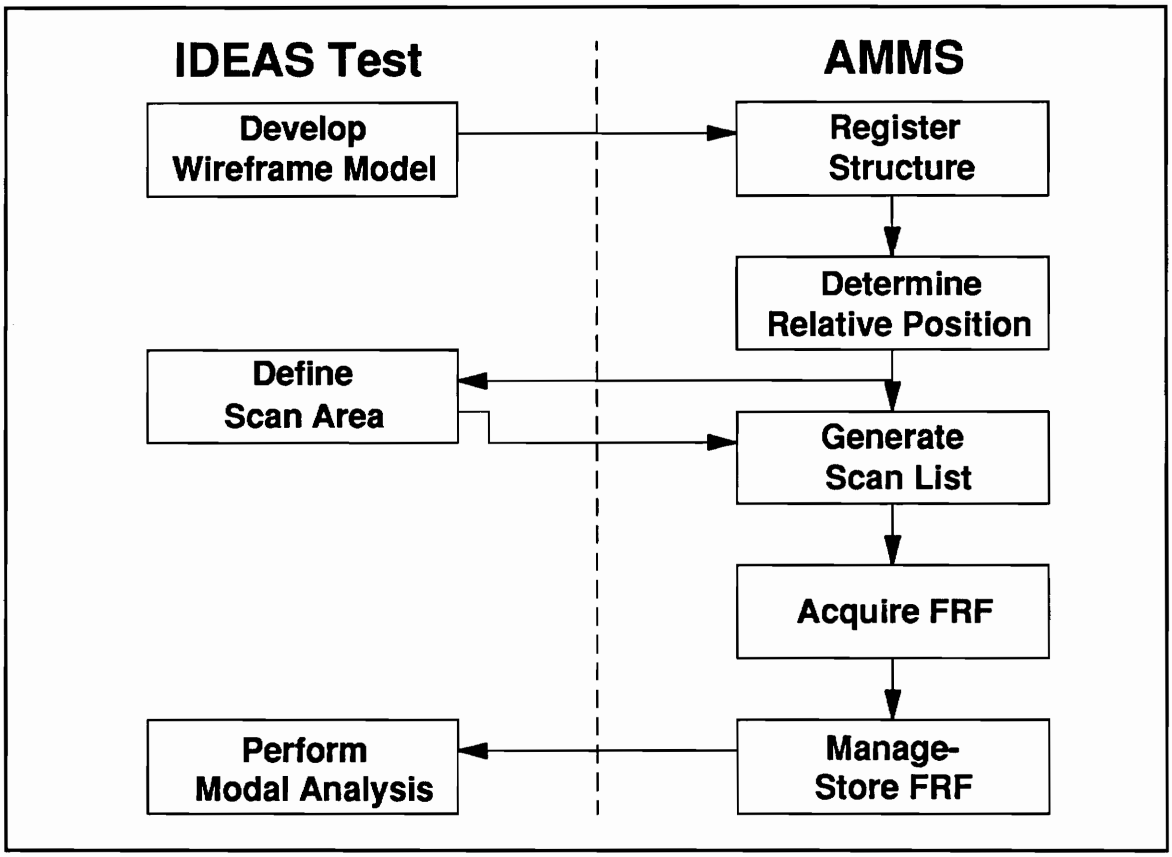

Figure 3.1 Flow Chart of Modal Test Automation Process.

further data acquisition. This simplified loop will repeat for all measurement points until the complete viewable structure is tested. Ninth, and finally, the user returns to I-DEAS Test for post-processing the FRF data in the modal analysis software package.

3.2 Automated Modal Test Scenario

One of the easiest means of understanding the AMMS system is to take the reader through a more detailed automated modal test scenario. Although the test scenario is numbered below most of the steps are tied together in a logical manner. To emphasize the automated procedure, Fig. 3.2 is shown. It depicts the AMMS tasks and software architecture. The interconnection of the task modules in this figure also corresponds to the various software modules. The logical progression of an automated modal test was the predecessor to the development of the AMMS software. This logical automated modal test scenario follows the following scheme:

1. The test structure is first modeled in I-DEAS Test family using the geometry modeling tools available. Other I-DEAS families like the Solid Modeling and the Finite Element Modeling packages may be used to aid in the development of an accurate wireframe model but are not required. Test is the only I-DEAS family required for the AMMS system. (Fig. 3.2, Module 1)

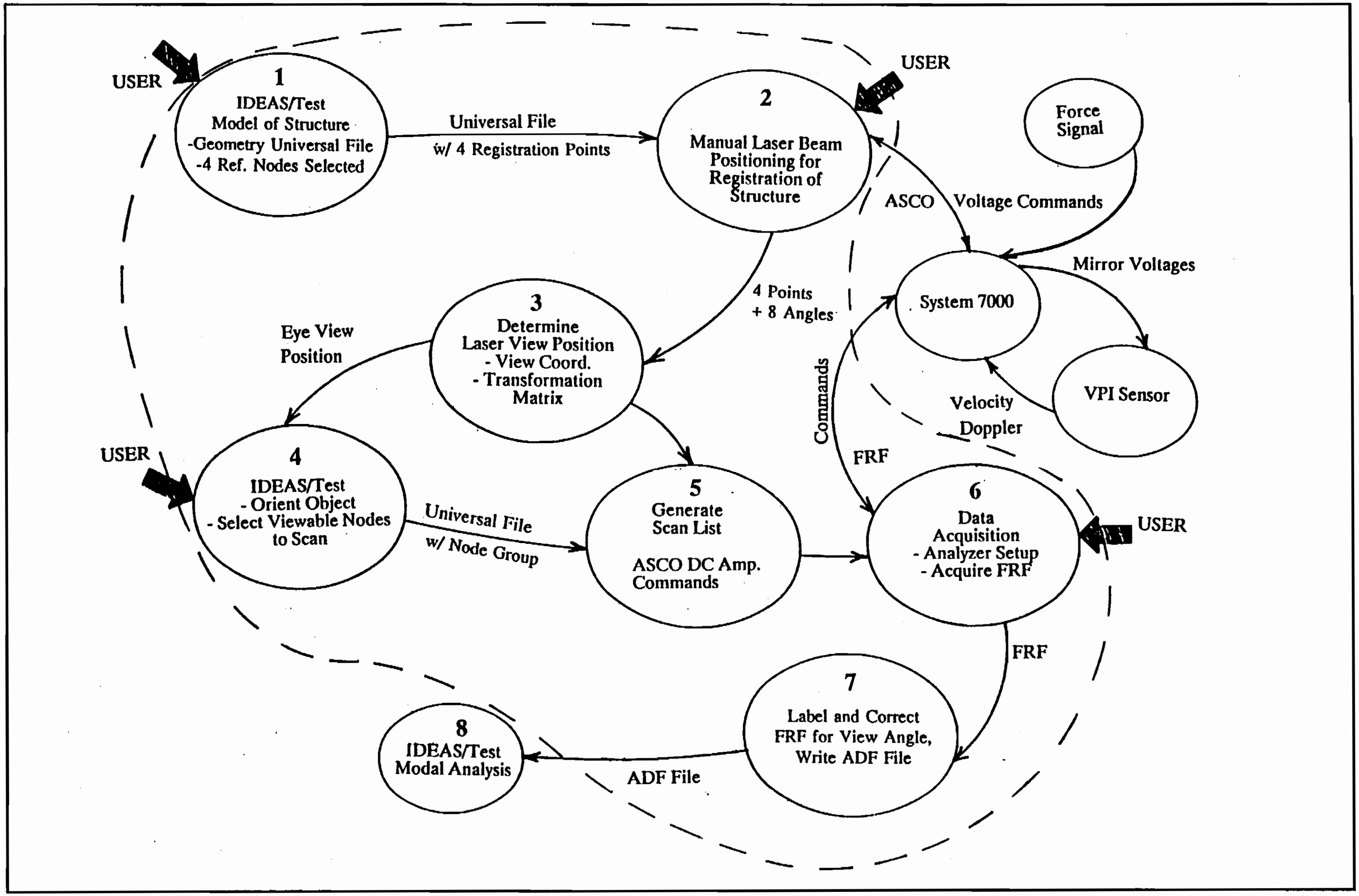

Figure 3.2 AMMS System Software Task and Data Flow Chart, (after, Agee [29]).

2. The wireframe model of the structure containing nodes and connectivity information is stored with a global Cartesian coordinate system in a Universal file format. (Fig. 3.2, Module 1)

3. The test structure is setup for a conventional EMA test including force transducer(s) and shaker(s).

4. The laser head (VPI Sensor) is placed at a distance from the structure such that the scanners in the *X* and/or *Y* directions are driven close to their 25° scan range. This process minimizes scan errors in subsequent steps.

5. Four reference points are selected on the viewable side of the structure as far away from on another as possible. The corresponding nodes are selected from the I-DEAS model. This provides the relative positions in space of these four points on the structure along with I-DEAS nodal coordinates. (Fig. 3.2, Module 1 and 1 to 2)

6. The laser beam is aimed at the 4 node locations on the structure. The scan angles in the *X* and *Y* directions are recorded. This procedure "registers" the structure with the laser head. (Fig. 3.2, Module 2)

7. The position of the laser head is computed in the I-DEAS global coordinated system using the nodal coordinates and the reference scan angles. The laser position is stored as a transformation matrix to be used later. (Fig. 3.2, Module 3)

8. Once the laser position information is known, the user selects within I-DEAS Test the viewable nodes or a subset of viewable nodes. The "nodes-to-scan" are grouped, stored, and written to a Universal file containing only the target node numbers. (Fig. 3.2, Module 4)

9. The scan list is created from the grouped node Universal file using the transformation matrix computed in 7. above. This list contains X and Y scan commands for the analyzer's channel 1 and 2 DAC. (Fig. 3.2, Module 5)

10. The user is lead through the setup of the FFT analyzer for the modal test by the use of a instrument-panel-type computer display. The "instrument" pushbuttons are activated by mouse clicks. (Fig. 3.2, Module 6)

11. Once the setup (steps 1-10) is completed the AMMS enters its automated acquisition mode. The laser beam is sent to a reference point in space then sent to the first node position in the scan list. FRFs and coherence functions are acquired. (Fig. 3.2, Module 6)

12. The calibrated FRF data are monitored, corrected for view angle, and stored in an I-DEAS Test ADF format on the computer workstation. Optionally, the FRFs may also be stored in a ZETA binary or ASCII compatible format. (Fig. 3.2, Module 7)

13. Steps 4-12 are repeated until all nodes in the scan list are scanned.

14. The mobility FRF data are now ready for I-DEAS Test modal parameter extraction and mode shape visualization. (Fig. 3.2, Module 8)

3.3 LSI Software Architecture

The key to the development of the AMMS system is the software that integrates the laser capability with the power of modern FFT analyzer technology. The integrating software is called Laser Systems Integrator (LSI) [34]. LSI was developed from a team effort however, a significant amount of the user interface software presented in this thesis is due to the efforts of Mr. Teck Awa. Figure 3.3 illustrates the AMMS software product development tools used in this project. The LSI application code for the AMMS was developed on an HP 9000/300 series workstation operating under HP-UX and X Windows system with a Zonic System 7000 FFT processor connection via an ethernet link. The LSI code utilizes FORTRAN and C programming languages, the X Window System *Xlib*, *Xt*-intrinsics, OSF/Motif *widgets*, ZETA graphics, and Zonic System 7000 ZETA

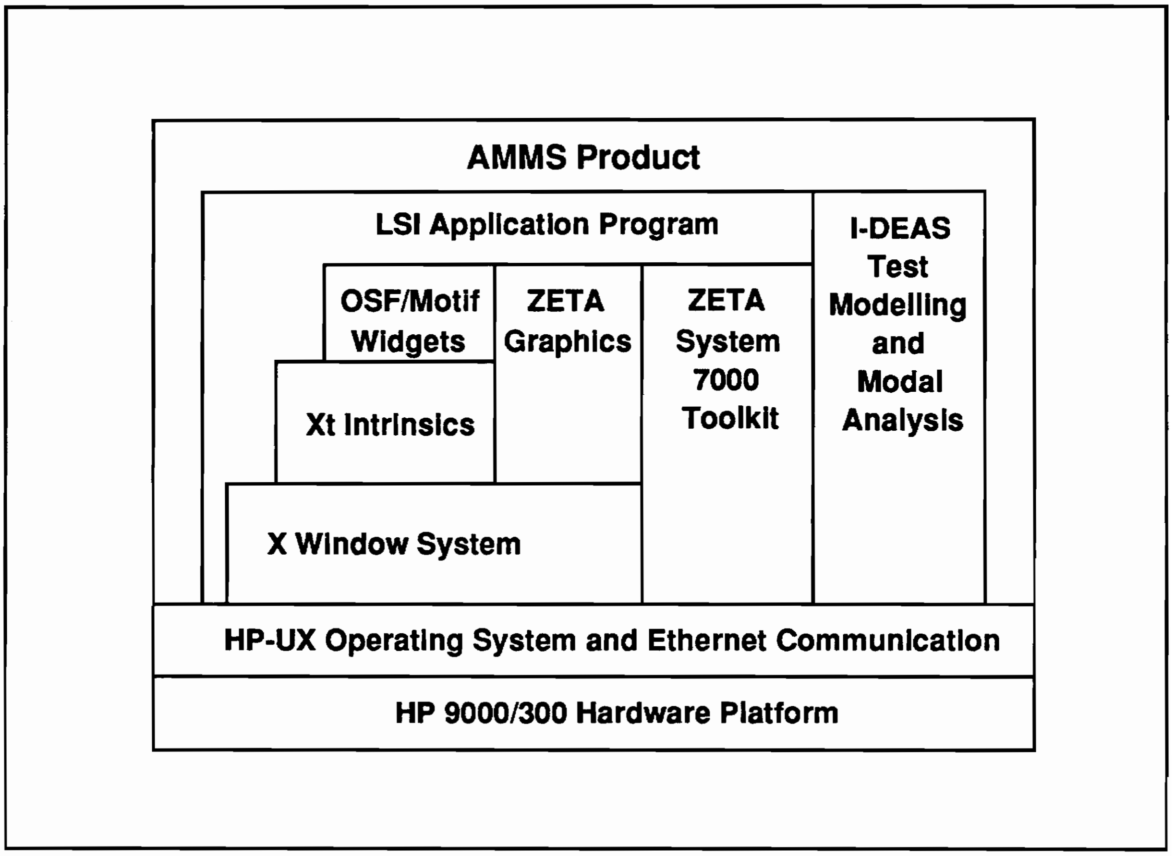

Figure 3.3 AMMS Product Development Tools, (adapted from Awa, [34]).

Programmers Toolkit. The LSI software was designed to complement the I-DEAS Test family geometry modeling and modal analysis capabilities.

LSI was developed in a modular form, thus, the software could be prototyped, tested, and debugged in smaller applications. The structure of the modules within the LSI software are shown in Fig. 3.4. The first level of the LSI structure chart is the application manager (or main menu) where the automated task is initiated. The hardware is initialized, program keyword and parameters are defined, X Windows are managed, and LSI system defaults are executed in this first level.

The second level of the LSI structure is the six (6) major tasks of the LSI software that corresponds to the six main tasks on the main AMMS menu. The six major LSI software modules of Fig. 3.4 are summarized as follows:

- 1.1 Module *EXIT*

  This main program module quits the LSI application.

- 1.2 Module *PROJECT NAME*

  This main program module serves to identify a particular modal test with a global project name. Serves as the default file naming system for the LSI file management task.

- 1.3 Module *LASER VIEW*

  A large main program module that has three (3) sub-modules that are required to determine the laser's position in the structure's global coordinated system.

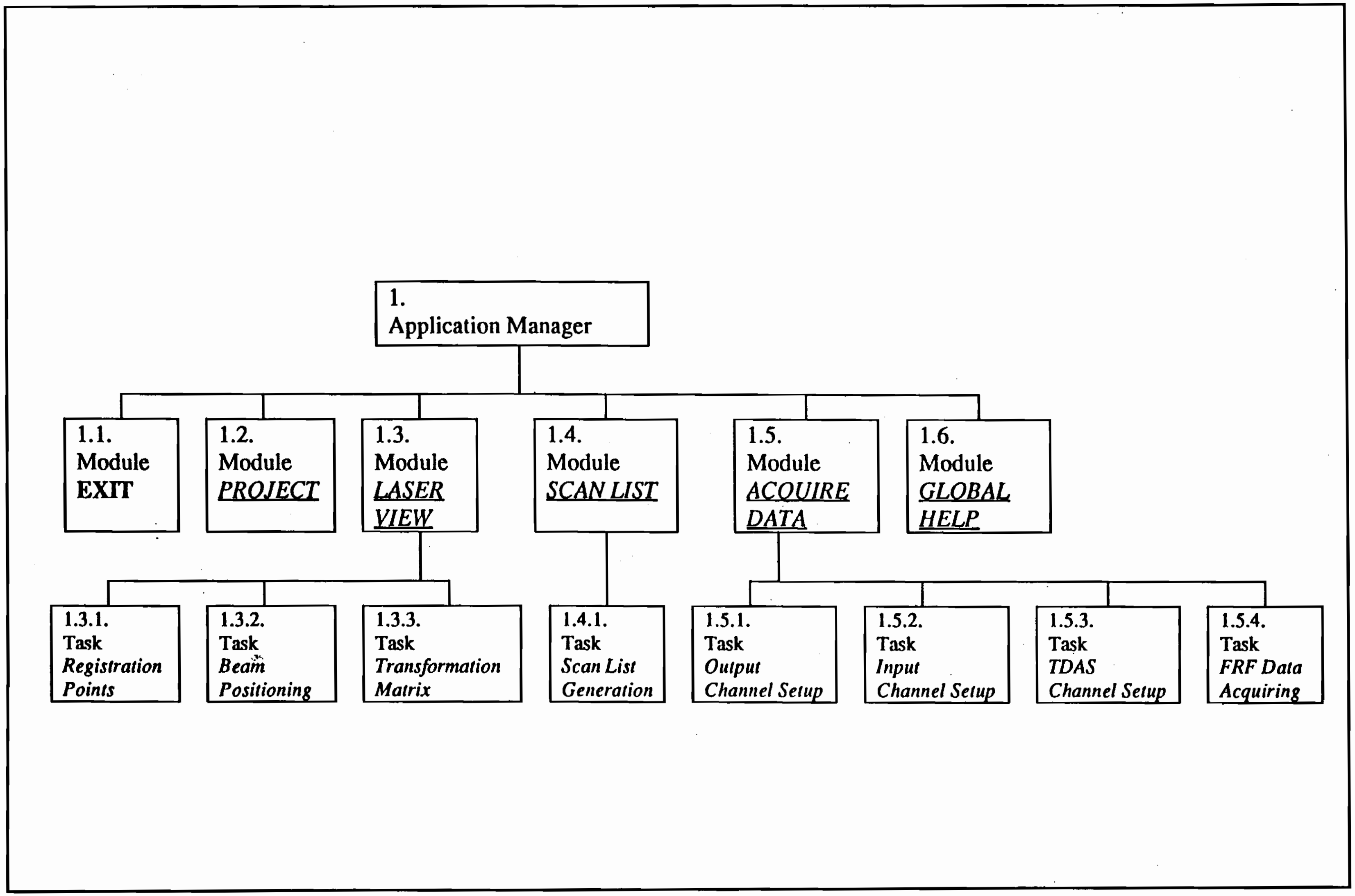

Figure 3.4 LSI Software Module Structure Chart, (adapted from Awa, [34]).

1.3.1 Task Module *REGISTRATION POINTS*

Reads the I-DEAS geometry file given four registration node numbers. It searches the structure's Universal geometry file an writes a new file with the four (4) node numbers and their global Cartesian coordinates. It creates the registration points file *project.reg*.

1.3.2 Task Module *BEAM POSITIONING*

Reads the registration points file, *project.reg*. Draws a laser "viewport" on the screen for manually positioning the laser beam with the system mouse. Stores *X* and *Y* scan angles for the four (4) beam position points in file *project.ang*.

1.3.3 Task Module *TRANSFORMATION MATRIX*

A large task module that reads the registration points file, *project.reg*, and reads the beam position file, *project.ang*. This task module then computes the transformation matrix and stores matrix in file *project.mat*. This task is mostly hidden from the user. Further discussion of the transformation matrix algorithm are the subject of Chapter 4 of this thesis.

- 1.4 Module <u>*SCAN LIST*</u>

This main program module reads the transformation matrix file, reads the I-DEAS grouped nodes-to-scan and geometry files, generates a scan list of X and Y voltage commands, and then stores this scan list in a file *project.lst*.

■ 1.5 Module *ACQUIRE DATA*

A large main program module that has four (4) sub-modules that are required to setup the System 7000 FFT analyzer output and input channels, setup the I-DEAS Test (Tdas) data manager, and acquire the FRF data.

1.5.1 Task Module *OUTPUT CHANNEL SETUP*

Reads the default output channel setup values either from *project.out* or from *default.out*, sets up the forcing function waveform type and amplitude, and then stores the setup as file *project.out.*

1.5.2 Task Module *INPUT CHANNEL SETUP*

Reads the default input channel setup values either from *project.in* or from *default.in*, sets up first three (3) input channels for: full-scale volts, sensitivity, label, and units. Selects autoranging parameters, window type, frequency range, zoom, block sizes and trigger conditions. Stores these setups as file *project.in.*

1.5.3 Task Module *TDAS CHANNEL SETUP*

Reads the default values either from file *project.tds* or from file *defaults.tds* for Tdas (Test) FRF management. Sets the location, sign, and direction for the reference (force) channel. Sets sign and direction for the response (velocity) channel. Stores the setups in file *project.tds*.

1.5.4 Task Module *ACQUIRE FRF DATA*

Sets up the System 7000 from the parameters set during the preceding setup modules by calling ZETA Toolkit routines. Reads the scan list file, *project.lst*. Acquires FRF, Coherence, and Time display of the Doppler envelop with ZETA routines. Stores the FRF data in Tdas format and optionally ZETA binary or ASCII format. Writes files *project.afu* for TDAS format, *project####.bin* for ZETA binary, and *project####.asc* for ZETA ASCII formats, where *####* in the filename is the response node number.

- 1.6 Module *HELP*

This main program module provides the global help messages. The help system is not fully implemented as of this time, however, provisions were built-in to the software structure to handle a sophisticated on-line help feature.

3.4 AMMS User Interface

A useful and friendly human interface was a primary design consideration during the LSI software development. A mouse-driven graphical software front-end was the most desirable user interface option for this modal test automation task. Since the development hardware platform was the HP 9000/300 series operating under HP-UX and X Windows, the LSI code was also developed under X Windows. The X Window works as a distributed, network-transparent, device-independent, multi-tasking windowing and graphics system [35]. The X Windows *Xlib*, *Xt* intrinsics, and *widgets* were use to create the comprehensive LSI menu system. Features of the LSI user interface include the following:

- Menu organization that logically follows the automated test scenario.
- Both popup and a tiled menu overlays.
- Shallow menu layers.
- Minimum keyboard input.
- Complete mouse driven menus and file I/O.
- Test instruments are setup and controlled by "software" buttons, slide bars, or toggle switches.
- Popup execution-feedback messages for important tasks; reporting either success, warnings, or failure.
- Local popup help menus built-in.

In the following sections of this chapter a brief presentation of the LSI user interface panels is provided. The sequence of the menu discussion and presentation of the menu panels is based on an automated test scenario similar to the one presented in section 3.2 above. The menu panels are discussed as a "new" modal test where there are no previously defined project setup defaults.

3.4.1 LSI Back Window

First, before the user sees the LSI Application Manager Menu Panel, the user starts LSI in a *hpterm* window. After user starts LSI this terminal window serves as the **Back Window** that ZETA and some of the LSI applications use for feedback to the user. Figure 3.5 shows an example of the **Back Window** immediately after LSI startup. Notice the program is started with the "lsi" command. What follows in the window next is the ethernet, System 7000, ZETA, etc., initialization procedure. The **Back Window** is an output window only; there are no user inputs to this window during execution of LSI.

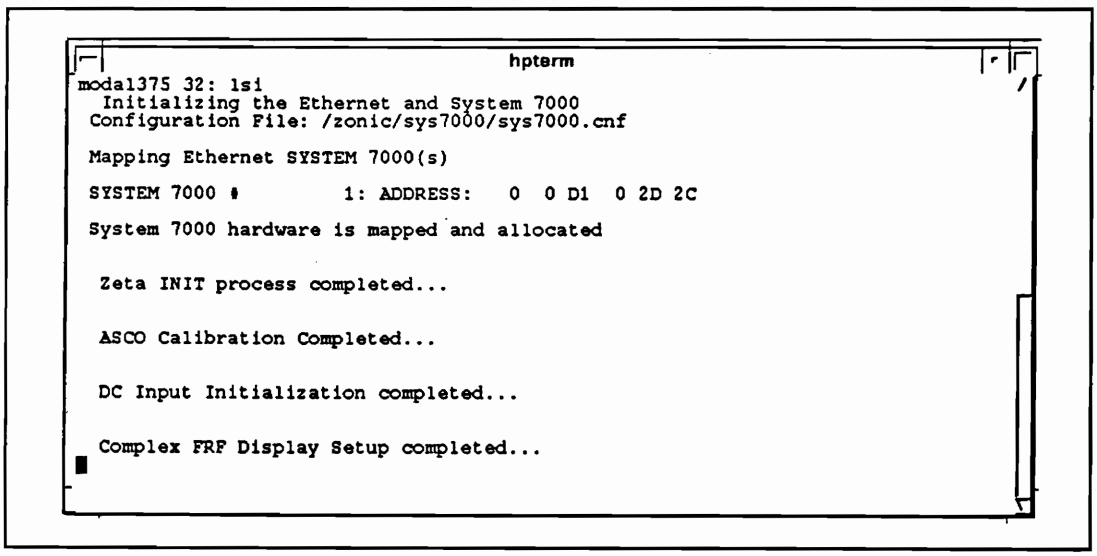

Figure 3.5 LSI Back Window Example.

3.4.2 LSI Application Manager Menu Panel

In Fig. 3.6 the LSI Application Manager panel or main menu panel is shown. This is the first menu that greets the user during the automated modal test. The features of this menu include the six (6) main task buttons; ***EXIT, PROJECT NAME, LASER VIEW, SCAN LIST, ACQUIRE DATA,*** and ***HELP.*** The ***PROJECT NAME*** button must always be selected first. All other buttons will produce an execution-feedback error without a project name. Other features of this main menu panel include its task tracking and feedback capability. With this capability, the main menu monitors and records the sequence of the automated test. The steps the user has taken in the process are displayed in this history window. One function of the history window is to provide the user the capability to retrace the steps that were followed in setting up the modal test.

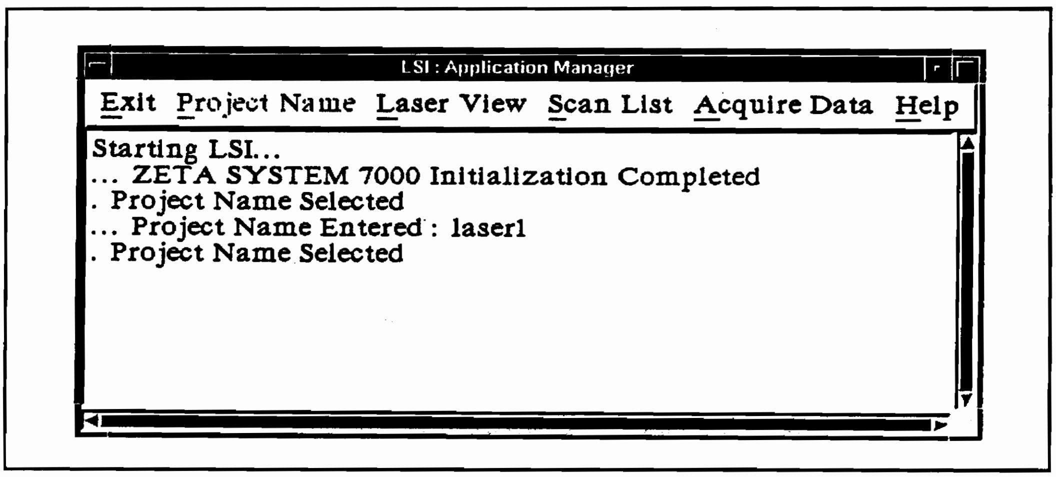

Figure 3.6 LSI Application Manager - Main Menu Panel.

Another function of the history window is to report on the file I/O status. If the data and setup files are read and written correctly a message to that effect is displayed in the history window. The main menu panel is visible at all times during the modal test. It is normally located in the upper left corner of the X terminal root window and all submenus popup at other screen locations; never over the main menu panel. To terminate the LSI software the user selects the ***EXIT*** button. This is the only ***EXIT*** and LSI may be terminated from any subprocess because the main menu stays visible at all times. The ***EXIT*** button on this panel closes the LSI menu system and the ethernet connection to the System 7000.

3.4.3 Project Name Panel

Figure 3.7 shows the second LSI menu the user will encounter; the LSI Project Name input panel will appear when the ***PROJECT NAME*** button is selected in the main menu. In this popup panel the user defines a project name that is to be associated with the modal test to follow. Essentially, the project name panel was created to follow the procedure that I-DEAS uses in its project files. To allow the AMMS system to be stopped and started at any point in the modal test and for data security reasons, LSI writes many files during the automated test. The management of these files is greatly simplified if they share a common *project* name and only different extensions.

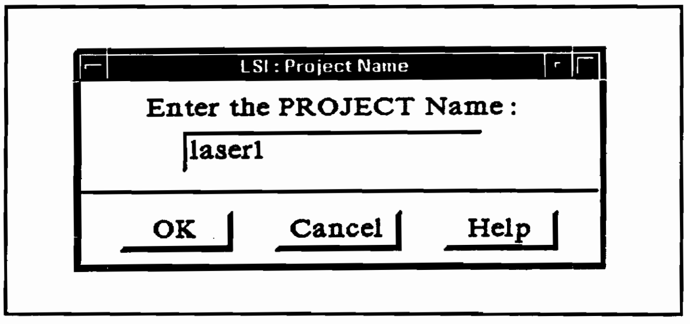

Figure 3.7 Project Name Input Panel.

Section 3.3 of this chapter gave a brief description of the project files written during an automated modal test. The project name is limited to twenty (20) characters by the text input area of the menu panel. Project name of eight (8) characters is recommended if there is a chance the ASCII FRF data will later be ported to a PC-DOS environment.

Most all of the LSI user interface popup menus software have three (3) action buttons at the bottom margin. The buttons ***OK, Cancel,*** and ***Help*** have the following meaning: a single mouse click on the ***OK*** button accepts the information on the menu panel. Feedback to the history window reports menu panel action. The ***Cancel*** button exits the menu panel without accepting changes. History window reports panel "canceled". The ***Help*** button is a local help feature that was included on each panel for developing the on-line help system. Currently there is very little on-line help available, however, a click on the ***Help*** button pops up a blank help window. History window reports "Local Help" selected.

3.4.4 Laser View Menu Panel

Figure 3.8 shows the popup panel that appears when the ***LASER VIEW*** button on the main menu is selected. The LSI Laser View menu panel has the three tasks that are required for determining the laser view position of the test structure. First, by clicking on the ***Registration Points*** button a popup panel as shown in Fig. 3.9 appears. On this menu panel the user is prompted to enter the I-DEAS Universal filename that contains the structure's geometry information.

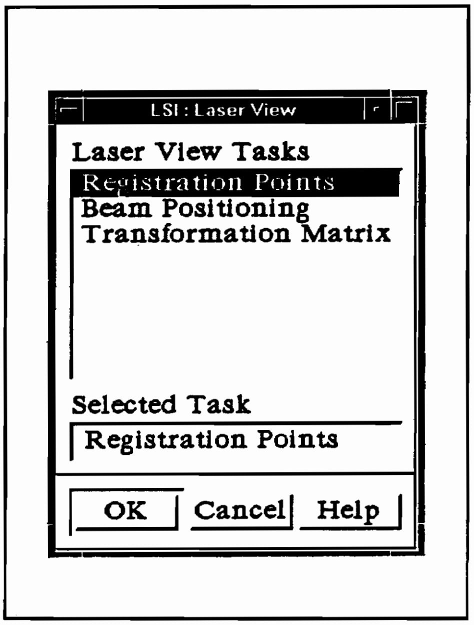

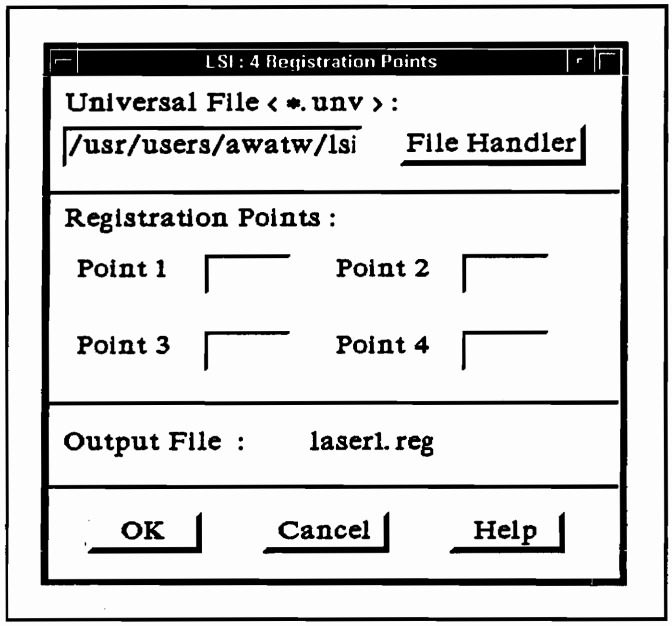

Figure 3.8 LSI Laser View Menu. **Figure 3.9** Registration Points Input Task Panel.

Button ***File Handler*** on the Registration Points panel (Fig. 3.9) is provided as a support menu that sorts the current working directory and allows the user to pick the Universal file from the displayed list. The ***File Handler*** panel is shown in Fig. 3.10.

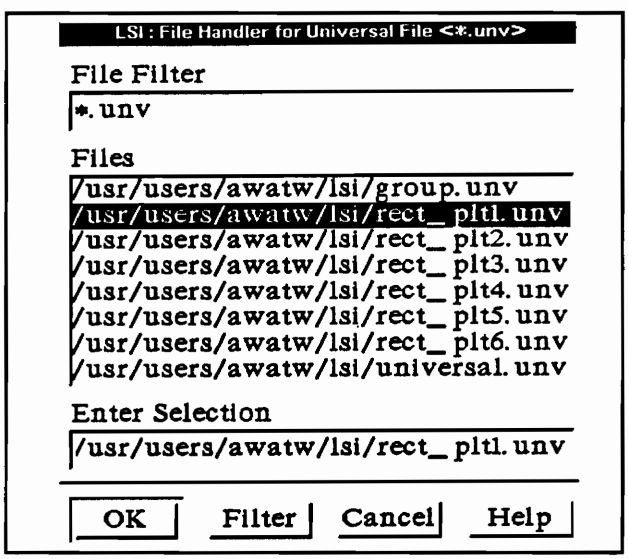

Figure 3.10 Universal File Handler.

Next, the user is requested to enter the four (4) node numbers that are properly spaced and are "viewable" by the laser (Fig. 3.9). The user then selects *OK* to accept the panel and then ***Cancel*** to close it. The user is then returned to the Laser View menu panel (Fig. 3.8).

The second task of determining the laser's view position is aiming the laser beam on the registration points of the structure. Selecting the ***Beam Positioning*** button pops up two windows as shown in Figs. 3.11 and 3.12. Figure 3.11 shows the LSI Beam Position task panel that contains the node numbers entered in the previous panel setup. It also contains an *X-Y* counter for monitoring the mouse movement on the companion LSI Viewport panel (Fig. 3.12). The large arrow buttons provide for fine (1 DAC step) laser beam movement.

The second menu that is displayed along with the beam positioning task is the LSI Viewport panel shown in Fig. 3.12. The viewport is a square window that corresponds to the laser's square field of view (4000 x 4000 DAC steps). The Cartesian coordinate system shown in the center of the viewport corresponds to the home-home position of the laser beam. To move the beam the mouse is moved to any arbitrary location and the user then clicks the left mouse button. The laser beam will jump to the corresponding location and on the screen a relative vector from the home-home position will be drawn to that point. The relative vector helps the user judge how to move the beam near the desired location. Once close to the desired location, the user must use the fine beam movement arrows on the other popup mouse control panel. When the laser beam is on the registration point the user clicks the small ***OK*** button beside the node number and the *X* and *Y* scan angles are recorded for that point. This registration procedure essentially repeats for the remaining three (3) node points. The ***Cancel*** button closes the window and the user is returned to the Laser View menu panel.

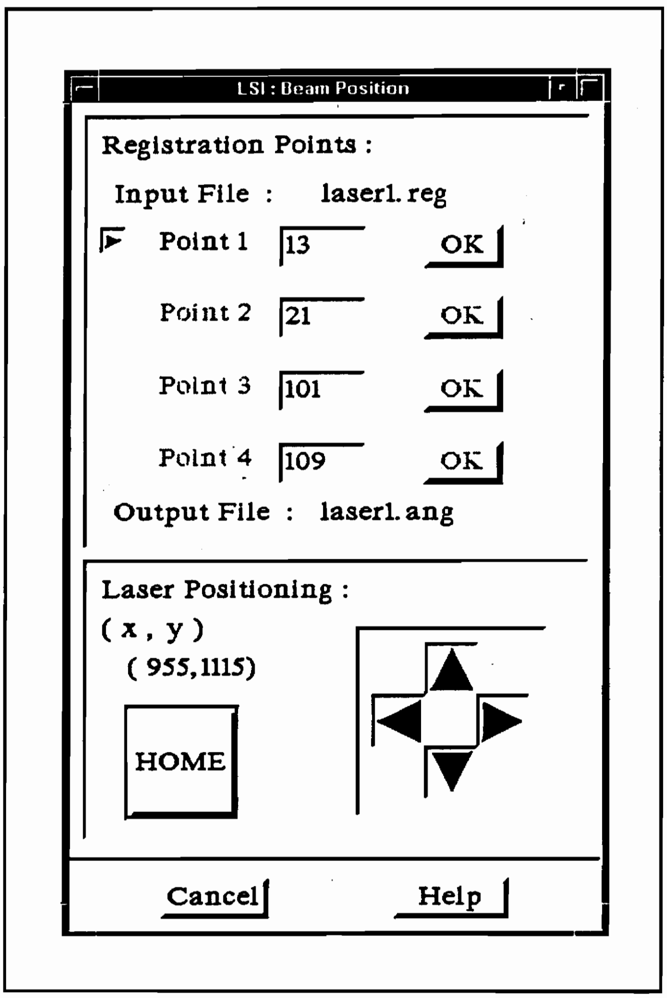

Figure 3.11 Beam Position Task-Laser Fine Movement Control Panel.

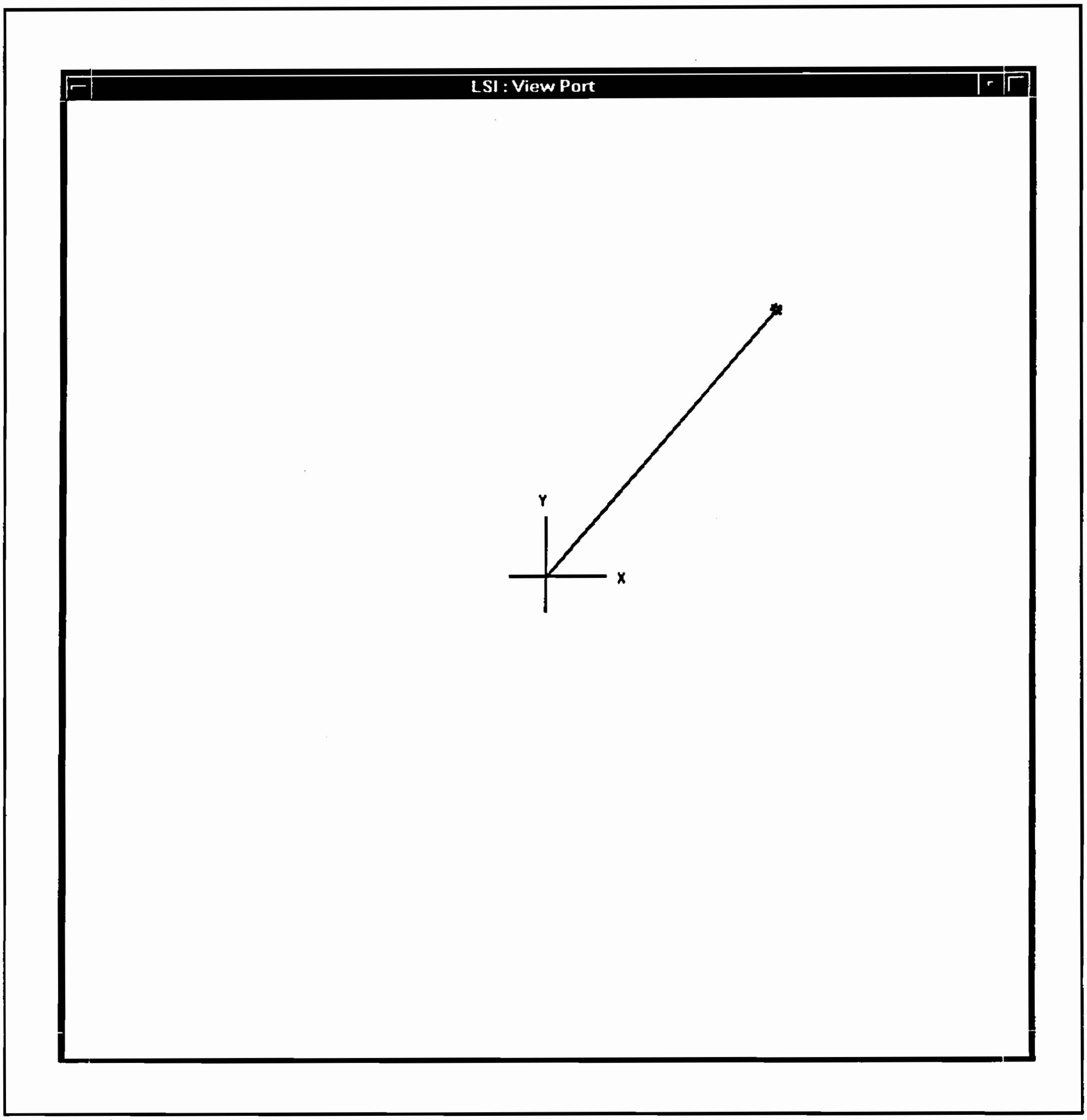

Figure 3.12 Beam Positioning Task-Laser ViewPort Panel.

The third task of determining the laser's view position is to calculate the laser's view of the structure. This is performed when the user selects the ***Transformation Matrix*** button from the Laser View menu panel (see Fig 3.8). The popup menu that follows this task is shown in Fig. 3.13.

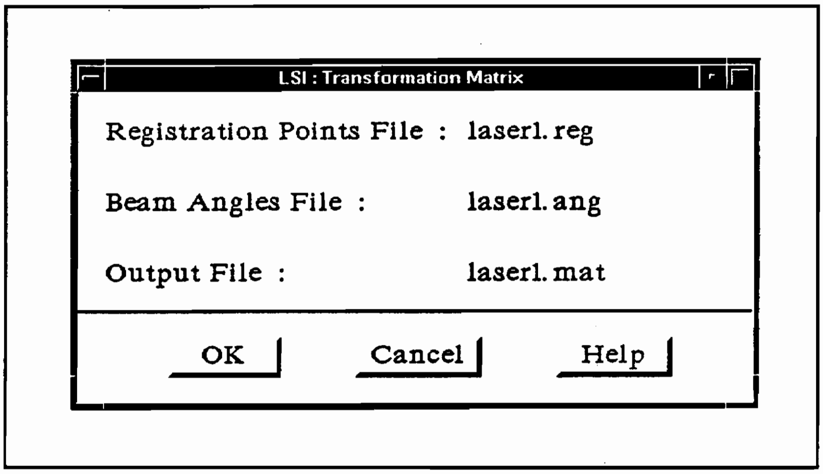

Figure 3.13 Transformation Matrix Menu Panel.

The Transformation Matrix panel is there to provide a check of the project file names before continuing with the calculation of the transformation matrix. The remainder of the process is hidden from the user. This routine reads the registration points file (*project.reg*) and the beam angle file (*project.ang*) and then computes the transformation matrix. The outcome of the transformation matrix computation is monitored and reported in the **Back Window**. If the procedure has errors or the program determines the solution has large inconsistences a warning message will be printed in the **Back Window**. After completion, an execution-feedback windows pops-up and reports; success, success with warnings, or failure. Once the transformation matrix routine is complete, the ***Cancel*** button closes the LSI Laser View menu panel and returns the user to the LSI Application Manager (Fig. 3.6).

3.4.5 Scan List Panel

The next step in the automated modal test scenario requires the development of a scan list. The ***SCAN LIST*** button on the main menu pops up the LSI Scan List menu panel shown in Fig. 3.14. This panel prompts the user enter the geometry Universal file and the grouped node file. The panel essentially requests the user to key in two filenames or use the ***File Handler*** (Fig. 3.10) button for each. Selecting ***OK*** opens and reads the Universal files and the transformation matrix file. It then performs the matrix multiplication on the nodal coordinates to develop the scan list of System 7000 ASCO commands (i.e. X and Y scan angles). Once the scan list is successful, the ***Cancel*** button closes the window and returns the user to the LSI Application Manager menu panel.

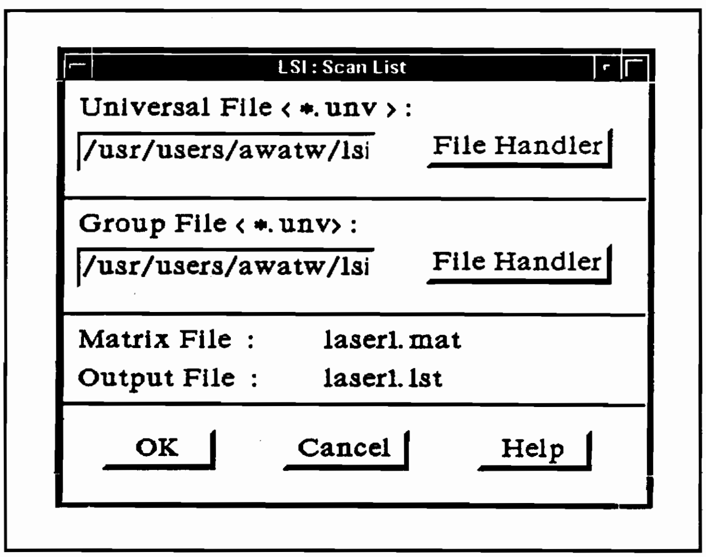

Figure 3.14 Generate Scan List Panel.

3.4.6 Acquire Data Menu Panel

Figure 3.15 shows the LSI Acquire Data menu panel when the ***ACQUIRE DATA*** button on the Application Manager is selected. This menu panel has three (3) acquire data tasks buttons: ***Output Channel Setup, Input Channel Setup,*** and ***FRF Data Acquiring.***

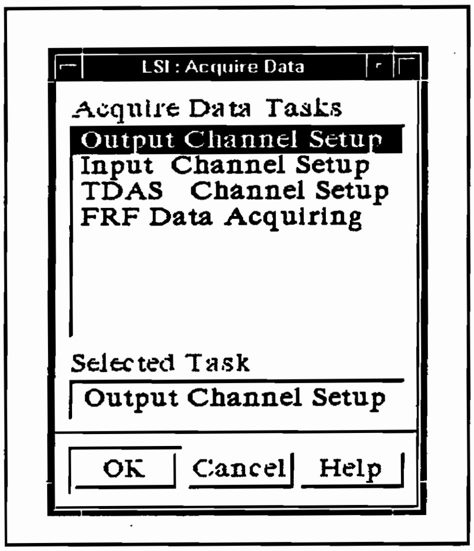

Figure 3.15 LSI Acquire Data Menu Panel.

Figure 3.16 shows Output Channel Setup panels. This panel is the System 7000 setup panel that controls the forcing function (ASCO, Channel 3) of the modal test. This mouse driven panel includes push-buttons for the user to select the desired waveform, frequency or bandwidth, burst time, and amplitude. The appearance of the Output Channel Setup panel varies depending on the type of output waveform selected. Figure 3.16 shows the typical random waveform output setup panel. ***OK*** accepts the form, ***Cancel*** closes and returns user to the Acquire Data menu panel.

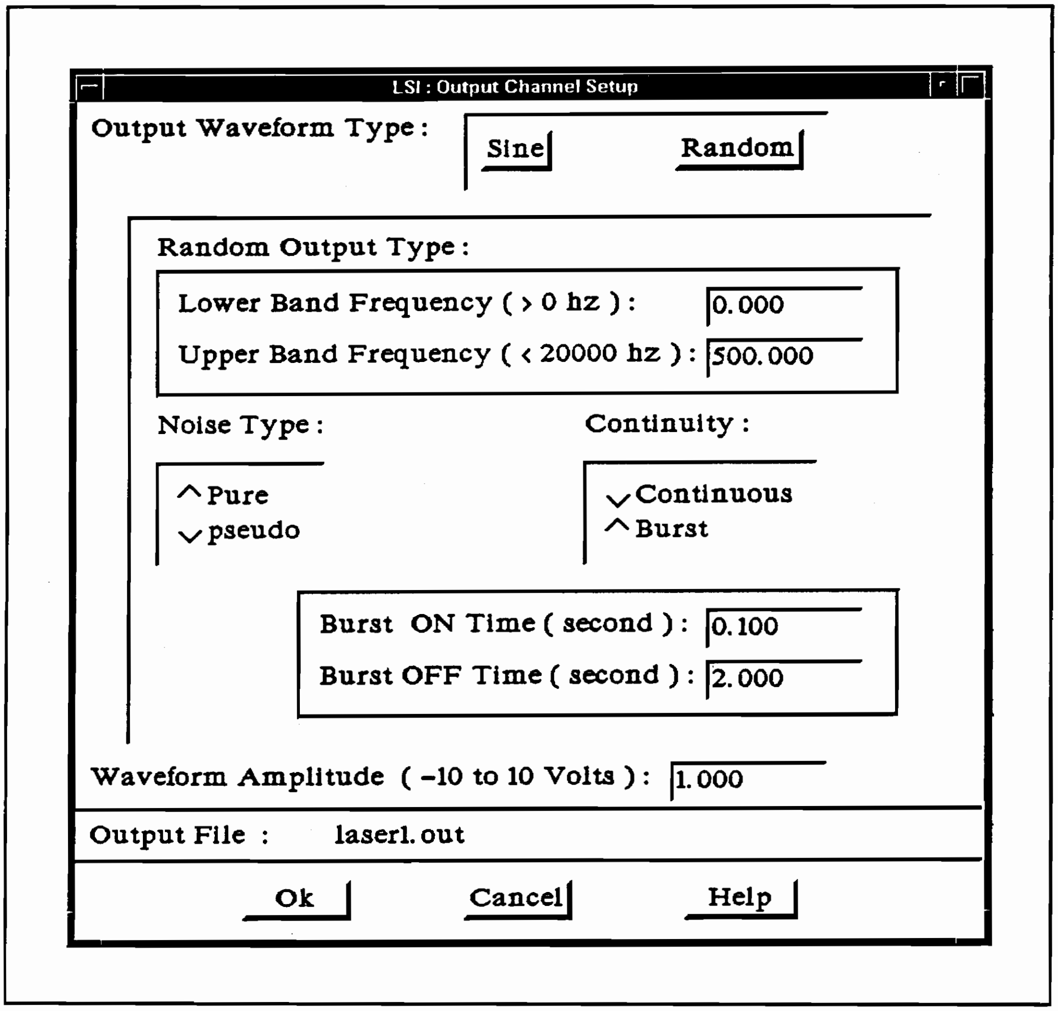

Figure 3.16 Output Channel Setup, Random Waveform Selected.

When the user selects the ***Input Channel Setup*** task button from the LSI Acquire Data menu panel, the LSI Input Channel Setup panel pops up. The System 7000 input setup is shown in Fig. 3.17. On the input setup panel, like the output panel, the analyzer is setup by simple keyboard inputs and mouse clicks on the buttons. Autoranging, input channel sensitivity, full-scale volts, units label, window type, analysis frequency, block size, trigger conditions, etc. can be selected.

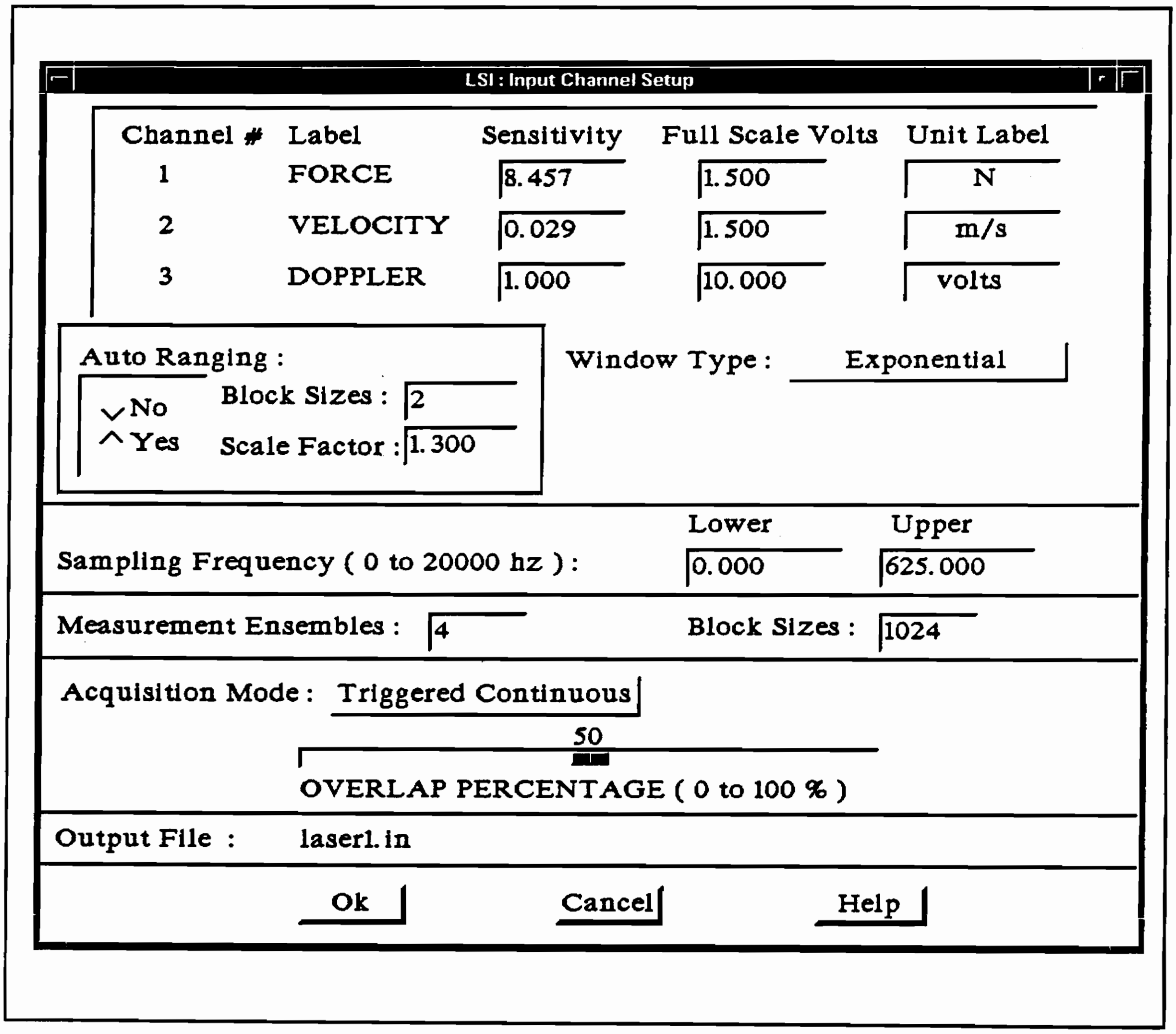

Figure 3.17 Input Channel Setup Panel.

If trigger input is selected on the Input Channel Setup panel then the Triggered Signal panel pops up. Figure 3.18 shows the LSI Triggered Signal panel where the user enters the trigger source, delay, level, and slope. ***OK*** accepts the form, ***Cancel*** closes and returns to the LSI Acquire Data menu panel.

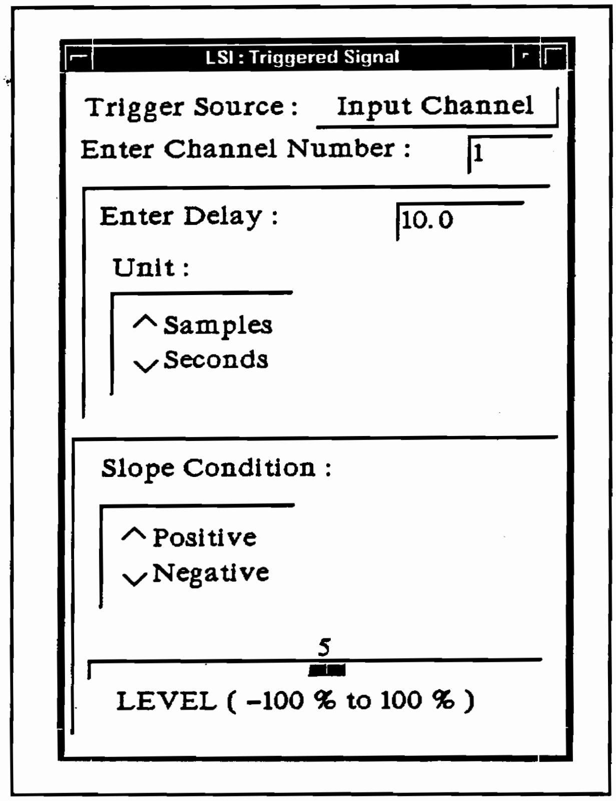

Figure 3.18 Triggered Input Signal Panel.

Once the user has setup the System 7000 for input conditions and forcing function output, the automated FRF data acquisition task is near. The final step before FRF acquisition begins is the I-DEAS Tdas (Test) data management task. At the LSI Acquire Data menu panel (Fig. 3.15), the user selects the ***FRF Data Acquiring*** button. This button pops up an I-DEAS Tdas Channel Setup panel shown in Fig 3.19. On this panel the user enters the node number corresponding to the force location, coordinated direction, and sign.

Direction and sign must also be entered for the response channel. The direction and sign are determined by the transducer's mounting relative to the global Cartesian coordinate system in the I-DEAS Test model. For example, a reference coordinate of **126Z+** indicates a force at the location of node number 126, with a positive force gage output aligned along the positive Z-axis. It is required that the user assume the primary response direction is out-of-plane or normal to the view plane of the laser when using this 1-D measurement system.

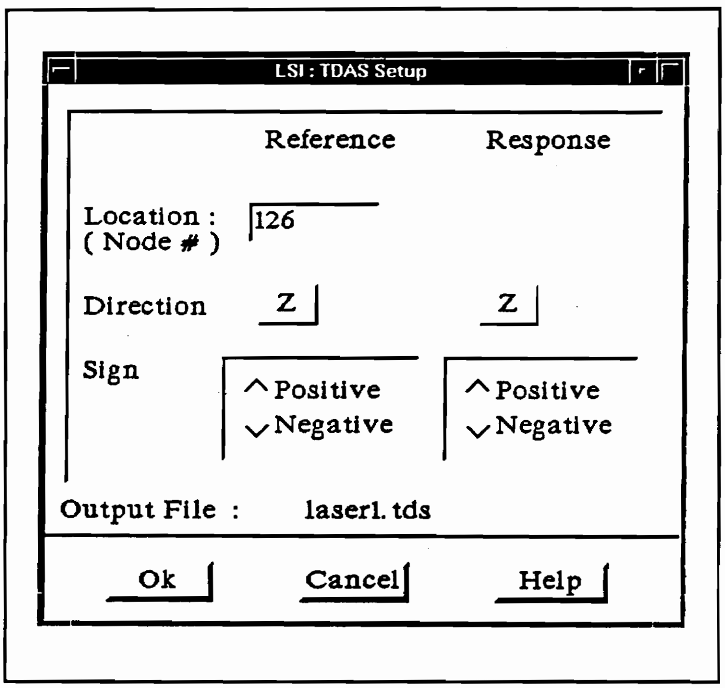

Figure 3.19 I-DEAS Test (Tdas) Channel Setup Panel.

The last menu panel before FRF acquisition is shown in Fig. 3.20. This panel entitled FRF Data Acquiring has two purposes. First, it provides the user the opportunity to check the project scan list filename and the Test ADF filename before data acquisition begins. Second, the user can select ZETA storage format (ASCII or binary) for the FRF data.

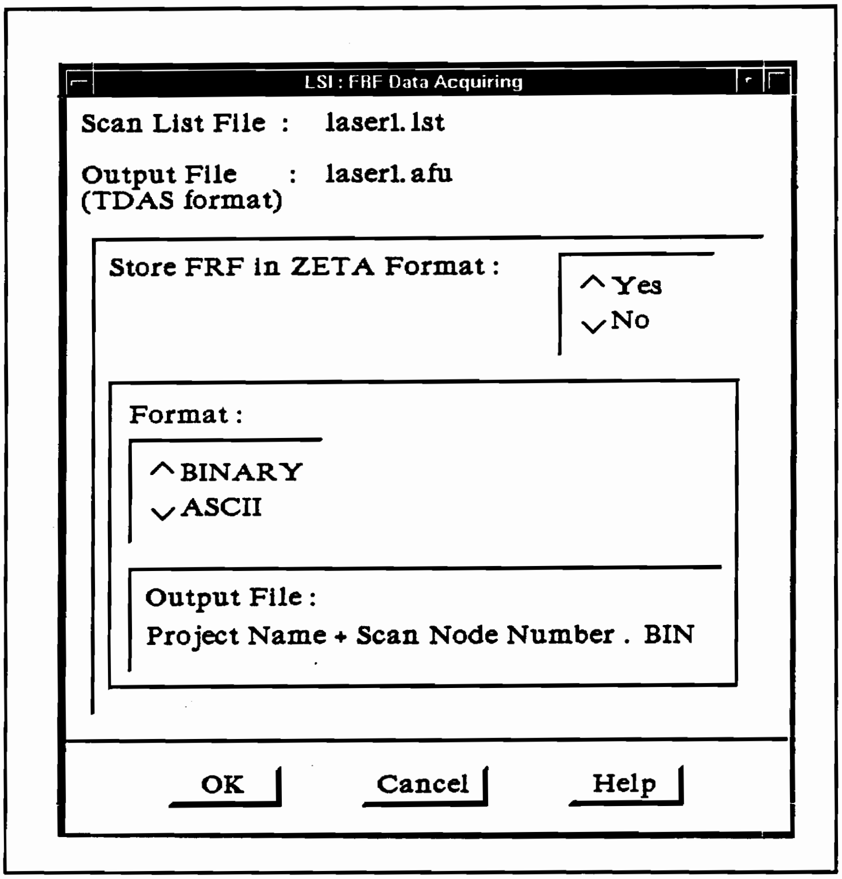

Figure 3.20 ZETA Format FRF Storage Options.

The ZETA FRF storage options is the last setup panel in the LSI software. When this optional storage panel is closed, the automated process go into the programmed scan and data acquisition mode. During the automated data acquisition process the FRF, coherence function, and time-domain Doppler envelope are displayed for each measurement point. Examples of the FRF and Coherence data obtained are presented in Chapter 5.

Chapter 4

Determination of the Laser Scan List

4.1 Scan List Overview

A scanning LDV measures the vibration velocity of a structure at discrete locations. In the AMMS system, the measurement locations on the structure correspond to the nodes of the I-DEAS Test model. When using the Test model two difficulties arise. First, the Test model will typically contains hundreds of nodes. Clearly marking each node location on the structure is nearly impossible. Second, manually positioning the laser is very time consuming and a waste of the laser's high-speed capabilities. Therefore, the desired approach is to program the computer to aim the laser beam at the measurement nodes. This is accomplished by generating a scan list of X and Y voltages to rotate the laser's scanning mirrors to place the beam on the measurement nodes. Thus, a key issue in the development of the AMMS system was the determination of the X and Y scan list.

The scan list is determined by the following procedure:

1. Choose four (4) registration nodes for a reference.

2. Physically aim the laser beam at the 4 nodes and record the mirror scan (deflection) angles.

3. From the registration node's relative position as established by the I-DEAS Test database and laser scan angles, determine the transformation matrix.

4. Use the transformation matrix to convert nodal coordinates to a <u>calibrated</u> scan list of *X* and *Y* mirror voltage commands.

It is the purpose of this chapter to summarizes the procedure for determining the *X* and *Y* scan angle list for automated mobility measurements on a test structure. However, the author would first like to acknowledge the members of the Laser Project team for their effort and especially Mr. Xiandi Zeng for his analytical developmental work and for his writing, testing, and de-bugging efforts on scan list determination. It is the intent of this thesis to present only an overview of the scan list algorithm. Reference [36] provides a more detailed development of the algorithm, its solution method, and its implementation into computer code.

4.2 Development of the Scan List Algorithm

4.2.1 Coordinate Systems

Figure 4.1 shows the relationship of the coordinates systems involved in determining the scan list. In Fig. 4.1 a general 2-D plate structure is shown with the VPI Sensor in a simplified EMA test setup. An arbitrary node point P is shown on the plate surface. The

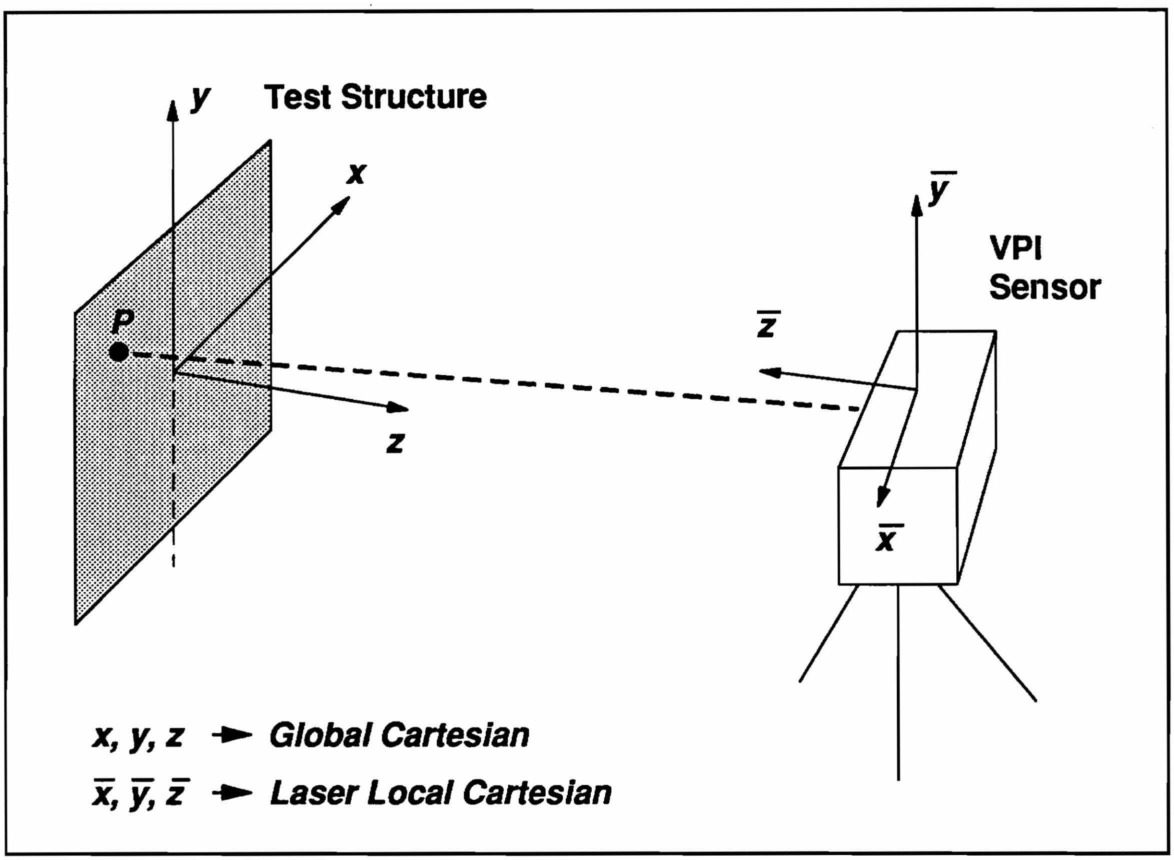

Figure 4.1 Definition of the Global and Laser Local Coordinate Systems, (adapted from Zeng, [36]).

position of the node is fully specified by the corresponding node location in the I-DEAS Test model. The nodal coordinates are defined by Test relative to its model's global Cartesian coordinate system shown in Fig 4.1 as (x, y, z) attached to the plate structure. Henceforth, this coordinate system will be referred to as the global coordinate system. The other coordinate system shown in the figure is the one attached to the laser head itself, denoted by $(\bar{x}, \bar{y}, \bar{z})$. This is the "laser local coordinate system" that is attached to the laser's scanning mirror system.

Two orthogonal mirrors are installed in the laser head to enable two-dimensional scanning. With a normal instrument setup, a voltage applied to the scan control of the X-mirror causes the laser beam to travel in the horizontal direction. A voltage applied to the scan control of the Y-mirror moves the beam in the vertical direction. The angle the scan mirrors rotate is proportional to the applied voltage. Thus, when the applied voltage to both scanners is zero, the laser takes the position referred to as "home" position. Based on this, Fig. 4.2 shows the four-quadrants of the laser scan positions. In quadrant **I**, both X and Y scan angles are positive. In quadrant **II**, X is negative, and Y is positive. Both X and Y are negative in quadrant **III**. In quadrant **IV**, scan angle X is positive, and scan angle Y is negative. Note, the laser positions defined in Fig. 4.2 are based on an observer standing behind the laser head viewing the test structure. This is the typical observation point during an EMA test. Fortunately the sign convention is made easier to remember by considering the sign of he input DC scan control voltage. When a <u>positive</u> voltage is applied to the X scanner the beam moves through a <u>positive</u>

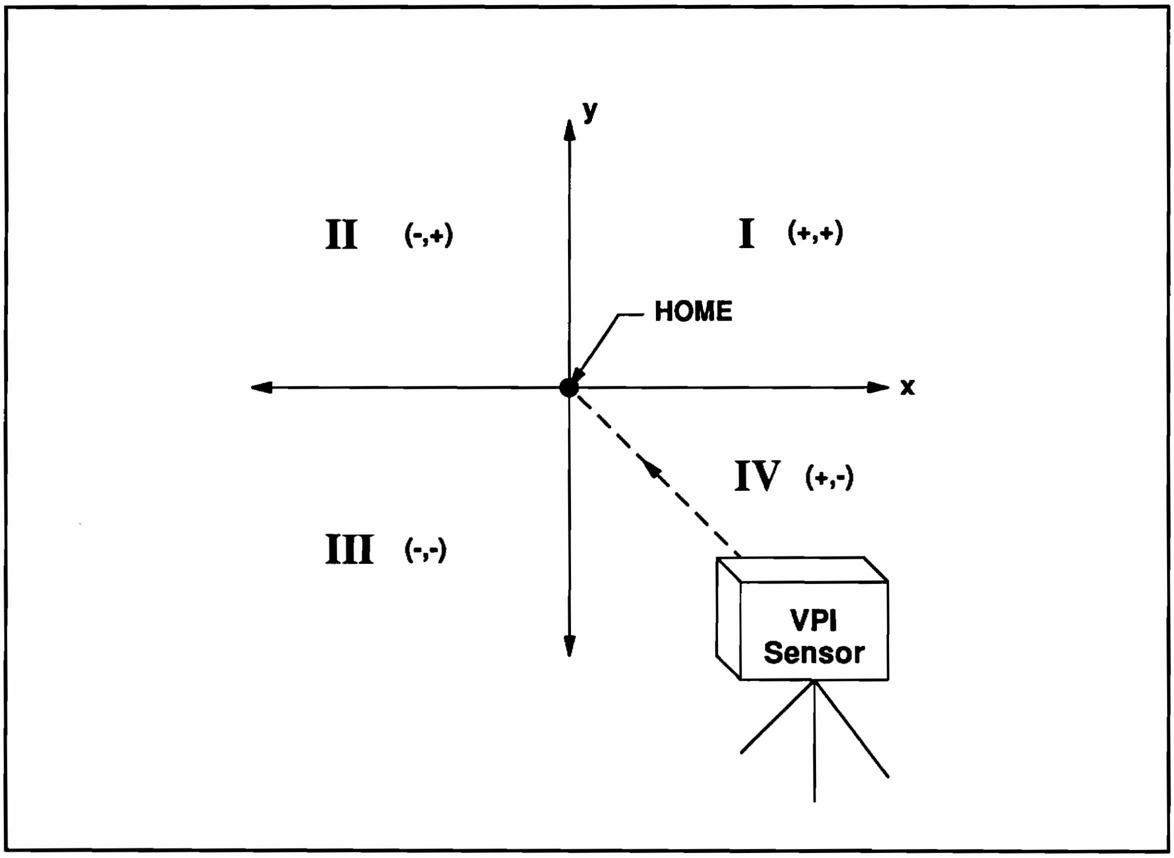

Figure 4.2 Laser Scan Angle Definitions, (adapted from Zeng, [36]).

(right) horizontal distance. For the Y scanner, a positive input voltage moves the beam through a positive (up) vertical distance (see Fig. 4.2).

4.2.2. The Scanner Model

Figure 4.3 shows the laser's mirror configuration and location of the laser local coordinate system. The two laser scan mirrors are installed in the laser head such that their axis of rotation is perpendicular to each other. At the home position, both the X and Y-mirrors are inclined at a 45 degree angle. The distance between the two mirrors is measured along the beam at the home position. This distance, called the separation distance of the reflection center, *dl*, is based on the mirror dimensions and maximum rotation angle. The particular VPI Sensor model used in this research had a separation distance, *dl*, of 46 mm.

Also shown in Fig. 4.3 is the laser local coordinate system ($\bar{x}$, $\bar{y}$, $\bar{z}$) with origin at $\bar{O}$. The laser local coordinate system is a right-hand system defined with the scan mirrors at home position. It is located on the surface of the Y-mirror at the point where the beam is reflected from the X-mirror. The $\bar{x}$-axis is on the Y-mirror surface and parallel to its axis of rotation. The $\bar{z}$-axis is along the laser beam when both mirrors are at the home position.

A point is space can be fully described by its coordinates relative to the laser local coordinate system however, there are two ways to do this. First, the point can be described in the usual Cartesian order ($\bar{x}$, $\bar{y}$, $\bar{z}$). Second, the point can be described in

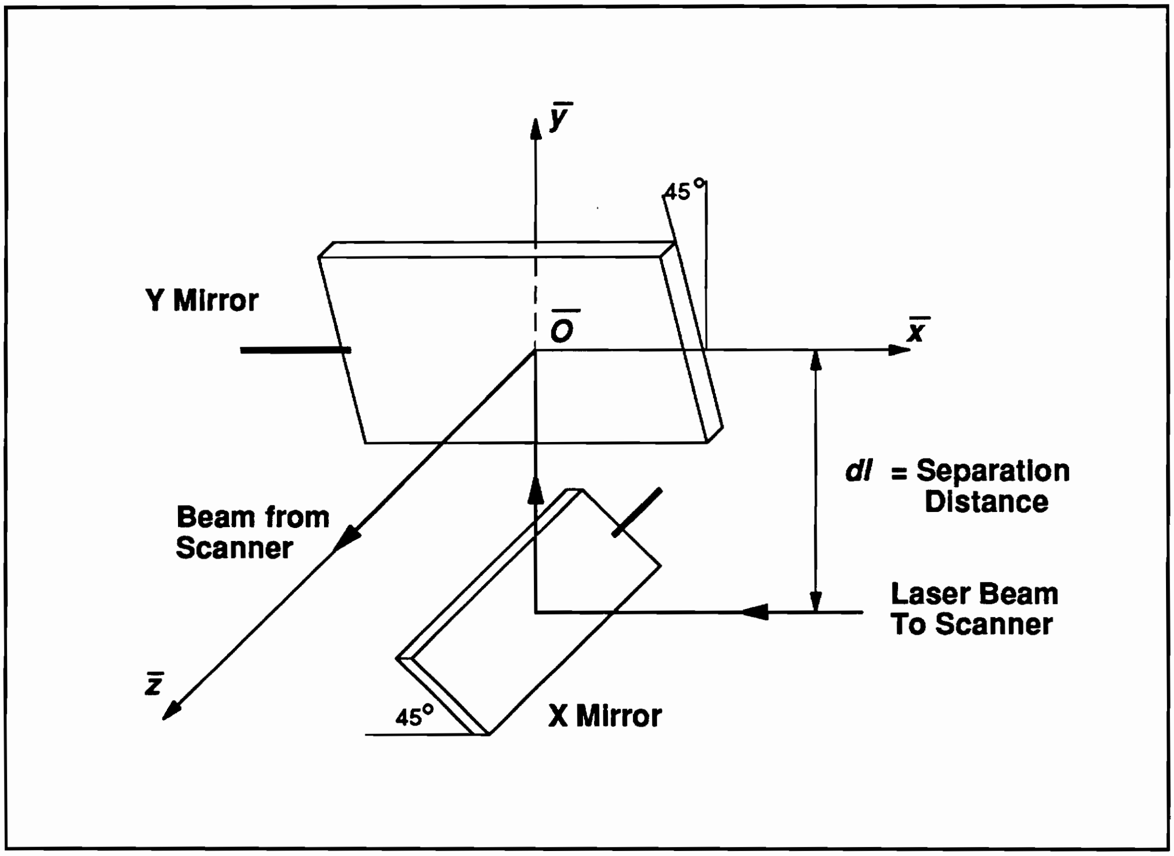

Figure 4.3 The Laser's Mirror Configuration and Local Laser Coordinate System, adapted from Zeng, [36]).

a scan list form of two scan angles and a distance from the origin to the point. In other words, X scan angle, Y scan angle, and range, R can be used to describe the point location. For this application, it is more convenient to describe the point in the scan list form. However, the two scan mirrors are separated by a fixed distance. Thus, the coordinate transformation between the Cartesian coordinates and the scan list requires some additional definitions and considerations.

When the X-mirror rotates the beam moves left or right of $\bar{O}$ along the $\bar{x}$-axis (see Fig. 4.3). This is equivalent to having an imaginary origin of the beam behind the Y-mirror [36]. When the X-mirror is rotated, the horizontal scan position is obtained by rotating the beam about the $\bar{y}$-axis through the imaginary center. Thus, the rotation angle is called $\theta_{\bar{y}}$. Similarly, when the Y-mirror rotates, the laser beam moves up or down. This rotation causes the imaginary origin point to travel along an arc whose radius is the mirror separation distance, dl. The vertical scan position is obtained by rotating the beam about the $\bar{x}$-axis. Thus, the rotation angle is called $\theta_{\bar{x}}$.

Now, the relationship between the scan angle definition and the scan coordinate definition can be defined. Maintaining a right-hand sign convention, it is defined that $\theta_{\bar{x}}$ is positive if it moves the beam to a positive $\bar{y}$, and $\theta_{\bar{x}}$ is negative if it moves the beam to a negative $\bar{y}$. The same sign convention is true for $\theta_{\bar{y}}$. Thus, the difference between the scan coordinate definition and the scan angle definitions is given by the following:

$$\theta_{\bar{x}} = Y \text{ scan angle} \tag{4.1}$$

$$\theta_{\bar{y}} = -X \text{ scan angle} \tag{4.2}$$

$$R = R \text{ (range)} \tag{4.3}$$

With the definitions of Eqs. (4.1) through (4.3), the relationship between the laser local Cartesian coordinates and the scan coordinates for a arbitrary point can be determined. Figure 4.4 shows the laser local coordinate system ($\bar{x}$, $\bar{y}$, $\bar{z}$) with origin at $\bar{O}$. Because both X and Y-mirrors are rotated from home, the point O' represents the new laser beam origin (imaginary point behind the Y-mirror). In Fig. 4.4, point P is an arbitrary point in which the laser beam has been aimed. The actual beam path is along line $O'P$. However a consistent origin for all measurement points is necessary. Thus, there is a way of using the geometry of the scanner model to reference all measurements through the laser local coordinate system attached to the Y-mirror at $\bar{O}$. In Fig. 4.4, vector $\bar{O}P$ with magnitude R represents the consistent laser origin model. From Fig 4.4, the following equations transfer the scan coordinates to the laser local Cartesian coordinate system for an arbitrary point in space.

$$\bar{x} = R \sin\phi \tag{4.4}$$

$$\bar{y} = R' \sin\theta_{\bar{x}} = R \cos\phi \sin\theta_{\bar{x}} \tag{4.5}$$

$$\bar{z} = R' \cos\theta_{\bar{x}} = R \cos\phi \cos\theta_{\bar{x}} \tag{4.6}$$

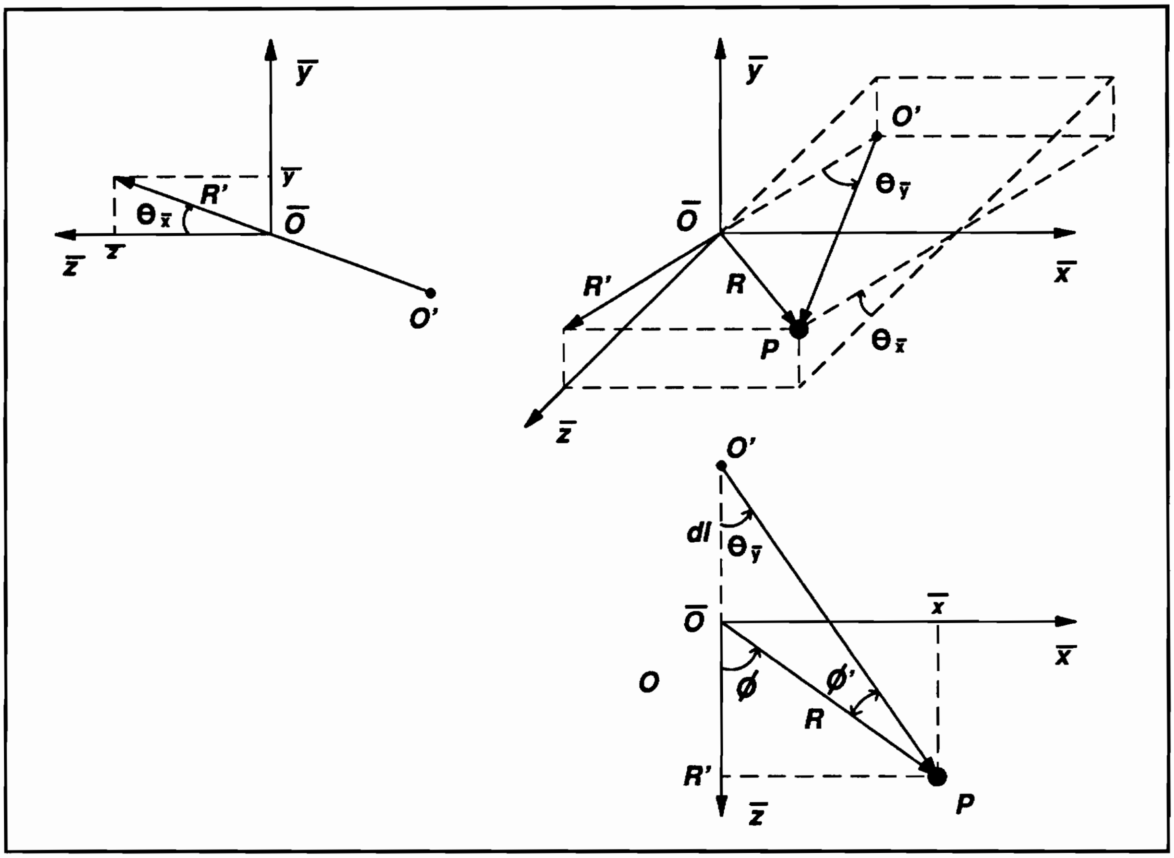

Figure 4.4 Relationship Between the Laser Local Cartesian and the Laser Local Scanning Coordinate; Moving Laser Origin Model, (adapted from Zeng, [36]).

and,

$$\phi = \phi' + \theta_{\bar{y}} \tag{4.7}$$

$$\phi' = \sin^{-1}\left(\frac{dl}{R}\sin\theta_{\bar{y}}\right) \tag{4.8}$$

where,

dl = mirror separation distance
R = range between laser local origin and point, P

The following equations transfer the Cartesian coordinate to the scan coordinate.

$$R = (\bar{x}^2 + \bar{y}^2 + \bar{z}^2)^{1/2} \tag{4.9}$$

$$\theta_{\bar{x}} = \tan^{-1}\left(\frac{\bar{y}}{\bar{z}}\right) \tag{4.10}$$

$$\theta_{\bar{y}} = \tan^{-1}\left(\frac{\bar{x}}{(R' + dl)}\right) \tag{4.11}$$

or rewritten as,

$$\theta_{\bar{y}} = \tan^{-1}\left(\frac{\bar{x}}{\left(\sqrt{\bar{y}^2 + \bar{z}^2} + dl\right)}\right) \tag{4.12}$$

Therefore, Eqs. (4.4) through (4.12) define the VPI Sensor scanner model. This model is used for the perpendicular scan mirror configuration shown in Fig. 4.3 only. If another mirror configuration is used, the above scanner model is invalid.

4.2.3 Transformation of Coordinate Systems

A point P in space can be specified in both the global and the laser local Cartesian coordinate systems. To compute a node scan list for the AMMS system, points in the laser local coordinate system must be defined relative to the global coordinate system attached to the structure. The coordinate system definition requires two parts, the origin position, and the orientation. The origin position is specified by its coordinates (a, b, c) in the global system. The orientation is specified by a 3 x 3 rotation matrix **[RT]** whose columns consist of the directions cosines of the three axes $(\bar{x}, \bar{y}, \bar{z})$ in the global coordinate system. This concept is aided by the sketch in Fig. 4.5. Point P is defined in two coordinate systems, therefore the relationship between the two systems can be determined. From Fig. 4.5, vector addition to point P gives:

$$\vec{R}_P = \vec{R}_o + \vec{\bar{R}}_P \tag{4.13}$$

And by projecting onto three axes, the above equation can be written in matrix form as:

$$\begin{Bmatrix} x \\ y \\ z \end{Bmatrix}_P = \begin{Bmatrix} a \\ b \\ c \end{Bmatrix} + [\mathbf{RT}] \begin{Bmatrix} \bar{x} \\ \bar{y} \\ \bar{z} \end{Bmatrix}_P \tag{4.14}$$

Where (a, b, c) are the laser local origin coordinates described in the global Cartesian system and where the rotation matrix, **[RT]** is defined as:

$$[\mathbf{RT}] = \begin{bmatrix} l_{\bar{x}} & l_{\bar{y}} & l_{\bar{z}} \\ m_{\bar{x}} & m_{\bar{y}} & m_{\bar{z}} \\ n_{\bar{x}} & n_{\bar{y}} & n_{\bar{z}} \end{bmatrix} \tag{4.15}$$

where l, m, and n are the direction cosines of each local axis in the global system.

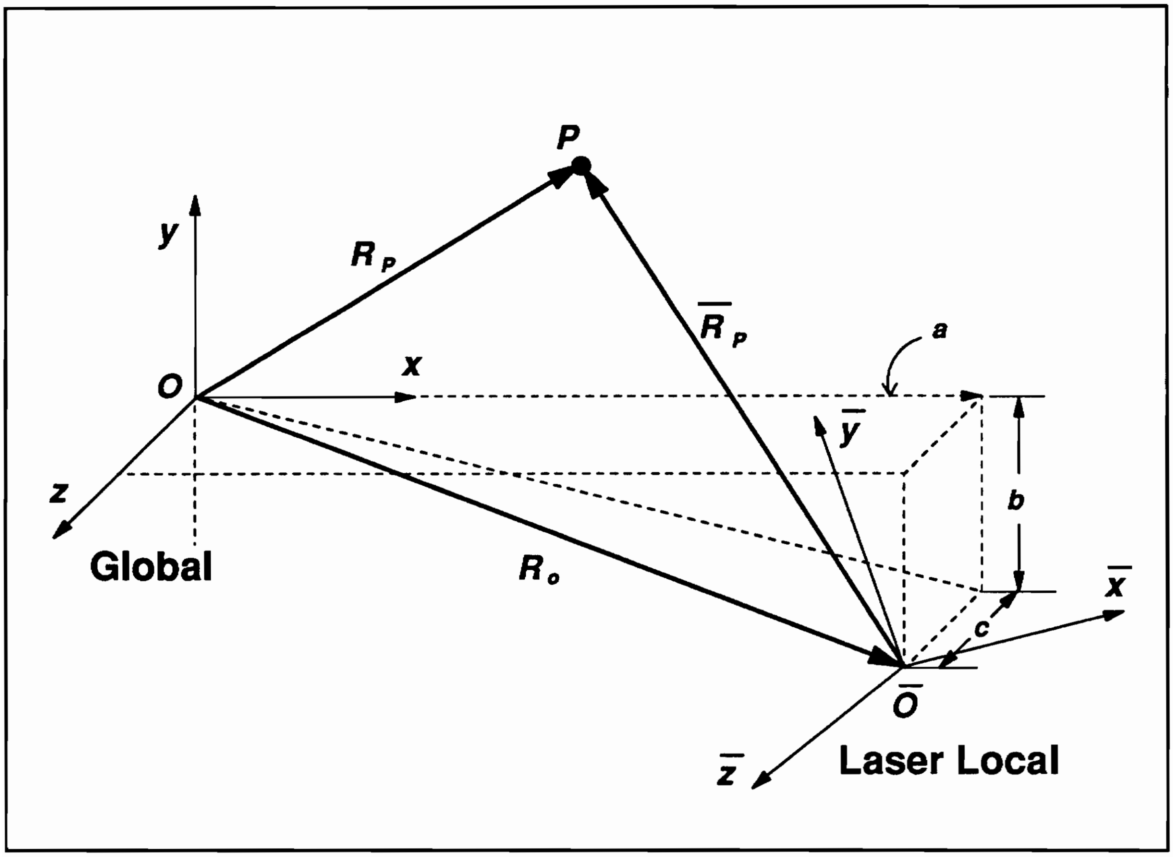

Figure 4.5 Definition of a Point *P* in Two Coordinate Systems: Laser Local, and Global Cartesian, (adapted from Zeng, [36]).

Now, if the global coordinates of point P are known (which they usually are from the I-DEAS Test model) and if the laser local origin coordinates and rotation matrix is known, the laser local Cartesian coordinates $(\bar{x}, \bar{y}, \bar{z})$ can be determined from Eq. (4.14). Once the laser local coordinates are known, the scan coordinates $(\theta_{\bar{x}}, \theta_{\bar{y}}, R)$ can be calculated from Eqs. (4.9) through (4.12). Finally, a scan list can be generated by Eq. (4.1) and (4.2) in the previous section.

Unfortunately, the laser position in space relative to the structure is unknown in a general modal test setup. However, the laser local origin coordinates and rotation matrix can be determined with physical measurements and the I-DEAS Test model geometry. The following section summarizes the method to solve for the laser local origin coordinates and rotation matrix.

4.2.4 Implementation of the Scan List Algorithm

During a modal test, the laser head is usually placed in a general location that can reasonably view the test structure. The laser position is selected based on a compromise of many variables including: total scan area size, optimum laser working distances, and many other physical constraints on the test setup. The exact laser position is never known before the EMA test. Therefore, it is necessary to compute the laser's position relative to the structure for each test setup, or laser view position.

As stated, the laser position consists of two parts that define it with respect to the global Cartesian system attached to the structure; the laser local origin coordinates and the rotation matrix. Both of these are unknown at the beginning of the modal test. However, after the laser head's position is fixed relative to the structure the relationship between the two coordinates systems is also fixed. If the beam is aimed at a point on the structure that corresponds to a node location in the I-DEAS model, then two pieces of information are known about that point. First, the global coordinates are known from the I-DEAS Test model, and second, the X and Y scan angles are known. The range, R is still unknown, but it can be determined if the laser is aimed at three or more registration points on the structure.

If three node points are used, as shown in Fig. 4.6, say points A, B, C, then there are three sets of transformation matrix equations similar to Eq. (4.14). This gives the nine (9) equations for points A, B, C as follows:

$$\begin{Bmatrix} x \\ y \\ z \end{Bmatrix}_A = \begin{Bmatrix} a \\ b \\ c \end{Bmatrix} + [\mathbf{RT}] \begin{Bmatrix} \bar{x} \\ \bar{y} \\ \bar{z} \end{Bmatrix}_A \tag{4.16}$$

$$\begin{Bmatrix} x \\ y \\ z \end{Bmatrix}_B = \begin{Bmatrix} a \\ b \\ c \end{Bmatrix} + [\mathbf{RT}] \begin{Bmatrix} \bar{x} \\ \bar{y} \\ \bar{z} \end{Bmatrix}_B \tag{4.17}$$

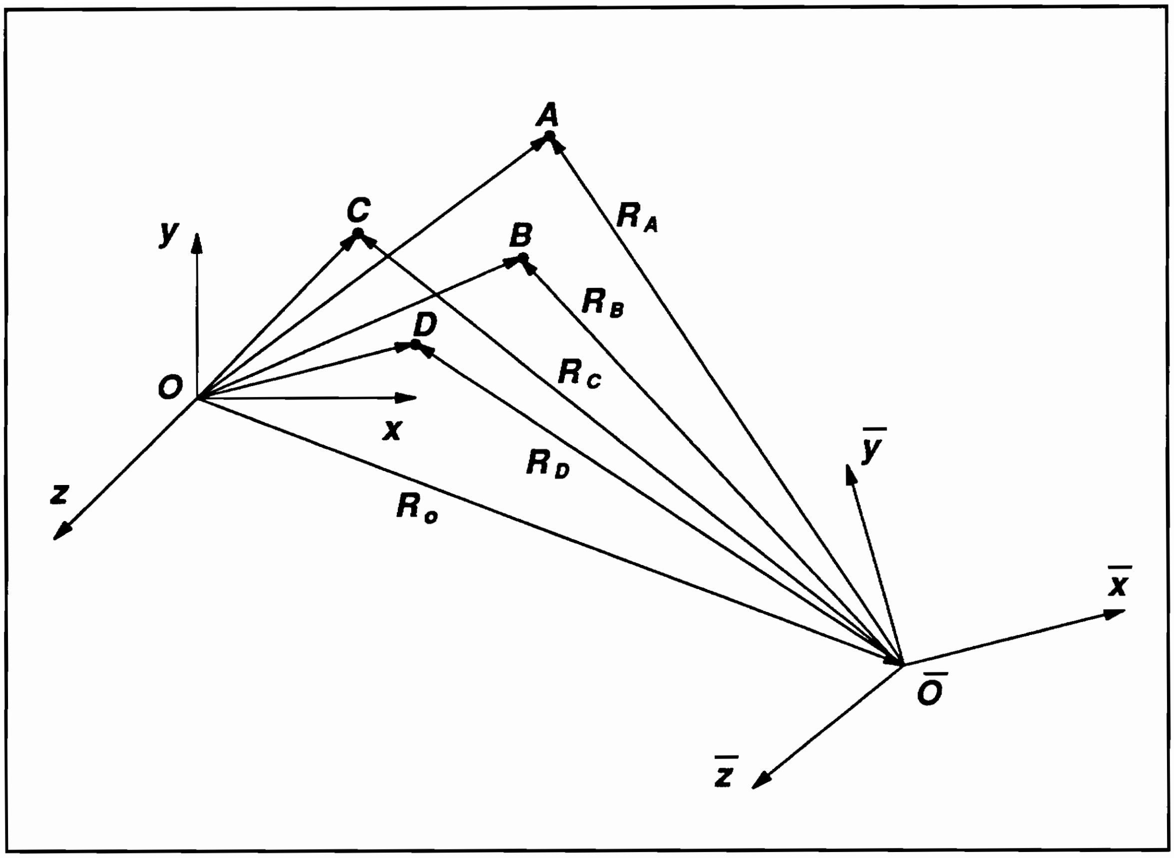

Figure 4.6 Relative Position and Range to Four Registration Points on the Test Structure, (adapted from Zeng, [36]).

$$\begin{Bmatrix} x \\ y \\ z \end{Bmatrix}_C = \begin{Bmatrix} a \\ b \\ c \end{Bmatrix} + [\mathbf{RT}] \begin{Bmatrix} \bar{x} \\ \bar{y} \\ \bar{z} \end{Bmatrix}_C \tag{4.18}$$

There are fifteen (15) unknowns in the above equations; 3 in the laser local origin coordinate, 9 in the rotation matrix, and 3 unknown ranges (R_A, R_B, R_C). It appears that more points are required to solve for all the unknowns in the above equations. However, the rotation matrix is an orthogonal matrix [37], implying there are 6 constraints among its 9 elements. These constraints on the vector norms and on the inner products are given as follows:

$$l_{\bar{x}}^2 + m_{\bar{x}}^2 + n_{\bar{x}}^2 = 1 \tag{4.19}$$

$$l_{\bar{y}}^2 + m_{\bar{y}}^2 + n_{\bar{y}}^2 = 1 \tag{4.20}$$

$$l_{\bar{z}}^2 + m_{\bar{z}}^2 + n_{\bar{z}}^2 = 1 \tag{4.21}$$

$$l_{\bar{x}} l_{\bar{y}} + m_{\bar{x}} m_{\bar{y}} + n_{\bar{x}} n_{\bar{y}} = 0 \tag{4.22}$$

$$l_{\bar{y}} l_{\bar{z}} + m_{\bar{y}} m_{\bar{z}} + n_{\bar{y}} n_{\bar{z}} = 0 \tag{4.23}$$

$$l_{\bar{z}} l_{\bar{x}} + m_{\bar{z}} m_{\bar{x}} + n_{\bar{z}} n_{\bar{x}} = 0 \tag{4.24}$$

There is now a total of fifteen equations for the fifteen unknowns. The fifteen equations are nonlinear, thus, it is extremely difficult to solve them simultaneously by iteration or other numerical methods. Reference [36] fully presents a geometrical solution method for these equations, therefore, it will not be repeated in this thesis. The reader is advised to consult this reference for specifics about the algorithm solution method. However, the basic three steps toward solving this system of 15 nonlinear equations is as follows: First, by using the geometry model (see Fig. 4.6), the ranges R_i can be calculated. Second, using the computed ranges the rotation matrix, **[RT]** can be determined. Third, the origin coordinate is then computed using the calculated ranges, rotation matrix, and global coordinates. The equations determining the ranges are simultaneously quadratic equations that will always give more that one solution. To get a unique range solution a fourth point, *D* (see Fig. 4.6) was added to the registration procedure. With four points, four 3-point combinations are available and each combination will give more than one range solution. A true range solution is chosen for each 3-point combination based on the fact that the true range is the same no matter which 3-point combination is used.

The selection of the "best" laser position was determined by using each position in turn to predict the beam deflection angles required to reach each of the four registration points. The actual beam deflection angles are, of course, known from the initial registration procedure of the experiment. The computed laser position that results in the minimum sum of the root-mean-square error is selected as the "best" description of the laser position relative to the I-DEAS Test global coordinate system. The sum of the RMS error, for node points $i = 1 \rightarrow 4$ is given by:

$$\mathcal{E}_{RMS} = \sum_{i=1}^{4} \left(\Delta\theta_{\bar{x}i}^2 + \Delta\theta_{\bar{y}i}^2 \right)^{1/2} \tag{4.25}$$

where,

$$\Delta\theta_{\bar{x}i} = \theta_{\bar{x}i,M} - \theta_{\bar{x}i,C} \tag{4.26}$$

$$\Delta\theta_{\bar{y}i} = \theta_{\bar{y}i,M} - \theta_{\bar{y}i,C} \tag{4.27}$$

and where, subscript M is the measured scan coordinate and subscript C is the computed scan coordinate.

Once the rotation matrix and origin coordinates are known, the scan list can be generated by rewriting Eq. (4.14) as follows:

$$\begin{Bmatrix} \bar{x} \\ \bar{y} \\ \bar{z} \end{Bmatrix}_P = [\mathbf{RT}]^T \left(\begin{Bmatrix} x \\ y \\ z \end{Bmatrix}_P - \begin{Bmatrix} a \\ b \\ c \end{Bmatrix} \right) \tag{4.28}$$

Where, $[\mathbf{RT}]^T$ is the transpose of the orthogonal rotation matrix.

With Eq. (4.28) all nodes to be scanned can be mapped from their I-DEAS global Cartesian coordinates to the laser local Cartesian coordinates. Next, Eqs. (4.9) through (4.12) are used to transfer the laser local coordinates to the laser scan coordinates. Last, Eqs. (4.1) and (4.2) can obtained the laser scan angle. However, this is not the final step in determining a laser scan list. The scan list transformation algorithm computes the scan angles for a purely analytical test setup with no scan errors is the scan list. The following section of this thesis presents the procedure for calibrating the scanners and ASCO DC voltage sources.

4.3 Laser Scanning Equipment Calibration Procedures.

4.3.1 Basic Calibration Principle

The basis for the scan accuracy of the AMMS system was to place the laser beam on a node as accurately as an accelerometer could be placed. This translated to a linear dimension of ±12.7 mm (±0.5 in). At first thought, this may seem like a relaxed design criterion considering the laser's specification of 0.5 mm beam resolution, and the 12-bit ASCOs driving the scanners. But, for example, when testing a large structure like an aircraft fuselage, a small angular error of a few DAC steps can mis-place the beam by quite a noticeable distance. Therefore, to prevent the user from recognizing a scanning error on a large structure, an angular scan precision requirement was set a 10 DAC steps or 0.0625° pointing accuracy.

During the experimental testing phase of the scan list algorithm, it was determined that the algorithm was extremely sensitive to errors in the registration point's scan angles. Therefore, something had to be done to discover the source of and to minimize the errors in the angular measurements. The two primary sources of error in the scan angle measurement were due to the simplifying assumptions made about the hardware. First, assuming the scan angle-to-input voltage was a nominal value of 2.5° per volt proved to be a gross error. Second, assuming the ZETA DC amplitude command was identical to the true ASCO output voltage also resulted in unacceptable error in the computed scan list.

Hence, what was required was two calibration functions. The first one would transform a scan angle to a true voltage (or vice-versa). The second one would convert true voltages to ZETA amplitude commands (or vice-versa). The scan angle transformation is given symbolically by the following transformation pair:

$$V_{cmd} \Rightarrow f(V_{cmd}) \Rightarrow V_t \Rightarrow g(V_t) \Rightarrow \theta \tag{4.29}$$

$$\theta \Rightarrow g^{-1}(\theta) \Rightarrow V_t \Rightarrow f^{-1}(V_t) \Rightarrow V_{cmd} \tag{4.30}$$

Where,

V_{cmd}	=	ZETA voltage amplitude command value
$f(V_t)$	=	command voltage to true voltage transformation function
$g(\theta)$	=	true voltage to scan angle transformation function
θ	=	mirror rotation angle (scan angle)
$(^{-1})$	=	inverse of the transformation function

Equation (4.29) above is used during the node registration precess to compute the $\theta_{\bar{x}}$ and $\theta_{\bar{y}}$ from the ZETA DC amplitude commands. These two calibrated angles are then used to determine the scan list transformation matrix. Conversely, Eq. (4.30) above is used on the transformed nodes selected for measurement. It computes the ZETA amplitude commands that are written to the *project.lst* (see section 3.3) file by the LSI software. Thus, after the transformation process, the *project.lst* file contains the <u>practical</u> scan list.

The following two sections describe the experimental calibration procedures for obtaining the transformation functions $f_i(V_t)$ and $g_i(\theta)$.

4.3.2 Laser Scanner Calibration Procedure

The development of the laser scan list algorithm identified the need for a better estimate of the X and Y scanner's voltage-to-angle calibration. The nominal value provided with the VPI Sensor proved to be a significant source of error when testing the algorithm with experimental data.

The laser scanner calibration test was developed to measure the mirror rotation angle as a function of DC voltage applied to the external BNC inputs. The scanner calibration test was designed to utilize the available test equipment and to utilize simple trigonometric relationships. The scanner calibration setup is shown in Fig. 4.7. Basically, the VPI Sensor was setup perpendicular to a surface and the beam was moved along the surface with a external voltage source. By measuring the input voltage and the relative distance traveled, the angle-per-volts could be determined. From Fig. 4.7 it is easily shown that the following relations hold:

For the X scanner,

$$\theta_y(V_t) = \tan^{-1}\left(\frac{X(V_t)}{R_o}\right) \tag{4.31}$$

For the Y scanner,

$$\theta_x(V_t) = -\tan^{-1}\left(\frac{Y(V_t)}{R_o}\right) \tag{4.32}$$

The scanner calibration procedure is summarized as follows:

- A steel measuring tape was attached to a rigid wall.

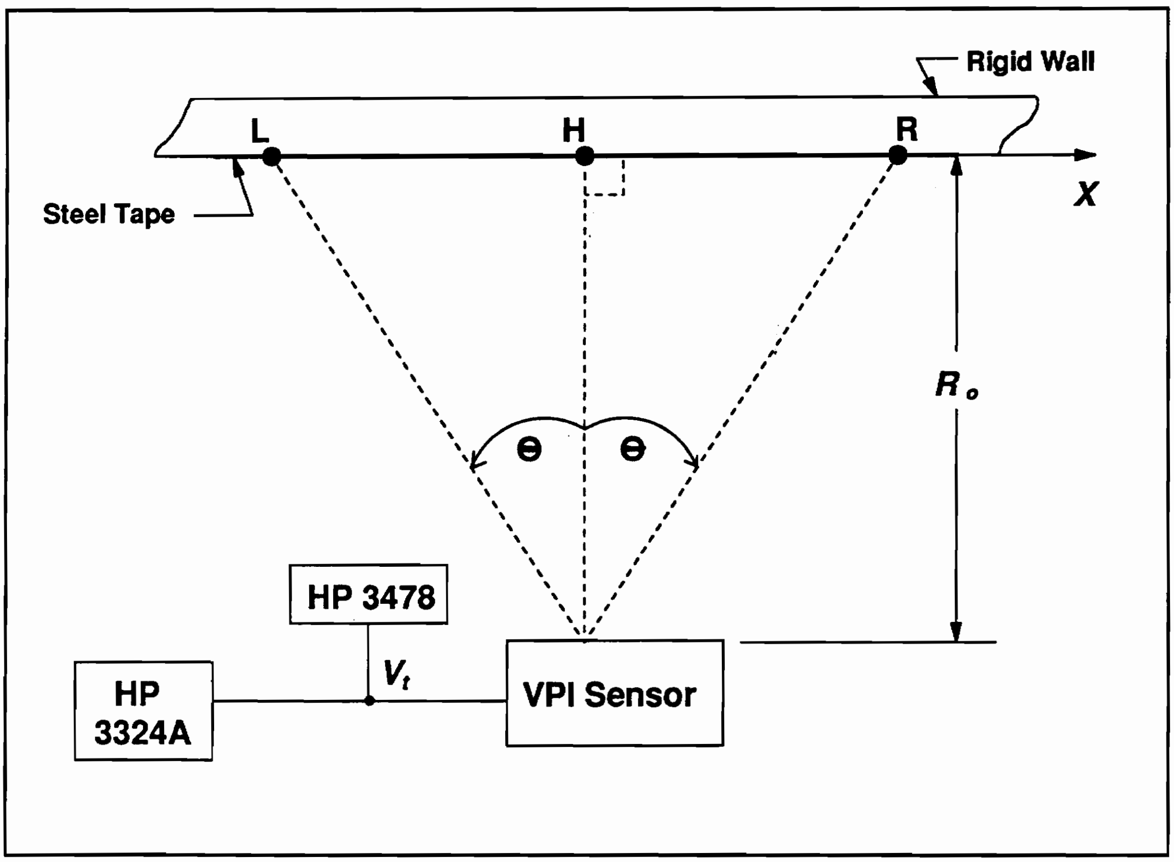

Figure 4.7 Laser Scanner Calibration Test Configuration.

- The laser head was located a distance, R_o from the steel tape. R_o was on the order of 10 m (33 ft) for a typical scanner calibration. At this distance the laser's <u>long</u> lens was required.

- In the test, R_o was designed to be as long as practical so uncertainties in its measurement would not factor into the calculated angles. Specifically, R_o was measured from the center of the tripod mounting hole on the laser-head to the wall using a surveyors tape.

- The laser head was setup as perpendicular to the wall as this crude experiment would allow. Equal ± full-scale voltages were applied to the scanners to make triangle leg L-H as nearly equal to leg R-H as possible (see Fig. 4.6).

- The laser's rear cover was removed to improve convection cooling across the scan control circuit boards and galvanometers to reduce thermal drift.

- After the laser was setup, all equipment was "powered-on" for a period of one-hour for improved thermal stability prior to taking measurements.

- The beam was stepped along the tape in 0.5 V DC increments supplied by the very stable DC voltage source in the HP 3324A function synthesizer.

- The true input voltage, V_t to the scan control circuit was measured by the HP-3478 multimeter. The HP synthesizer's amplitude LED display is not accurate enough for use in this calibration work. The impedance of the "load" on the synthesizer is only 50Ω due to the impedance matching connector. A nominal ± 5 % tolerance on the internal resistance is enough to cause the LED display to be off slightly from the true voltage output.

- The laser's X-scanner was operated through several full-right, home, full-left cycles for a complete measurement. The procedure was then repeated for the Y-scanner with the exception of traveling the full range. Due to limitations of the test facility, the Y-scanner was only calibrated to three-fifths (3/5) of full scale.

- For safety reasons, and to increase readability of the beam location on the measuring tape, a blue tinted filter was installed over the laser's aperture. This effectively decreased the laser's output power, and decreased the beam diameter.

Results of the laser scanner calibration are plotted in the following figures. In Figs. 4.8 and 4.9, the experimental calibration curve for the X and Y-scanners, respectively is shown with the data points indicated as circles. These two figures show a linear regression line drawn through the data points with its equation shown on the graph. The equations shown are of the slope-intercept form, ($y = mx + b$), where m is the slope in

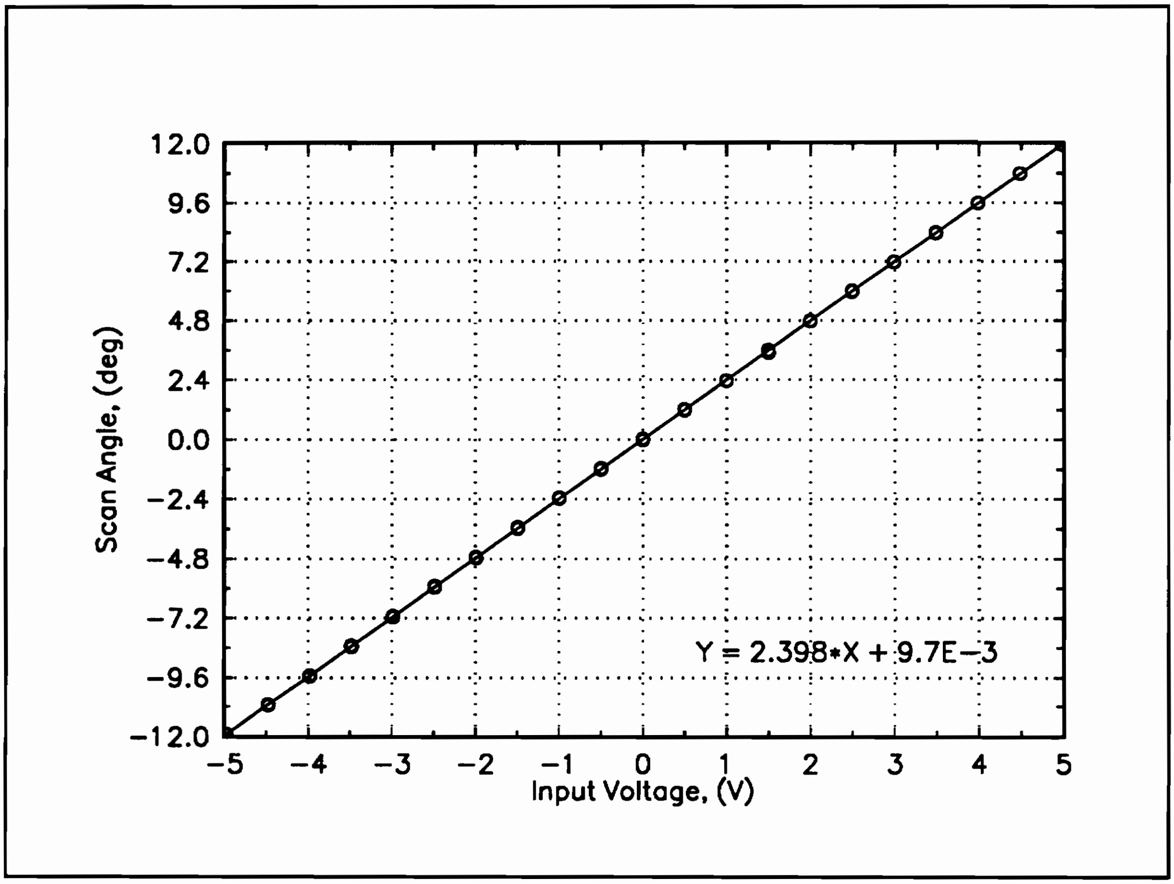

Figure 4.8 *X*-Scanner Angle-to-Voltage Calibration Curve. Linear Regression Curve Fit Equation Shown.

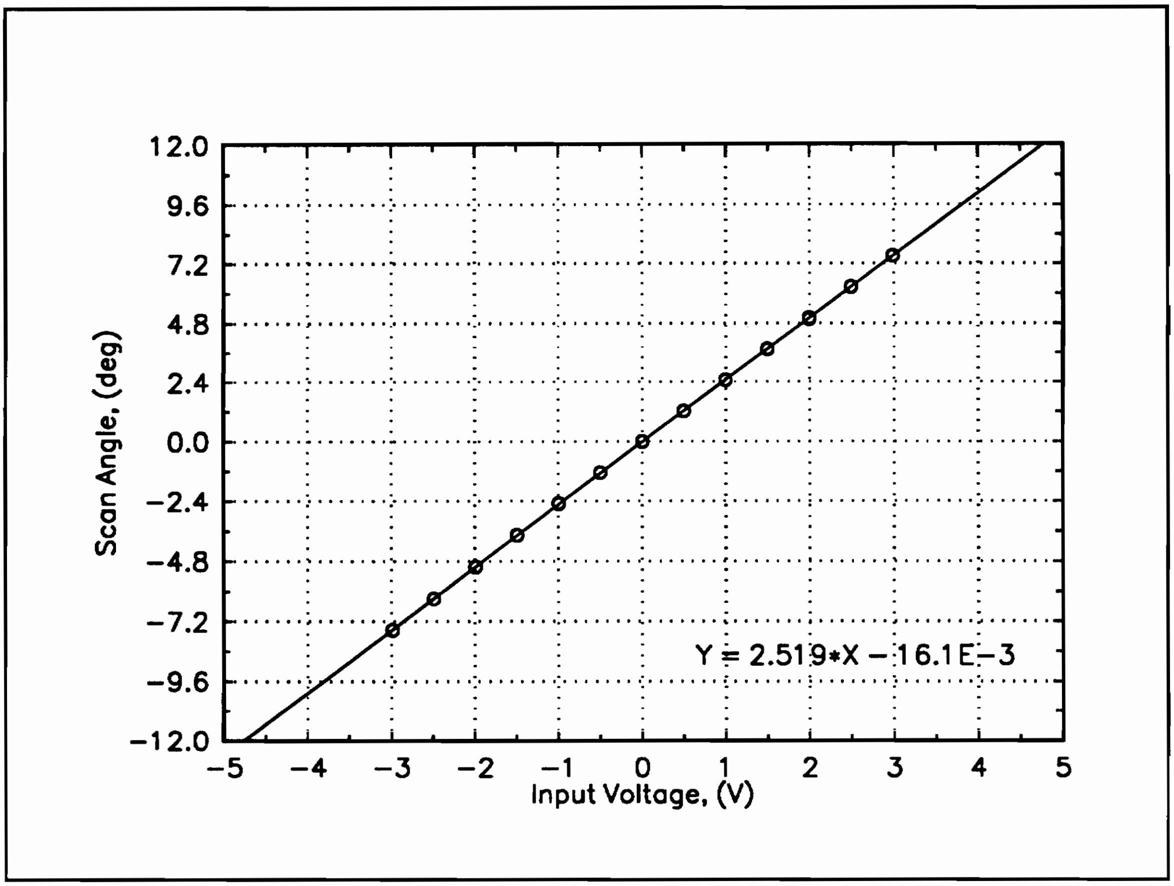

Figure 4.9 *Y*-Scanner Angle-to-Voltage Calibration Curve. Linear Regression Curve Fit Equation Shown.

units of degree-per-volt, and where b is the intercept in units of degree. The linear "fit" is very good as indicated by a computed correlation coefficient of 1.0, and typical residual values less than three DAC steps for both X and Y scanners. The residuals were later found to be due to the nonlinearity in the scanners. For example, the calibrations shown in Fig. 4.8 and Fig. 4.9 result in a true voltage-to-scan angle transformation function of:

$$g_x(V_t) = 2.398 V_t + 9.7\mathrm{E}{-3}$$

$$g_y(V_t) = 2.519 V_t + 16.1\mathrm{E}{-3}$$

During the scanner tests it was discovered that the beam did not return to the original home position after each measurement cycle. The home position shifted depending on the approach direction. This shift implied the galvanometer system had a hysteresis loop of 0.035°. Fig 4.10 is a "zoomed-in" view of the X-scanner calibration curve. This figure shows the hysteresis loop along with galvanometer thermal drift. The scan history in this figure is: 1=home, move far right, return from far right to home, 2=left-going hysteresis home, move far left, return from far left to home, 3=right-going hysteresis home, etc. It is clear that the difference in the 1 to 2 homes is a hysteresis effect. To evaluate the hysteresis as a function of time the laser was again cycled far right to a new home=4. The hysteresis is the difference between points 3 and 4 which is again about 0.035°.

The scanner calibration work also uncovered a thermal drift problem in the scanner electronics and the galvanometers. In Fig. 4.10, the difference in the homes for points 1 and 3 illustrates the thermally induced scanner drift. Additional ventilation was added

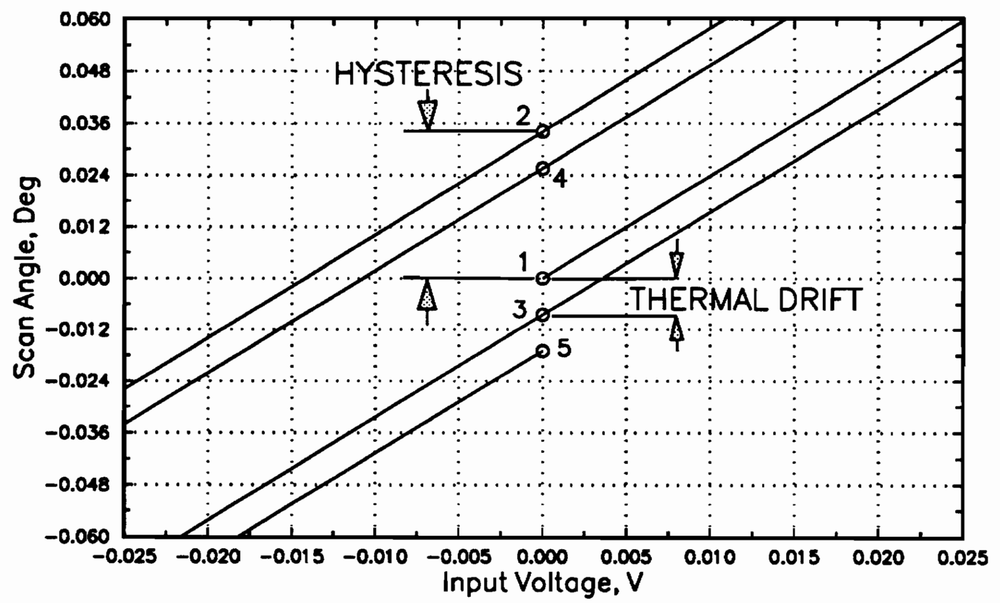

Figure 4.10 *X*-Scanner Calibration Curve, Home Region Showing Hysteresis and Thermal Drift Phenomenon.

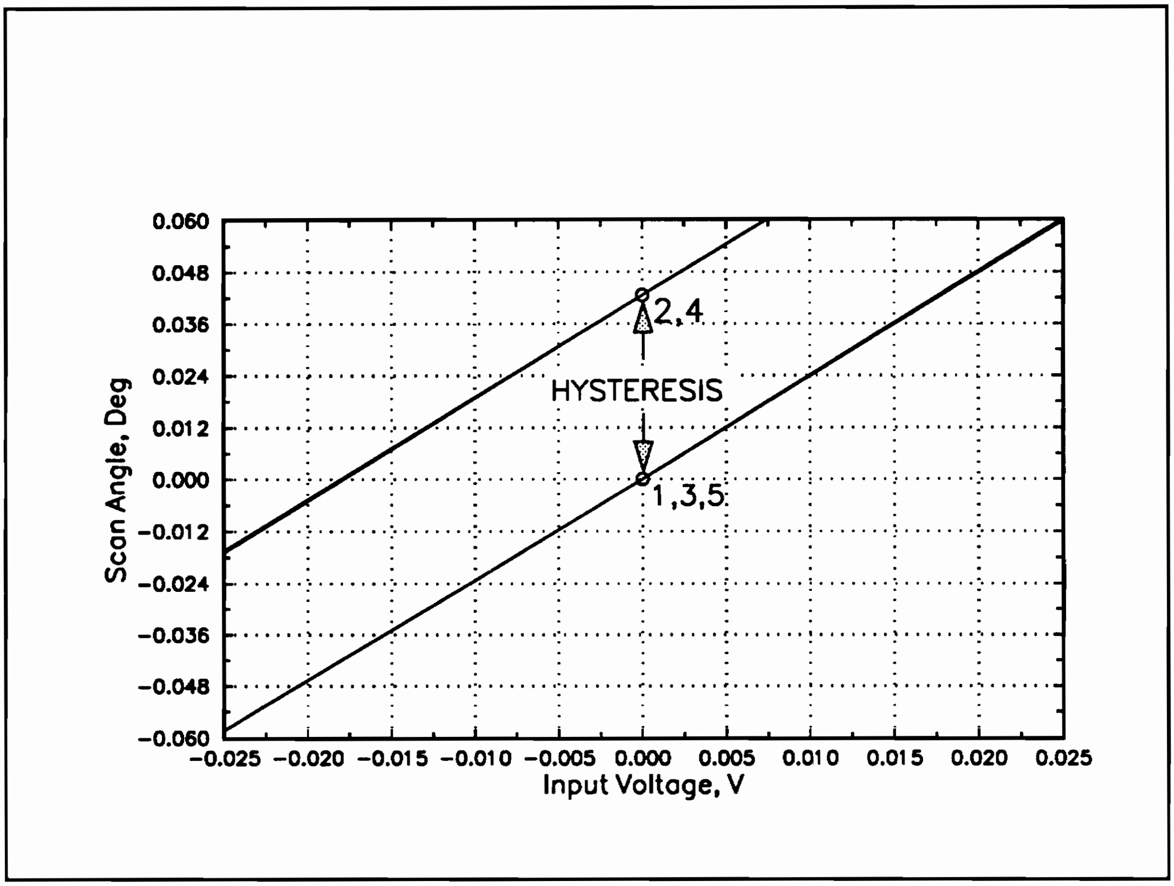

Figure 4.11 *X*-Scanner Calibration Curve, the Home Region After Improved Ventilation In Laser Housing.

to the electronics side of the laser housing to virtually eliminate the drift. Fig. 4.11 shows the "zoomed-in" view of the X-scanner calibration curve after the improved ventilation was added. In this figure, the thermal drift has been corrected but the hysteresis loop remains. The hysteresis loop is inherent in the design of the scanning system.

It is clear that the pointing accuracy of the laser is limited by the hysteresis unless a total path history is kept on each scanner after each laser start-up. This would be impractical to implement, so this residual scan error remains in the system. However, to minimize the total scan error, the rest of the scanning process was designed to minimize the additional accumulated errors. The following sections present the procedure for calibration of the rest of the scan equipment, and the methods used to minimize the scan errors.

4.3.3 ASCO DC Output Calibration Procedure

The galvanometer calibration functions only represent one-half of the scan angle-to-scan list transformation given by Eqs. (4.29) and (4.30). The second-half of the scan list transformation function relies on the ZETA DC amplitude command-to-true voltage calibration function. This relationship is required because the LSI software treats a scan angle as a DAC amplitude <u>command</u>, while the laser scanners require a <u>voltage</u> to make a scan angle.

A small calibration program was written to automatically step the ASCO channels through its 4096 DC output levels, and capture the voltage on the HPIB controlled HP 3478 multimeter. The program stored the DC voltage data in a "look-up" table file along with its ZETA amplitude command. This calibration procedure required approximately 75 minutes per-channel to complete the look-up table.

The resulting look-up table was an very large data file, and since it required nearly 2½ hours to measure both ASCO channels, a faster and simpler calibration method was desired. Therefore, a linear regression analysis was performed on both of the 4096 data point files. Another linear regression analysis was performed on a small sample of the 4096 files: the zero point, the extreme positive, and the extreme negative points. A typical example of this data is plotted in Fig 4.12 for ASCO channel 1 (X). In this figure, the slope-intercept form of the equation for the 3-point curve fit is shown. One would expect the slope of this line to be nearly one, however, the slope of the line is nearly one-half (½). This is because the voltage divider/LP-filter circuit (see Fig. 2.6) was installed for the calibration test. It was preferred to calibrate the entire ASCO output circuit with one test and represent it with one calibration function. However, this calibration method results in a unique calibration function depending on the resistance of the voltage divider circuit.

A comparison of the regression equations for the 4096 data point files and the 3 data point files was made. The difference between the 3-point fit and the 4096-point fit was found to be less than one-fifth of a DAC step at full-scale output. Thus, the 3-point method was preferred over a 4096-point curve fit, and over a 4096-point look-up table.

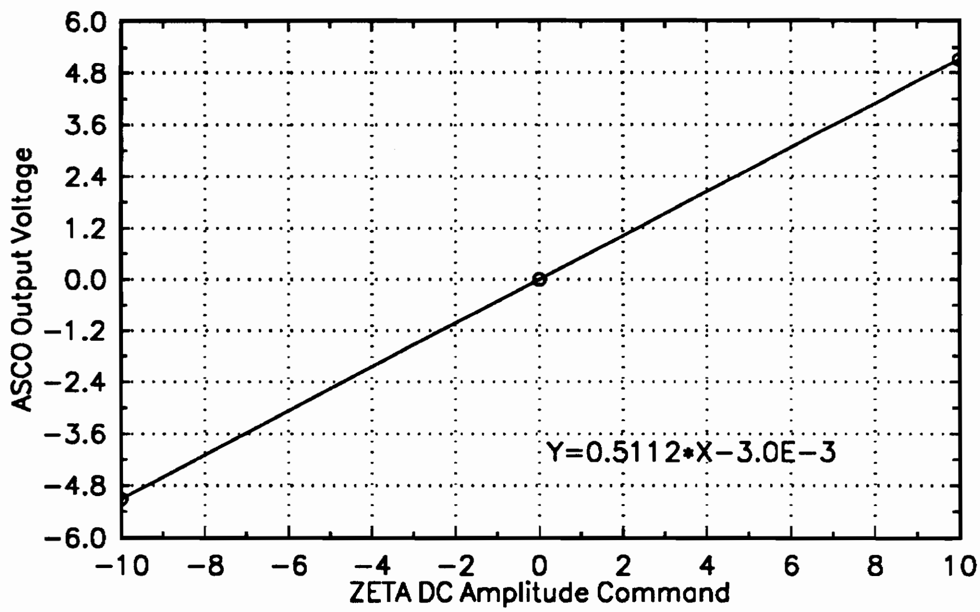

Figure 4.12 Typical ASCO Channel ZETA Amplitude Command-to-True Voltage Calibration Curve.

4.4 Laser Scan List Sensitivities

The determination of the laser position and the scan list has sensitivities to anything that will reflect itself in an angular position error. The first sensitivity is the scanner calibration. This demands a full calibration of each scanner, and each DAC as described in the previous sections of this chapter. Second, hysteresis sensitivity in inherent in the scanner design and cannot be removed with out controller redesign. To reduce the impact of the scanner hysteresis, the AMMS user is required to place the laser as close to the structure as possible so that the scanners will be forced to use as much of its scan range as possible. This results in the 0.035° of hysteresis being very small compared to the mirror deflection angles needed to target the registration points. That is, the hysteresis will be about 0.3 percent of the registration point beam deflection angle. The third sensitivity is the thermally induced drift-type (see Fig. 4.10). Over a relatively short time this could result in inconsistent angle measurements. This sensitivity was virtually eliminated by additional laser housing heat vents.

The last piece of strategy to minimized errors in the automated laser scanning is to realize that the hysteresis exists and that positioning consistency can only be obtained by approaching the target node from the same direction. Thus, when a movement to the next node is to be made, the laser is sent to a scanning origin. This origin has been established somewhat arbitrarily as the full-scale up-far right scanner position. This means that any scan node is always approached from the top down and from right to left.

No matter what the hysteresis, the strategy will at worst shift the scan set up and to the right an angular shift equivalent to the hysteresis in the respective scanners.

4.5 Laser Position Test Results

Laser Scan test on an 458 x 427 mm steel plate 2.5 mm thick resulted in a worst case scan position error of 0.88 degrees before the following issues were discovered, corrected, minimized, or worked around.

- Hysteresis evaluation
- Full-range *X* and *Y* scanner calibration
- Full-range scanner use in registration point measurement
- Use of four registration points
- Selection of the "best" laser position
- Account for the moving laser origin in the scan list algorithm development
- Use of a scanning origin from which all laser positions are approached

After the implementation of these strategies the same scanner test was performed. The new accuracy of pointing was 0.053°. This includes the 0.035° of hysteresis. This value represents a 94 percent reduction in the scan error, a significant achievement to say the least!

Chapter 5

Application of the Automated Mobility Measurement System

5.1 Line-of-Sight Velocity Correction Method

Along with the advantages of the automated scanning laser system come some constraints. The laser measures the structural velocities along its line-of-sight (LOS) to the structural target point. It is different from measurements using a conventional accelerometer. An accelerometer measures the acceleration normal to the surface of the surface of the vibrating structure. This is a major advantage as this usually conforms to an outward normal direction used in the analytical model for the test article. It is not the case for the laser system. Figure 5.1 shows the possible scan range of the laser on a simple rectangular plate structure. It is clear that the laser's measurement beam is rarely aimed exactly perpendicular to the plate. Obviously, it cannot be perpendicular to the plate at all measurement nodes from one view position. There is only one point where the laser actually measures the outward normal velocity; i.e., directly in the center of the scan area at the home position.

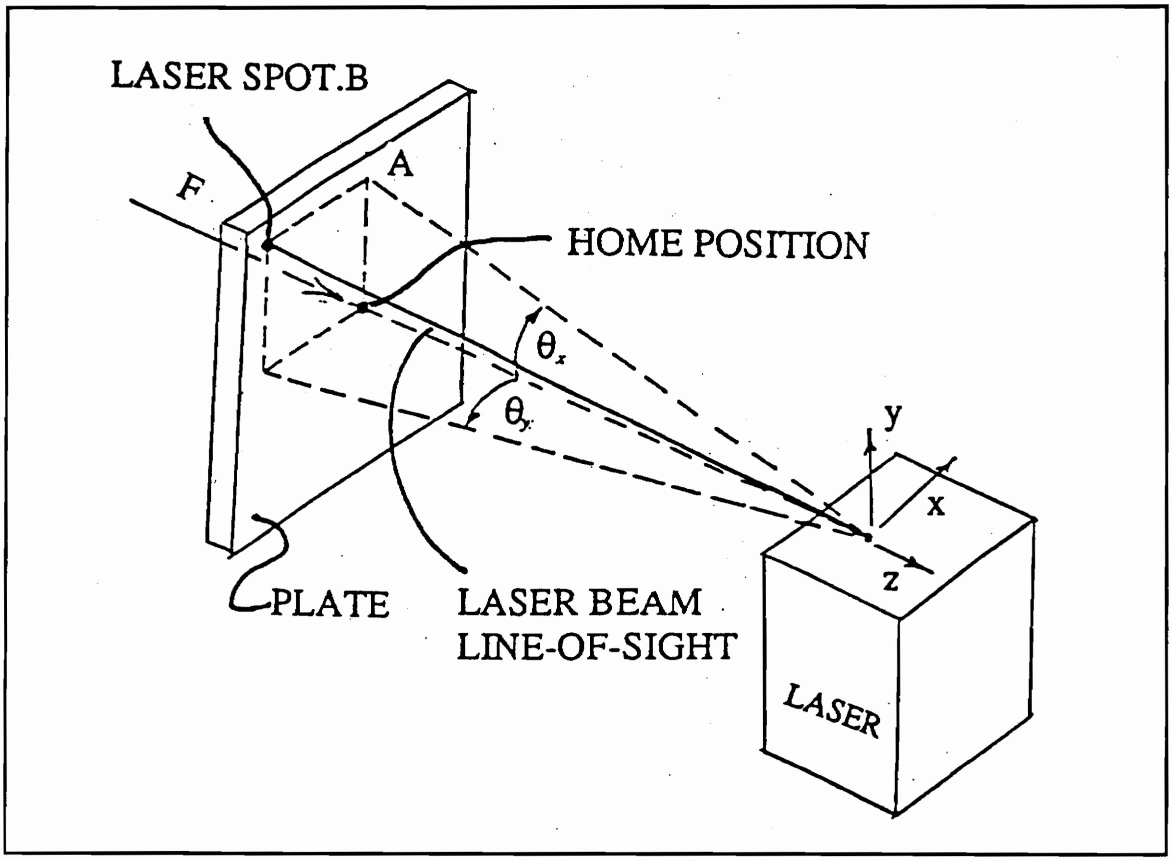

Figure 5.1 Laser-Plate Relationship Showing Line-of-Sight Measurement, (after Mitchell [39]).

If, however, one thinks of many structures and their modal motions, there is usually one dominant motion direction. Consider an aircraft wing mode. The motion is generally normal to the chordal plane of the wing. Under such circumstances the problem can be classed as a one-dimensional modal analysis problem. In those 1-D cases, the line-of-sight measurements can be corrected for the view angles involved. Reference [39] presents a method to correct the laser-based velocity measurement for the effect of the laser scan angle. For the plate example in Fig. 5.1, Ref. [39] shows the true outward normal velocity can be written in terms of the measurable LOS motion and the scan coordinates (i.e., scan angles) as follows:

$$V_z = \frac{V'_{LOS}}{\cos\theta_{\bar{x}} \cos\theta_{\bar{y}}} \tag{5.1}$$

where,

V_z = true outward normal velocity
V'_{LOS} = relative line-of-sight velocity (no laser-head motion)
$\theta_{\bar{x}}, \theta_{\bar{y}}$ = scan coordinates

From Eq. (5.1) it is clear that line-of-sight velocity is a foreshortened version of the true outward normal that is desired. The maximum deviation of the line-of-sight velocity is dependent on the allowable mirror rotation angle of the laser scanner system. With the scanners limited to ± 12.5° rotation angle, the maximum deviation of the line-of-sight velocity is given by:

$$V'_{LOS} = (\cos 12.5°)^2 V_z = 0.9532\, V_z \tag{5.2}$$

All mobility FRFs obtained with the AMMS system are corrected by Eq. (5.2) for scan angle. It is implemented as a FFT analyzer channel sensitivity that is a function of both $\theta_{\bar{x}}$ and $\theta_{\bar{y}}$. It should be pointed out that the home position should be aimed closely perpendicular to the assumed 1-D plane of vibration.

5.2 Correlated Laser Motions

5.2.1 Laser-head Motion Correction Method

Another consideration when using an LDV for velocity measurements is its sensitivity to its own motion. The laser measures the velocity of a vibrating surface relative to itself along the line-of-sight. If the laser-head is moving, the Doppler system will detect its motion along the same line-of-sight. Therefore, laser stability during the measurement is important especially if the laser-head motion (along the LOS) is highly correlated with the surface velocity of the vibrating test structure. The situation for correlated head motion can easily arise if the shaker used for the EMA is connected to the same "ground" the laser tripod is resting on. Correlated laser-head vibration could be caused by the forcing function traveling through an air-borne noise path. This vibration will phasewise add to the structure motion to yield the net output laser-measured velocity signal.

Correlated head vibration can be completely corrected for by installing a triaxial accelerometer on the laser-head itself and measuring the three acceleration components. If correlated laser-head motion is a problem in practice, however, a good estimate of the true structural velocity can be obtained with only one accelerometer located along the laser's $\bar{z}$-axis as shown in Fig. 5.2.

In Fig. 5.2, the laser itself has two velocity components shown; V_{Hx} and V_{Hz}. These motions represent an out-of-plane and one of the in-plane motions that influence the LOS velocity measurement. Velocity component V_{Hy} along the y-axis (not shown) also influences the LOS velocity measurement. General 3-axis head motion and how to correct the velocity measurement for it is presented in the following discussion.

When there is no correlated head motion, the output of the laser is equal to the line-of-sight velocity. That is,

$$V_{OUT} = V'_{LOS} \tag{5.3}$$

But, the line-of-sight vector, in general, depends on head motion. If there is correlated head motion during the experiment then $V_{OUT} \neq V'_{LOS}$. Instead, the laser output velocity is a vector sum of the line-of-sight surface velocity and the laser-head velocity components (see Fig. 5.2) given by,

$$\vec{V}_{OUT} = \vec{V}_{LOS} \pm \vec{V}_{Hz} \tag{5.4}$$

where, (dropping the vector $\rightarrow$ notation)

V_{LOS} = relative line-of-sight velocity vector <u>with</u> x and y head motion

V_{Hz} = laser-head velocity component in the outward normal direction, z

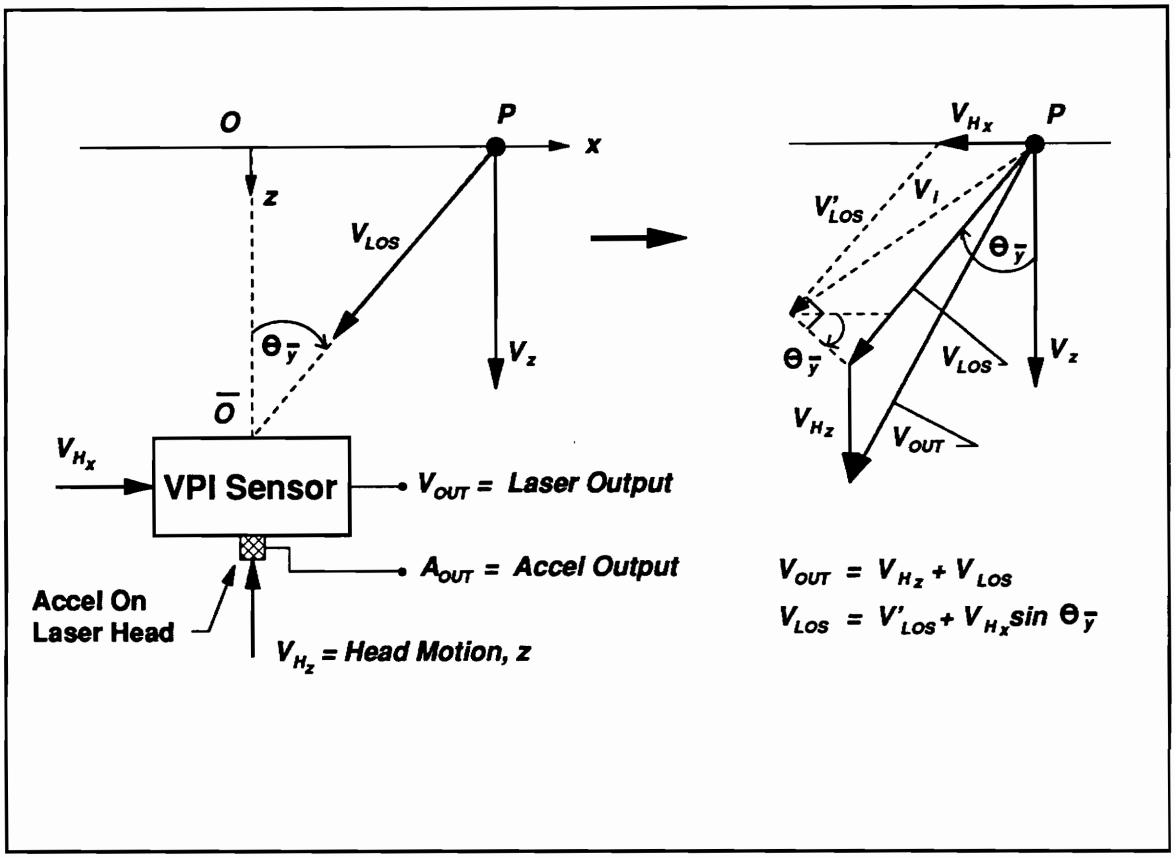

Figure 5.2 Measurement of Velocity of Point, P with Correlated Laser-Head Motion, V_{Hz} and V_{Hx}.

and where,

$$V_{LOS} = V'_{LOS} \pm \sin\theta_{\bar{y}}\left(V_{Hx}\right) \pm \sin\theta_{\bar{x}}\left(V_{Hy}\right) \tag{5.5}$$

Substituting eq. (5.5) into Eq. (5.4) and expanding gives,

$$V_{OUT} = V'_{LOS} \pm V_{Hz} \pm \sin\theta_{\bar{y}}\left(V_{Hx}\right) \pm \sin\theta_{\bar{x}}\left(V_{Hy}\right) \tag{5.6}$$

where,

V'_{LOS}	=	relative line-of-sight velocity with <u>no</u> head motion
V_{Hx}	=	correlated laser-head motion, x direction
V_{Hy}	=	correlated laser-head motion, y direction
$\theta_{\bar{x}}$	=	x scan coordinate
$\theta_{\bar{y}}$	=	y scan coordinate

By substituting the two maximum scan angles of 12.5°, Eq. (5.6) can be simplified to,

$$V_{OUT} = V'_{LOS} \pm V_{Hz} \pm \sin(12.5°)\left(V_{Hx} \pm V_{Hy}\right) \tag{5.7}$$

By substituting the true outward normal component V_z from Eq. (5.1) and again assuming maximum scan angles of 12.5°, the following equation gives the output of the laser when there is correlated motion on all 3-coordinate axes:

$$V_{OUT} = V_z\left(\cos\theta_{\bar{x}}\cos\theta_{\bar{y}}\right) \pm V_{Hz} \pm 0.2166\left(V_{Hx} \pm V_{Hy}\right) \quad ; \ \theta_{\bar{x}} = \theta_{\bar{y}} = 12.5° \tag{5.8}$$

The implication of Eq. (5.8) is that laser-head motions in the in-plane directions (V_{Hx} and V_{Hy}) are only about 21 % effective at the maximum scan angle of 12.5°; even less at smaller scan angles. While the out-of-plane component (V_{Hz}) is 100 % effective and independent of scan angle. Therefore, this is the most critical laser-head motion direction. If one can minimize the in-plane head vibrations or otherwise neglect them because they are senond order effects, then only one accelerometer is required to compensate for correlated head motion. Using one accelerometer is not the best correction procedure, but, it can improve the estimate of the FRF in a noisy environment without the need for a triaxial accelerometer, 3 additional FFT channels, and a complicated data post-processing task. This analysis assumed that there was no in-plane motions in the response; i.e. 1-D outward motion only.

5.1.2 Correlated Head Motion Model

In the preceding section of this thesis the effects of correlated laser-head motion on the LOS velocity measurement was developed. Once it has been determined that laser vibrations are effecting the FRF measurements, the following three-channel FFT analysis can be employed to approximately correct for these motions with only one accelerometer. The accelerometer as previously shown, should be mounted on the laser-head aligned with the outward normal axis (z) of the structure.

The correlated laser-head motion model is shown in Fig. 5.3. The model used in this analysis is a single-input-multiple-output (SIMO) model. It is single input because the forcing function, $F(t)$ travels through the system through two paths. First, the forcing function path through the transfer function, $H_1(f)$ is the normal excitation and structural dynamic response that we are trying to measure. Its this path that causes structural

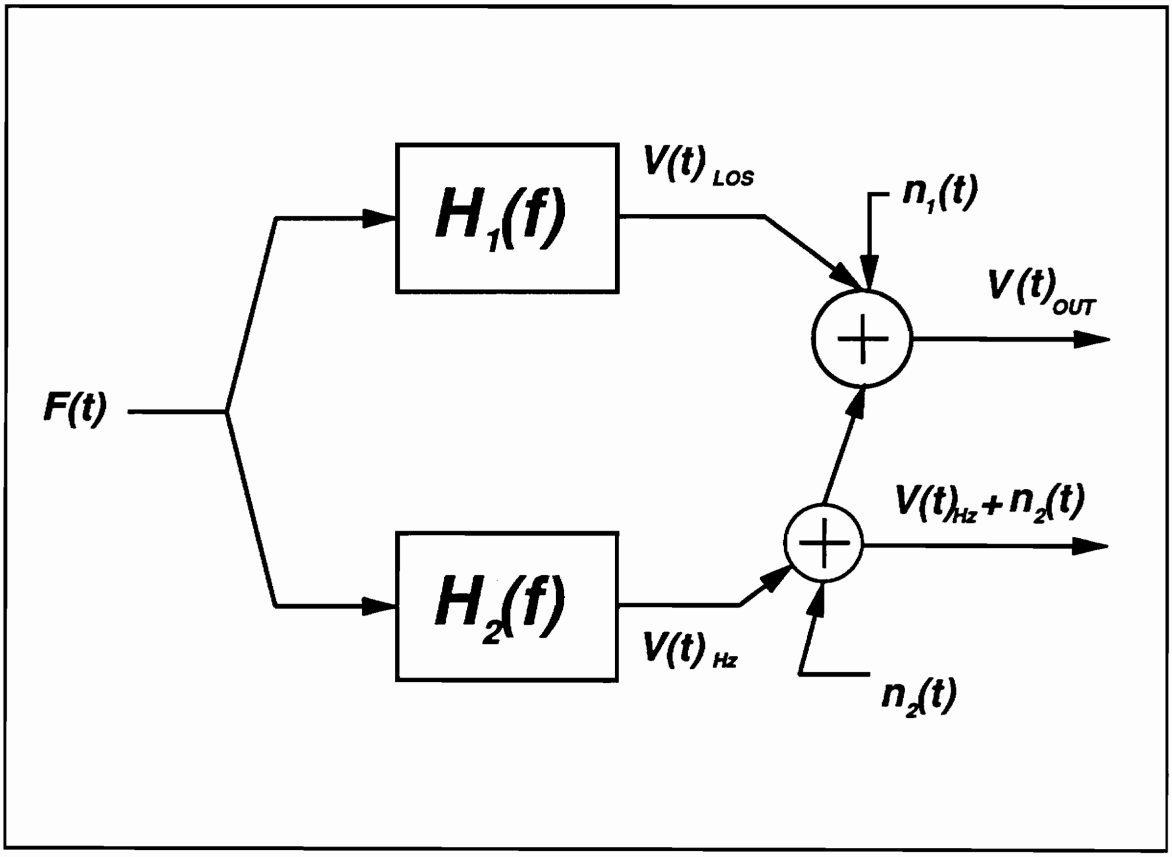

Figure 5.3 Correlated laser head motion model.

surface vibrations that are sensed by the LDV system. Second, the forcing function path through transfer function, $H_2(f)$ is the unwanted, but present force path that shakes the laser during the modal test. Since $F(t)$ travels two different path and arrives at the final summation point, it is reflected as an increase in relative velocity output of the laser, $V(t)_{OUT}$. Furthermore, since $F(t)$ originates from the same source, is very likely that the laser-head motion, $V(t)_{Hz}$ will be strongly correlated with the line-of-sight velocity, $V(t)_{LOS}$. Thus, the laser-head motion contaminates the FRF measurement of the structure that we are after. No amount of ensemble averaging will remove the bias error caused by laser-head motions. Therefore, from the previous section of this chapter, Eq. (5.8) can be written without the in-plane velocity terms as:

$$V_{OUT} = V_z\left(\cos\theta_{\bar{x}}\ \cos\theta_{\bar{y}}\right) \pm V_{Hz} \tag{5.9}$$

and by returning to line-of-sight nomenclature we have:

$$V_{OUT} = V_{LOS} \pm V_{Hz} \tag{5.10}$$

where,

$$V_{LOS} = V'_{LOS} \quad \Bigg| \begin{matrix} V_{Hx} \\ V_{Hy} \end{matrix} = 0 \tag{5.11}$$

Equation (5.10) is the same expression we started in Eq. (5.4). From here the correlated laser-head motion model can be developed. As shown in Fig. 5.3, collection of terms at the main summation point and dropping the (t) and (f) designations:

$$V_{OUT} = V_{LOS} + n_1 + V_{Hz} + n_2 \tag{5.12}$$

where, n_1 and n_2 are measurement noise terms.

From Fig. 5.3 it can bee seen that:

$$V_{Hz} = F\,H_2 \tag{5.13}$$

Now, from Eq. (5.11) we have:

$$V_{OUT} = F\,H_1 + F\,n_1 + F\,H_2 + F\,n_2 \tag{5.14}$$

Next we take the Fourier Transform of Eqs. (5.12) and (5.13) respectively and multiply both through by the complex conjugate (*) of the force channel F. Thus, we have:

$$G_{F\,V_{OUT}} = G_{F\,V_{LOS}} + G_{F\,n_1} + G_{F\,V_{Hz}} + G_{F\,n_2} \tag{5.15}$$

and,

$$H_1 = \frac{G_{F\,V_{LOS}}}{G_{F\,F}} \tag{5.16}$$

It is now evident that the two noise terms drop out of Eq. (5.15) because they are uncorrelated with the input force. From Eqs. (5.13) and (5.16) we can rewrite Eq. (5.15) as:

$$G_{F\,V_{OUT}} = G_{FF}\,H_1 + G_{F\,V_{Hz}} \tag{5.17}$$

Now, by simply rearranging Eq. (5.17), we can solve for the structure's FRF:

$$H_1 = \frac{G_{F\,V_{OUT}} - G_{F\,V_{Hz}}}{G_{F\,F}} \tag{5.18}$$

Thus, Eq (5.18) gives the one-accelerometer method for FRF corrections when the laser-head is vibrating such that its motion is highly correlated to the force channel. Note that for Eq. (5.18) the signal from the accelerometer mounted on the laser-head must first be integrated to a velocity and the laser output velocity signal should be corrected for laser scan angle given by Eq. (5.1).

The one-accelerometer correction method has one very distinct application for large aircraft structures. It would be extremely useful when the laser is place under the wing pointing upward for a measurement and when the laser is placed near the shaker support column. The shaker support column are grounded directly to the test facility in most cases. In this test situation the primary direction of correlated head motion would be along the outward normal direction.

The correlated laser-head motion equations in the preceding section were developed based on the assumption that the laser vibrations during a modal test were in some way correlated with the forcing function of the test. If the laser experiences vibrations from other sources that are not correlated with the force signal steps can be taken to minimize this effect on the FRF measurement. Transient motions caused by external events can be averaged out of the measurement if a sufficient number of measurement ensembles are acquired. The effects of other uncorrelated motions (i.e., output noise) can be minimized if the proper unbiased frequency response function estimator is used [22]. This is of H_1 and ${}^cH$ so their use is recommended when using a LDV for structural dynamics measurement. The use of H_2 is not recommended as it is a biased estimator in the presence of laser output noise.

5.2 Rectangular Plate Test: An AMMS Application

The content of this thesis has primarily been focused on the development of laser-based automated mobility measurement system for structural dynamics measurement. However, in this section of the thesis an application of the AMMS is discussed. The mobility measurement task first requires that an I-DEAS Test model of the test structure be developed. Figure 5.4 shows the I-DEAS wireframe model of a 458 x 427 mm flat rectangular plate of thickness 2.5 mm. The model has conventional node numbering along with a Test established global Cartesian coordinate system with its origin located in the center of the plate at node N61. The rectangular plate model shown has 121 nodes defining its geometry. The model also has 4 nodes added in the center to identify the location of one non-symmetric threaded hole and a node each of the four corners 25.4 mm from each edge that also identifies threaded mounting holes. Thus, the total number of nodes in this plate model is 129 (121 regular nodes + 3 connectivity nodes, + 5 "hole" nodes). The plate model geometry and connectivity listing is stored in the Universal file format so that it can easily be read into the AMMS by the LSI software.

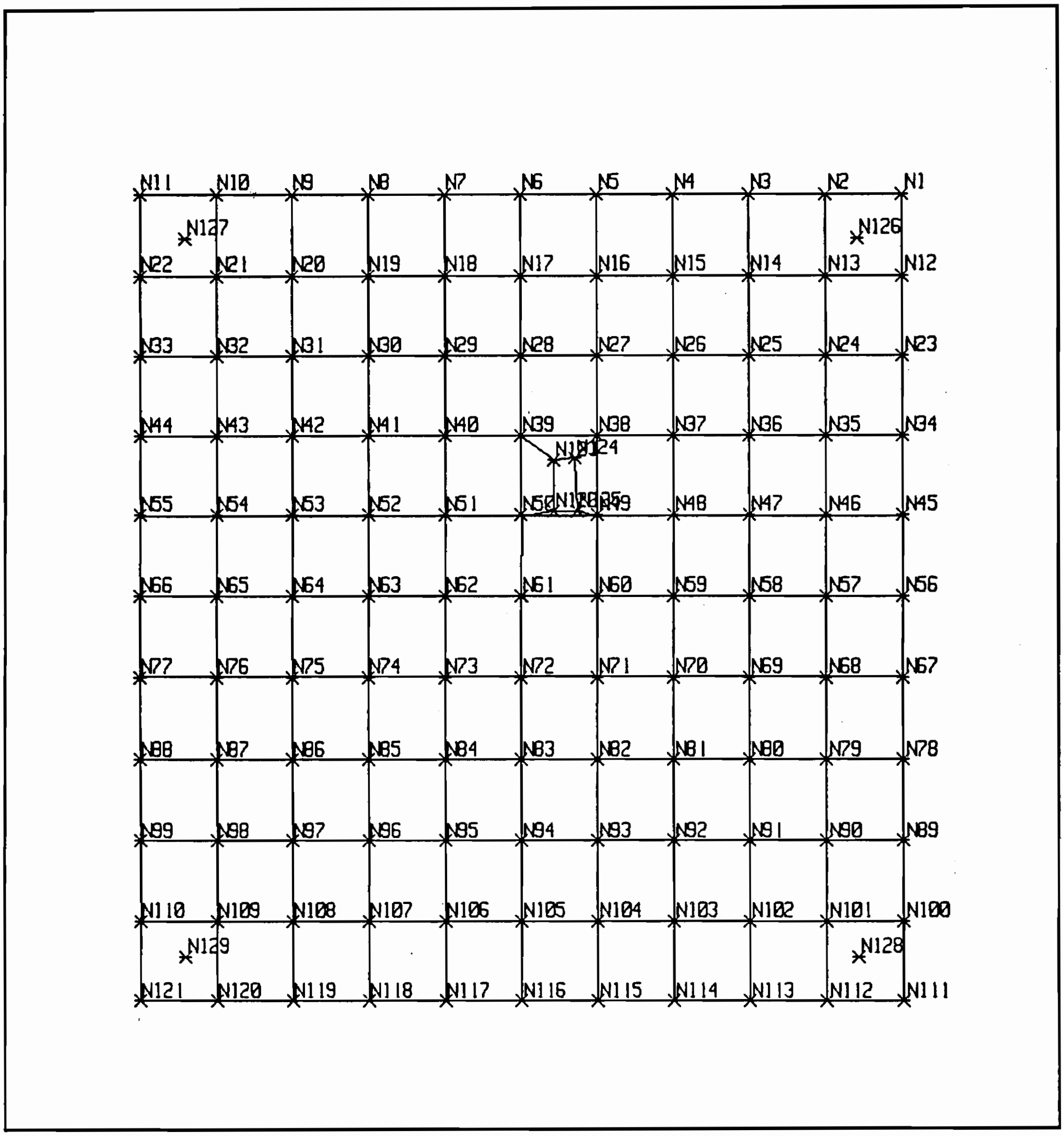

Figure 5.4 I-DEAS Test Wireframe Model of a 458 x 427 mm Steel Plate with Node Numbers Shown, (after Agee, [29]).

Once the plate geometry was modeled, the actual plate was setup for the experimental modal test. In general, the plate was tested with free-free boundary conditions. Four widely spaced nodes near the outer boundary of the plate were selected as reference points. Here nodes N13, N21, N101, and N109 were selected and used as the registration points. The laser was place approximately 1.2 m in front of the plate which would allow for a full-view of the plate from one laser location. This setup also forced the scanners to use at least 80 percent of their full-scale deflection during the critical registration point logging process. Next, the LSI software determined the laser position relative to the Test coordinate system. The nodal transformation matrix was computed and applied to a second Universal file containing only the node numbers selected for scanning. Finally, a scan list was developed and the automated acquisition sequence was initiated.

To begin the test, a shaker and force gage was attached through an adhesive mounting base at node N14.

5.3 Typical Results of a Plate Mobility FRF Measurement

The first structure tested with the AMMS system is the flat rectangular plate described in the preceding section. To begin the experimental measurement it was decided to keep the excitation frequency relatively low because the plate was known to have many resonances below 500 Hz. An FFT analysis range of 0 to 300 Hz was selected for the first test. Other test parameters included the use of a burst random excitation signal, an exponential window, and FFT averages of 15 data ensembles. The analyzer setup included triggered input on the force channel with a 2 % pre-trigger value, autoranging full-scale voltage of the ASCIs, and input overload monitor and reject enabled.

The typical laser-based mobility FRFs and associated coherence function measurements are shown in Figs. 5.5 through 5.7. The figures show FRFs with coherence for three different response point locations (same driving point, node N14) for the rectangular plate example described above. Figure 5.5 shows the important driving point mobility at node N14. Notice that the coherence function is very high for this measurement except at the antiresonances where the surface velocity response is very low and the signal at these frequencies contain very little structural dynamic information; mostly noise. Figures 5.6 and 5.7 show other typical FRF and coherence function measurements for response location N28 and N61 respectively. The coherence function in Fig 5.6 again is low at the antiresonances. If there is a concern about the accuracy of the FRF in these regions, then further averaging may be used or the complex FRF estimator, ${}^{c}H$, may be used to determine the structure's FRF. ${}^{c}H$ was not implemented in the AMMS system when these plate FRF measurements were taken. Figure 5.7 shows yet another quality laser-based FRF and coherence function measurement at node N61.

In a experimental modal test that followed later on the same rectangular plate structure the analysis frequency was increased to a upper frequency of 600 Hz. The plate was changed slightly from the test described above because an accelerometer was attached on

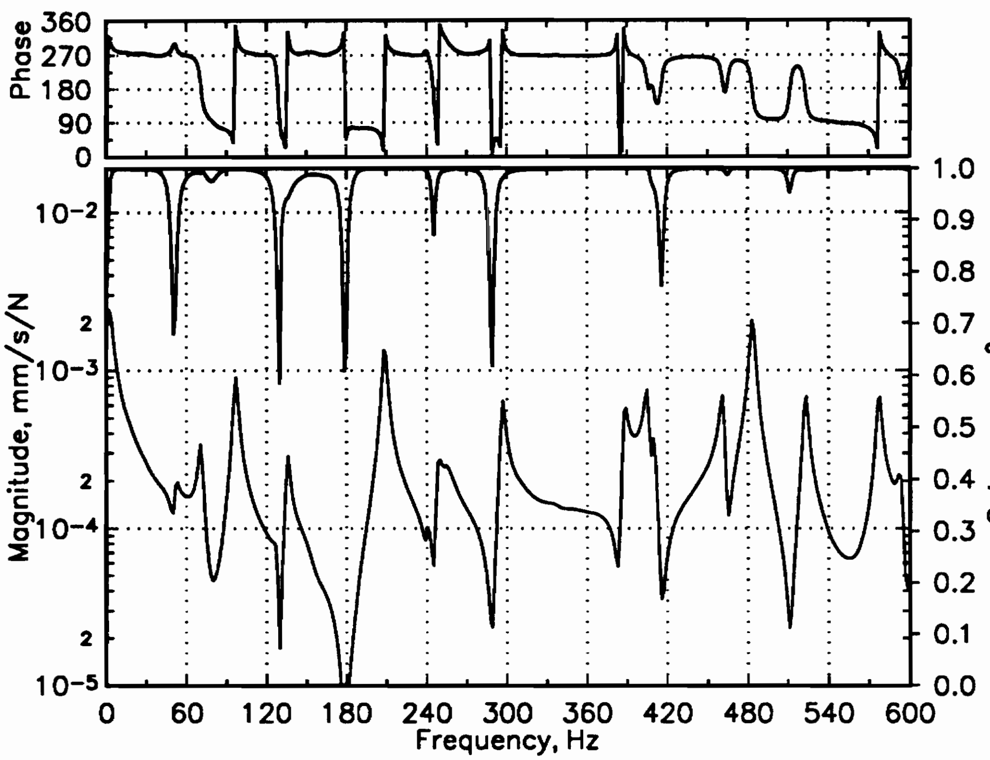

Figure 5.5 Laser-Based FRF and Coherence of a Rectangular Plate, Driving Point - N126, Response Point - N26.

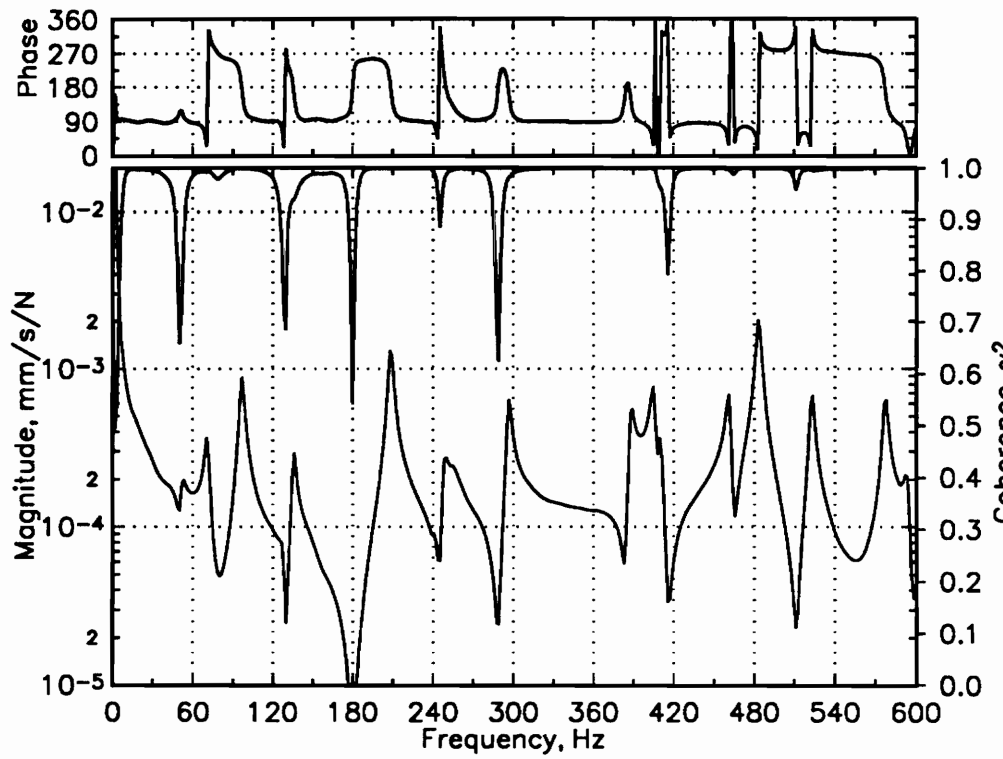

Figure 5.6 Accelerometer-Based FRF and Coherence of a Rectangular Plate, Driving Point - N126, Response Point - N26.

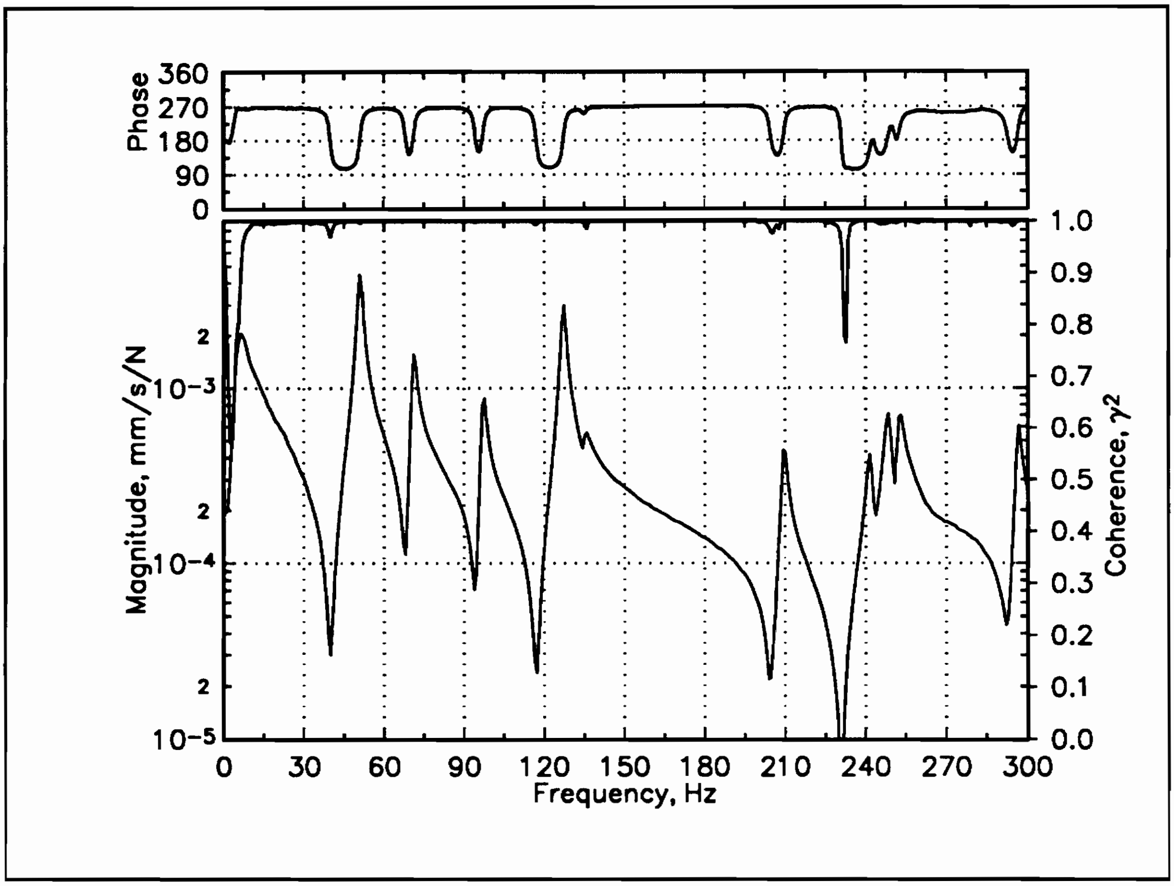

Figure 5.7 Laser-Based FRF and Coherence of a Rectangular Plate, Driving Point - N14, Response Point - N14.

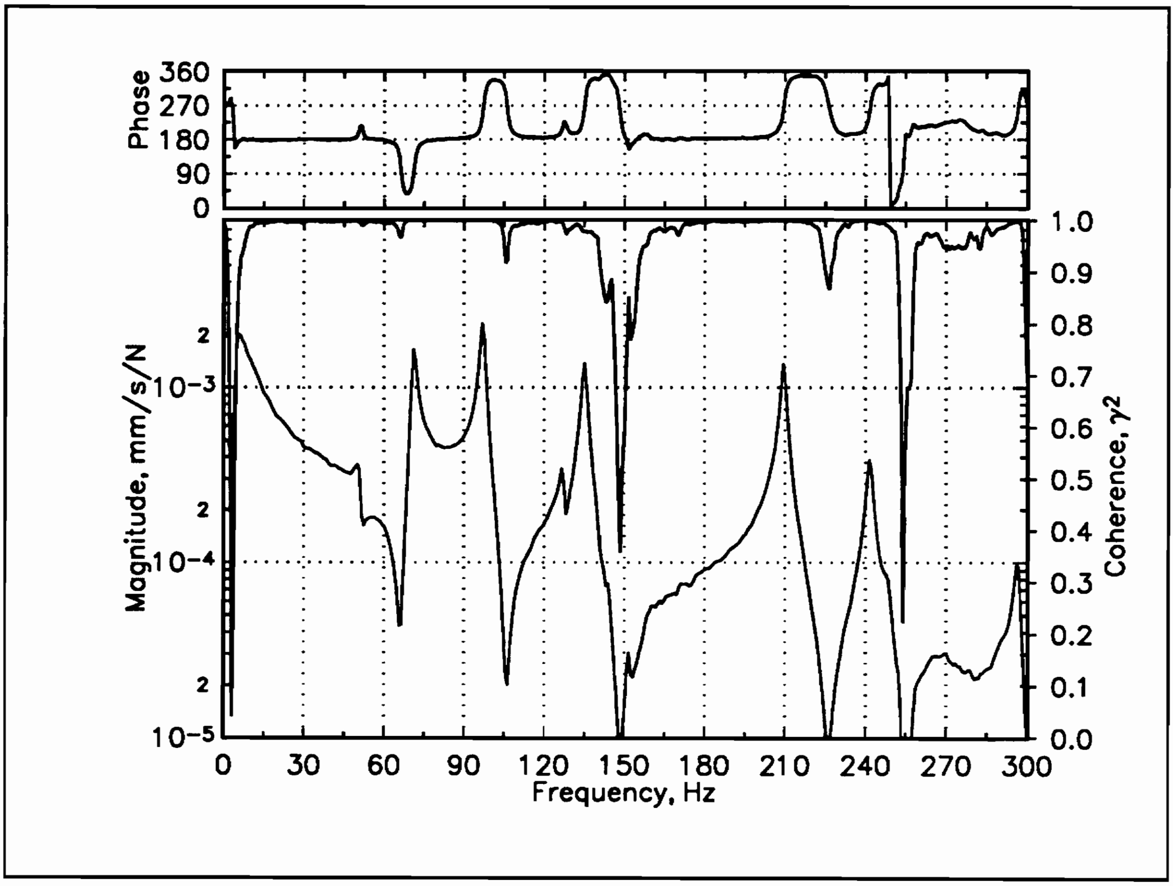

Figure 5.8 Laser-Based FRF and Coherence of Rectangular Plate, Driving Point - N14, Response Point - N28.

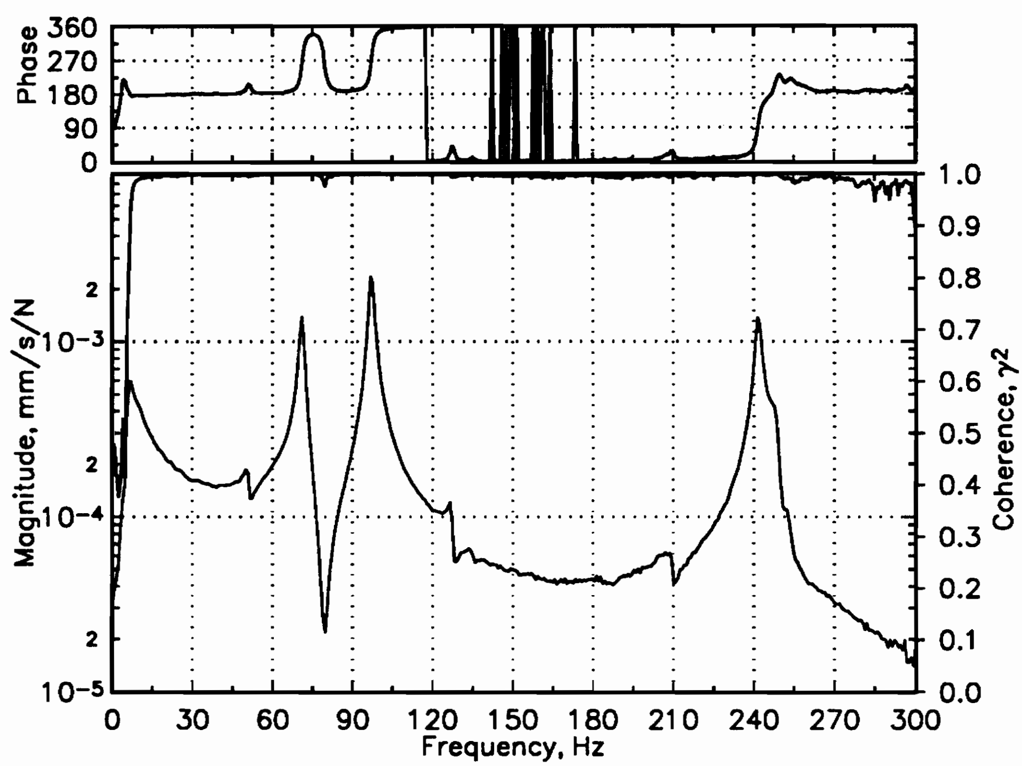

Figure 5.9 Laser-Based FRF and Coherence of a Rectangular Plate, Driving Point - N14, Response Point - N61.

the back side at node N26 and the driving point was moved to node N126. Figure 5.8 shows the laser-based mobility FRF measurement and coherence function for this test. Again, the coherence was very high except in the antiresonances. Figure 5.9 shows the associated accelerometer-based FRF measurement (integrated to mobility). Notice that the coherence function is very similar to the coherence in the previous laser FRF of Fig. 5.8. In fact, even when the two figures are overlaid, it is difficult to determine one from the other. These two figures provide only one example of a laser-based FRF compared to an accelerometer-based FRF, but it demonstrates that quality FRF data can approach that of conventional accelerometers.

Chapter 6

Conclusions and Recommendations

6.1 Conclusions

The purpose of this research was to develop the first product in a series of laser-based high technology products for structural dynamics measurement and analysis. The automated mobility measurement system (AMMS) presented in this thesis introduced a new concept involving the linking of a scanning laser Doppler velocimeter to a conventional computer-controlled multichannel FFT processor. This instrumentation complex was automated and integrated by development of the hardware controlling software entitled Laser Systems Integrator (LSI). LSI was developed as a user-friendly, logically organized, and menu-driven engineering tool for automated modal testing. The automated laser system further depends on the geometric modelling capabilities of a popular commercial engineering software package; I-DEAS Test. The post-processing support for the AMMS system is also provided by I-DEAS Test modal analysis capabilities.

This laser-based AMMS system allows non-contacting structural dynamic measurements to be made in industrial-type environments differing from typical measurement laser holographic methods. Simple experimental setup is a key feature of this system. The AMMS system provides for large scale modal testing without the need for hundreds of accelerometers, charge amplifiers, cables, and simultaneous acquisition channels; thus, the system makes the task of FRF measurement more efficient for large modal tests. A major advance in the implementation of this system is that the very time-consuming task of acquiring mobility FRF data for modal analysis can be automated, thus, relieving expensive staff of the tedious measurement task and perhaps allowing them more time for data collection or data analysis.

AMMS system features like lack of mass loading the structure, of multiple transducers, of the time required to detach, move, and reattach transducers, of having to instruct the FFT processor to acquire data, of having to do all the bookkeeping of FRF information, and of having to direct the measurement results to the modal analysis software, accumulates time savings that result in a very efficient data acquisition and modal analysis interface system.

6.2 Recommendations for Future Work

There are various issues involved with the precision of the scanning system used in the AMMS system that require attention. Therefore, the following recommendations are made for development of the AMMS system into a commercially viable engineering tool.

- The System 7000 ASCO's do not consistently come on-line with the same command-to-voltage calibration each time. It was determined that the ASCO's need to be calibrated each time the unit is turned-on. Errors on the order of 13.5 DAC steps at full-scale can occur if this is not done. The present work-around solution is to calibrated them once and leave the System 7000 powered-on continuously. The recommended action is:

  a.) Include a DC digital voltmeter with IEEE-488 (or RS-232) interface that can be used to automatically calibrated each ASCO upon system start-up. A 3-point slope-intercept calibration is sufficient to characterize the command-to-voltage relationship. Or,

  b.) Correct the problem at the source. Redesign the System 7000 DC output to come-up stable and consistent from unit-to-unit and from start-up to start-up. This appears to be the best long-term solution to alleviate this problem.

- The hysteresis in the scanner galvanometers must be calibrated with each laser unit and the full-scale angular deflection must be determined or controlled. Presently the least squares regression line through the zero-full right-hysteresis zero-full left-zero data set should be used during the reference point setup while the full right-hysteresis zero data set should be used to determine the calibration during scanning. This difference is caused by the use of a "scanning origin" or reference point at the full right-full up scan position. The scan will always come at the node point from the same direction. The recommended action is:

a.) Calibrate the scanners for every production unit. There is some concern that this calibration may change over time (or usage). Since the hysteresis maybe caused by friction in the galvanometer bearings, the friction may change as the instrument bearings wear-in. Or,

b.) Install a set of integral feedback controllers for the scanners. These controllers must also include a scanner thermal blanket temperature controller that can reduce the thermal drift by a factor of 10. This appears to be the best long-term solution to eliminate the hysteresis and thermal drift problems.

- The accuracy of the scanning depends upon the angular separation of the registration points on the structure. To minimize the effect of scanner hysteresis on the scan list, the laser should be placed close enough to the structure so that the angular separation angle in at least one direction during the registration point logging procedure is at least 20°, but less than or equal to 25°. Additionally, for improved laser measurement performance from difficult surfaces the laser should be place at one of its optimum working distances from the structure. Action recommended is:

a.) Add a subroutine to the LSI software after the registration point selection panel and prior to registration point logging task that computes the upper-bound laser range, $R_{L,max}$ from the laser to the structure using the largest of:

$$R_{max,x} = 2.84\,\Delta X_{max} \tag{6.1}$$

$$R_{max,y} = 2.84\,\Delta Y_{max} \tag{6.2}$$

$$R_{L,max} = \max\left(R_{max,x}\ ;\ R_{max,y}\right) \tag{6.3}$$

The lower-bound laser range, $R_{L,min}$ from the laser to the structure should be set at:

$$R_{min,x} = 2.26\,\Delta X_{max} \tag{6.4}$$

$$R_{min,y} = 2.26\,\Delta Y_{max} \tag{6.5}$$

$$R_{L,min} = \max\left(R_{min,x}\ ;\ R_{min,y}\right) \tag{6.6}$$

where ΔX_{max} and ΔY_{max} are the maximum global Cartesian distances between the registration nodes.

It is recommended that the laser be placed at any one of the optimum working distances, d listed in the VPI Sensor documentation [16] or given by:

$$d = 1700 \pm n \times 210 \quad \text{mm}, \qquad n=0,1,2,... \tag{6.7}$$

User prompts should be added to the LSI program to use optimum working distances (these can be listed for the user), to use registration points as far apart as practical, and to "group" nodes to scan inside the area defined by the registration nodes.

- Finally, the last recommendation is associated with the application of the laser-based AMMS system to large structures like an aircraft fuselage or other aerospace structure. The problem of precision scanning is amplified at the long distances required for testing the structure. These applications require more stringent specifications; thus, demanding more precise measurements and laser beam control. It is recommended that the feasibility of a high-resolution scanner version of the AMMS system be studied. It is visualized that this model of the AMMS system would incorporate the improved scanner control, the corrections for scanner nonlinearity, and the laser-head motion correction algorithm presented in Chapter 5 of this thesis.

List of References

1. Mitchell, L. D., A. L. Wicks, and R. L. West, "Structural Imaging Using Laser Technology," *Department of Mechanical Engineering Research Proposal Number 90-1622-04*, Virginia Polytechnic Institute and State University, Blacksburg, Virginia, April 1990.

2. Hurst, C. J., C. E. Knight, and L. D. Mitchell, et al, *Investigation of the Potential for Noise Reduction of a Reciprocating Compressor*, January 1, 1990 to August 15, 1990, Department of Mechanical Engineering, Virginia Polytechnic Institute and State University, Blacksburg, Virginia.

3. Hunt, D. L., S. P. Weiss, W. M. West, et al, "Development and Implementation of a Shuttle Modal Inspection System," *Sound and Vibration*, Vol. 24, No. 8, August 1990, pp. 34-42.

4. West, W. M., "Illustration of the Use of Modal Assurance Criteria to Detect Structural Changes in Orbiter Test Specimens," *Proceedings of the International Modal Analysis Conference IV*, Vol. I, Kissimmee, Florida, February 1986, pp. 1-6.

5. Tranter, J. T., "The application of Computers to Machinery Predictive Maintenance," *Sound and Vibration*, Vol. 24, No. 12, December 1990, pp. 14-19.

6. Oliver, D.E., and Jaeger, P. E., "A Unique Laser Doppler Vibrometer: Role in Design an Non-Destructive Testing," *Proceedings of the 37th International Instrument Symposium*, San Diego, California, Instrument Society of America, May 1991, pp. 11-21.

7. Barker, A. J., Jaeger P. E., and Oliver, D. E., "Non-contacting Vibration Measurement: Role in Design and Industrial Applications," *Proceedings of the 3rd International Conference of Stress Analysis by Thermoelastic Techniques*, Vol. 1084, March 1989, p. 293

8. Zonic Corporation, "System 7000 Parallel Signal Processor," *Bulletin No. 7000-S89-5M*, Milford, Ohio, 1989.

9. Hewlett Packard Company, "HP 3565S Multichannel Measurement System," *Test and Measurement Catalog*, Santa Clara, CA 1991.

10. PCB Piezotronics, *Smart Sensing*, Company Catalog G-500 and Supplement to Catalog G500, Depew, NY, November 1991.

11. PCB Piezotronics, *Modal Array Sensing Systems: Structcel, Flexcel and Data Harvester*, Company Brochure No. SFDH890, Depew, NY, August 1990.

12. Tektronix Inc., *SI5010 Programmable Scanner*, Company Brochure No. 3SI-6464, Beaverton, Oregon, August 1990.

13. Tektronix Inc., *Fastscan 2600FS Software*, Company Brochure No. 3JW-7878, Beaverton, Oregon, October 1990.

14. PCB Piezotronics, *ICP Sensors for Dynamic Measurements*, Company Catalog SF-20, Depew, NY, September 1991.

15. Ometron Limited, "Random/Service Data Acquisition Software," *VPI Vibration Measurement Technical Note*, No. 4/9320/1/3590, London, England. 1990.

16. Ometron Limited, *VPI Sensor Operators Manual*, London, England, 1987.

17. Dossing, O., *Structural Testing Part 1: Mechanical Mobility Measurements*, Bruel and Kjaer, Company Document No. BR0507-11, Naerum, Denmark, April 1988.

18. Bendat, J. S., and A. G. Piersol, *Random Data: Analysis and Measurement Procedures*, 2nd ed., John Wiley-Interscience, New York 1986.

19. Sharpton, W. R., and A. L. Wicks, *Experimental Modal Analysis*, Seminar, 1988 SAE International Congress & Exposition, Detroit, MI, March 1988, Sponsored by The Society of Automotive Engineers, Continuing Education, Warrendale, Pennsylvania.

20. Hewlett Packard Company, *The Fundamentals of Signal Analysis*, Company Application Note 243, Santa Clara, CA, 1989.

21. Mitchell, L. D., "Concepts in Mechanical Mobility and Impedance," *Supplement to Mobility and Impedance Program Users Guide*, ed. 1.1, Mechanical

Engineering Department, Virginia Polytechnic Institute and State University, March 1987.

22. Wicks, A. L., and L. D. Mitchell, "Methods for the Estimation of Frequency-Response Functions in the Presence of Uncorrelated Noise, A review," *International Journal of Analytical and Experimental Modal Analysis*, Vol. 2, No. 3, July 1987, pp. 109-112.

23. Mitchell, L. D., "An Improved Method for the Fast Fourier Transform (FFT) Calculation of the Frequency Response Function," *Proceedings of the First European Signal Processing Conference EUSIPCO-80 - Short Communication and Post Digest*, Swiss Federal Institute of Technology, Lausanne, Switzerland, September, 1980, pp. 159-160.

24. Mitchell, L. D., "Improved Methods for the Fast Fourier Transform (FFT) Calculation of the Frequency Response Function," *Journal of the Mechanical Design, Transactions of the ASME*, 104, April, 1982, pp. 277-279.

25. Agee, B. L., A. D. Kelly, and L. D. Mitchell, "Finite Element Model Updating Using Laser-Based Experimental Dynamics for Noise Prediction Purposes," *Proceedings of the 1991 National Conference on Noise Control Engineering*, Tarrytown, New York, July 1991, pp. 657-666.

26. Dossing, O., "The Prediction of Transducer Mass-Leading Effects and Identification of Dynamic Mass," *Proceedings of the International Modal Analysis Conference IX*, Vol. I, Florence, Italy, April 1991., pp. 306-312.

27. Wicks, A. L., A. Kubler, and M. Insalaco, "A Comparison of Angular Acceleration and Translational Acceleration Measurements on a Free-Free Beam," *Sensors, Journal for Machine Perception*, Vol. XII, No. 2, May, 1989

28. Sun F. P., and L. D. Mitchell, "Two-Dimensional Velocity Data Smoothing and Structural Angular Velocity Extraction Using a DFT-IDFT Technique," *Proceedings of the Thirteenth Biennial ASME Conference for Mechanical Vibration and Noise*, Miami, Florida, September, 1991, pp 303-309.

29. Agee, B. L., X. Zeng, L. D. Mitchell, and M. Schiefer, "An Automated Mechanical Mobility Measurement System for Acquiring Data for Experimental Modal Analysis," *Proceedings of the International Modal Analysis Conference X*, San Diego, CA, February 3-7 1992, pp. 211-218.

30. Smith, R. J., *Circuits, Devices, and Systems*, 4th ed., John Wiley & Sons, New York, 1983.

31. Zonic Corporation, *ZETA Software: The Language of the System 7000*, Company Brochure No. ZETA(10M)690, Milford, Ohio, June, 1990.

32. Halliday, D., and Resnick, R., *Fundamentals of Physics*, 2nd ed., John Wiley & Sons, New York, 1981.

33. Drain, L. E., *The Laser Doppler Technique*, John Wiley & Sons, New York, 1980.

34. Awa, T. W., and L. D. Mitchell, "Year 1 LSI Software Development," *Department of Mechanical Engineering Laser Project Technical Report*, Virginia Polytechnic Institute and State University, Blacksburg, Virginia, September, 1991.

35. Jones, O., *Introduction to the X Window System*, Prentice-Hall, New Jersey, 1989.

36. Zeng, X., L. D. Mitchell, and B. L. Agee, "The Determination of the Scanning List for A Laser-Based MObility Measurement System: Algorithm and Implementation," *Department of Mechanical Engineering Technical Report to Zonic Corporation*, Virginia Polytechnic Institute and State University, Blacksburg, Virginia, January 1992.

37. Anton, H., *Elementary Linear Algebra*, 4th ed., John Wiley & Sons, New York, 1884, pp. 189-220.

38. Walpole, R. E., and R. H. Myers, *Probability and Statistics for Engineers and Scientists*, 3rd ed., Macmillian Publishing Company, New York, 1978, pp. 315-352.

39. Mitchell, L. D., K. Kochersberger, and R. L. West, "Measurement of a One-Dimensional Mobility Using a Laser-Doppler Velocimeter," *Proceedings of The Society of Experimental Mechanics Spring Conference*, Milwaukee, WI, June 10-13, 1991, pp. 846-853.

Vita

Barry L. Agee was born on August 31, 1962. He grew up in Floyd, Virginia and in June, 1980 he graduated from Floyd County High School. He attended New River Community College in Dublin, Virginia and graduated Magna Cum Laude with an Associate in Applied Science degree in Drafting and Design Technology in May, 1982. In July, 1982 he began working at Newport News Shipbuilding in Newport News, Virginia as a designer in the Submarine Overhaul Design Department. In August, 1987 Barry enrolled at the Virginia Polytechnic Institute and State University, in Blacksburg, Virginia. He graduate Cum Laude with a Bachelor of Science in Mechanical Engineering degree in May 1990. Based on his achievements as and undergraduate research assistant, he was awarded a two-year scholarship by the Virginia Center for Innovative Technology for graduate study. In May, 1990 Barry began his graduate work at Virginia Tech and in February, 1992 he completed the requirements for the degree of Master of Science in Mechanical Engineering. Upon leaving Virginia Tech, Barry began working for Eastman Chemical Company in Kingsport, Tennessee as a mechanical engineer in the Engineering Mechanics and Analysis Group.

Barry L. Agee